DEVELOPMENT OF NOVEL STRATEGIES FOR RAPID SYNTHESIS OF SILICOALUMINOPHOSPHATE MOLECULAR SIEVES IN NON-AQUEOUS MEDIA AND CATALYTIC APPLICATION STUDIES ON METAL SUPPORTED SAPO-35

THESIS

SUBMITTED IN PARTIAL FULFILMENT OF THE REQUIREMENTS
FOR THE AWARD OF THE DEGREE OF

Doctor of Philosophy

IN

CHEMISTRY

BY

S SURESH

(Roll No. 716192)

Research Supervisor

Dr. N. Venkatathri

DEPARTMENT OF CHEMISTRY
NATIONAL INSTITUTE OF TECHNOLOGY WARANGAL
WARANGAL – 506 004, TELANGANA, INDIA

JULY – 2021

DECLARATION

This is to declare that the work presented in the thesis entitled "**Development of Novel Strategies for Rapid Synthesis of Silicoaluminophosphate Molecular Sieves in Non-Aqueous Media and Catalytic Application Studies on Metal Supported SAPO-35"** is a bonafide work done by me under the supervision of Dr. N. Venkatathri, Associate Professor in the Department of Chemistry, and was not submitted elsewhere for the award of any degree. I declare that this written submission represents my ideas in my own words. Where others' opinions or concepts have been included, I have adequately cited and referenced the sources. I also declare that I have adhered to all principles of academic honesty and integrity and have not misrepresented or fabricated or falsified any idea/data/fact/ source in my submission. I understand that any violation of the above will be a cause for disciplinary action by the Institute and can also evoke penal action from the sources which have thus not been appropriately cited or from whom proper permission has not been taken when needed.

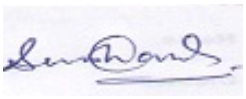

Date: **13.07.2021** (**S. Suresh)**

Place: **NIT Warangal** Roll No.: **716192**

Dr. N. Venkatathri
Associate Professor
Department of Chemistry
National Institute of Technology
Warangal - 506 004
Telangana, India

Mobile: +91-9491319976
Email: venkatathrin@yahoo.com

CERTIFICATE

This is to certify that the work presented in the thesis entitled "**Development of Novel Strategies for Rapid Synthesis of Silicoaluminophosphate Molecular Sieves in Non-Aqueous Media and Catalytic Application Studies on Metal Supported SAPO-35"** is a bonafide work carried out by **Mr. S. Suresh** for the degree of Doctor of Philosophy in Chemistry, National Institute of Technology, Warangal (Telangana), India, under my supervision and that the same has not been submitted elsewhere for a degree.

Date: **13.07.2021**
Place: **NIT Warangal**

Dr. N. Venkatathri
Thesis Supervisor

This thesis is dedicated to my beloved Parents

Acknowledgments

Acknowledgments

During my Doctoral Research work, I have received assistance and support from the following people:

First and foremost, I am genuinely indebted, and I express my earnest gratitude for my Research Supervisor **Dr. N. Venkatathri**, Associate Professor, Department of Chemistry, National Institute of Technology Warangal, for his valuable expertise and astute guidance. His unabated enthusiasm, which stems from his absolute command over the subject, has been a constant source of inspiration for me to work hard, and the outcome is expressed in the form of this thesis.

I am grateful to **The Director**, National Institute of Technology Warangal, for allowing me to carry out the work and allowing me to submit in the form of a thesis.

I express my gratitude to the Doctoral Scrutiny Committee members: **Dr. Vishnu Shanker**, Chairman and Head, Department of Chemistry, **Prof. K. Laxma Reddy**, Department of Chemistry, **Prof. K. V. Gobi,** Department of Chemistry, and **Dr. T. V. Appa Rao**, Department of Physics, NIT Warangal for their detailed review, constructive suggestions and excellent advice during the progress of this research work.

My sincere thanks are due to former Heads Prof. V. Rajeswar Rao, Prof. K. V. Gobi, of the Department of Chemistry during the period of my research work.

I want to thank all the faculty members from Chemistry Department, namely Prof. A. Ramachandraiah (HAG), Prof. K. Laxma Reddy (HAG), Prof. V. Rajeswar Rao (HAG), Dr. Vishnu Shanker, Dr. D. Kashinath, Dr. B. Srinivas, Dr. K. Hari Prasad, Dr. S. Nagarajan, Dr. M. RaghaSudha, Dr. Ch. Jugun Prakash, Dr. Ravinder Pawar, Dr. Mukul Pradhan, Dr. Rajeshkhanna Gaddam, Dr. V. Rajeshkumar, and the other faculty members for their valuable advice and encouragement throughout the research work.

I convey my special thanks from the bottom of my heart to my seniors, Dr. A. Rajini, Dr. M. Nooka Raju, Dr. A. Ajay Kumar, Dr. Suman Chirra and my juniors Mr. Srinath Goskula, Mr. Sripal Reddy Gujjula, Mrs. Radha Nagarapu for their continuous support and encouragement in every step of my research work.

I want to convey my heartfelt thanks to Dr. K. Vimal Kumar, Dr. Yugender Kotagiri, Dr. Santosh Biradar, Dr. K. Chaitanya Kumar, Dr. T. Surender, Dr. M. Satya Narayana, Research Scholars, and Department of Chemistry for their fathomless support in technical discussions.

With all happiness, I acknowledge the cheerful assistance rendered by all my research colleagues, Dr. V. Krishnaiah, Dr. Srinivas Pavurala, Mr. Ashutosh Kumar Yadav, Dr. E. Hari Mohan, Mr. Phani Kumar, Dr. T. Vikram Sagar, Dr. Sagar Vijay Kumar, Dr. Lingala Suresh, Dr. B. Mayuri, Mrs. Poshala Soumya, Dr. Rajitha, Dr. G. Ramesh, Dr. N. V. Bharath, Dr. S. Nagaraju, Dr. B. Paplal, Dr. P. Vinay, Dr. T. Sanjeeva, Mr. Neeli Satyanarayana, Dr. Sunil Kumar Venishetty, Mr. Shekar Kummari, Mr. K Sampath, Mr. M. Srikanth, Mr. P. Babji, Mr. K. Vijendhar, Mr. G. Ambedkar, Mr. Ch. Raju, Mr. T. Danunjay Rao, Mr. R. Venkatesh, Mr. K. Sathish, Mr. A. Naveen Reddy, Mr. A. Bhargava Sai, Mr. P. Venkatesham, Ms. M. Shireesha, Ms. G. Siva Parvathi, Mrs. Santwana, Mrs. Divya, Mrs. T. Shireesha, Mrs. B. Sravanthi, Mr. P. Vara prasad, Mr. R. Arun Kumar, Ms. Akanksha, Mr. B. Anjaiah, Mr. B. Prashanth, Mr. K. Madhu, and other research scholar friends for their generous support.

I am grateful to the lab assistants Mr. G. Santhosh, Mr. Praveen, Mr. Srinivas, Mr. T. Kiran Kumar, Mr. P. Heerulal, Mrs. Shaheen Begum, Mr. B. Sadanandam, Mr. K. Kehsvulu, Mrs. A. Rajini, Mrs. Ganga Bhavani, Ms. K. Kavya and other supporting staff of the Department of Chemistry, NIT Warangal for their cooperation.

I have been blessed with continuous moral support and boundless inspiration from my parents, Sri. Siliveri Sathya Goud Garu and Smt. Siliveri Padma Garu, My wife Manisha, My Brother's Siliveri Ramesh, Siliveri Naresh, my closest friends Manasa Samavedam, Hithavani Rapaka, Venu Chennaboina, Madhu Ade, and Aarti Gautam and all other family members. Their love and affection have been motivating forces behind what I am today.

Above all, I fail to find apt words to thank Mr. Sagar Janampelli (Quality Assurance Officer at Bharat Petroleum Corporation Limited), Siva Sai Kuma Pinnepalli (University of Missouri Kansas City, USA) Nathan A. Oyler (University of Missouri Kansas City, USA), Deepak Joshi (CSIR-Indian Institute of Petroleum, Dehradun, India) and Padmakar (CSIR-Indian Institute of Chemical Technology, Hyderabad, India) for their experimental and moral support for my thesis work.

With encouragement and support, I could complete my doctoral work successfully. I much acknowledge DST-SERB (EMR/2014/000629) Government of India and the Ministry of Human Resource Development, Govt. of India, for financial assistance in the form of Institute fellowship.

Last but not least, it gives me immense pleasure to express my heartfelt thanks to all those who have been with me and lend me the necessary help in every possible way throughout my thesis work.

Date: **12.07.2021** **S Suresh**

ABBREVIATIONS

IUPAC	International Union for Pure and Applied Chemistry
nm	Nanometre
cm	Centimeter
Å	Angstrom
θ	Theta
λ	Lambda
eV	Electron volt
ε	Epsilon
υ	Neu
mL	milli Litre
μL	micro Litre
M	Molarity
mM	milli Molar
h	Hour
mins	minutes
^{o}C	Degree centigrade
μm	Micro metre
g	Grams
mg	milli Grams
mmol	milli Mole
RT	Room Temperature
rpm	Rotations per minute
SEM	Scanning Electron Microscopy
TEM	Transmission Electron Microscopy
XRD	X-ray Diffraction
FTIR	Fourier Transform Infra Red
UV	Ultra-violet
XPS	X-ray Photoelectron Spectroscopy

CONTENTS

Table of Contents

CHAPTER-I

Introduction - need, objective, and scope.

Abstract

The present work described in this thesis is mainly focused on the synthesis and characterisation of silicoaluminophosphates (SAPOs) in non-aqueous media as solid state heterogeneous catalyst supports through different route of synthesis. Various synthesis strategies were explored to observe structural formation and to identify features that enhance the stability and catalytic activity of small pore SAPOs and metal supported SAPOs for various catalytic applications. The primary characterisation techniques used include powder X-ray diffraction spectroscopy (PXRD), Scanning electron microscope (SEM), Fourier transform infrared spectroscopy (FT-IR), Magic Angle Spinning-Nuclear Magnetic Resonance spectroscopy (MAS-NMR), Brunauer–Emmett–Teller (BET) analysis and X-ray photoelectron spectroscopy (XPS). Microporous SAPO-35 (Levyne type) synthesised in a non-aqueous media by using different inorganic promoters ($HClO_4^-$, HF, H_3PO_4, and $NaNO_3$) to enhance the rate of crystallization. The study revealed that, when a small amount of inorganic promoter was added to the reaction mixture, this will enhance the speed of the nucleation process of the gel and which leads to faster crystal growth, All the materials synthesized using various promoters have exhibited similar characteristics as that of the standard SAPO-35 (material synthesized without using promoters). Further investigated on Methanol to olefin catalytic application from these study the catalytic performance in terms of yield and selectivity of these materials in the MTO conversion reaction is found to be similar with the performance of standard material. In another study an Aluminophosphate with sequence number Six Teen (AST) type framework silico alumino phosphate (SAPO-16) molecular sieve is successfully synthesized through an eco-friendly, economic and a faster crystallization method by microwave treatment. The faster crystallization in case of microwave treatment is due to the direct formation of SAPO-16, whereas in case of conventional hydrothermal aqueous media synthesis, it is forming through SAPO-L lamellar intermediate which takes around 24-48 h in aqueous media and 360 h in non-aqueous media at the same temperature. The synthesized SAPO-16 was found to be economic and efficient catalyst for Benzaldehyde acetalization reaction, the catalytic activity on Benzaldehyde acetalization reaction shows that the reactants have a maximum of 80 % benzaldehyde conversion in 8 h. Further SAPO-35 material was doped with TiO_2 anatase by sol-gel method with different weight ratios and photocatalytic performance of methylene blue degradation under sunlight radiation by the synthesized TiO_2/SAPO-35 was analyzed. The TiO_2/SAPO-35

composites degrade the methylene blue under sunlight irradiation in 25 minutes against 90 minuts for pure TiO_2 anatase. The fine dispersion of TiO_2 anatase Nano particles on the surface of the microporous SAPO-35 resulted in the increased ability of dye degradation. Further, Pd metal loaded on the surface of SAPO-35 using borohydride reduction method and resulting Pd/SAPO-35 materials used to study on Suzuki-Miyaura Cross Coupling reaction of benzene boronic acid conversion and it was given 99% with the Pd/SAPO-35 in 5 min under microwave irradiation. In summary, small pore SAPO materials were synthesised and evaluated for their performance for environmental control applications and identified frameworks as a structural feature that enhances catalytic applications.

Chapter 1
Introduction

I.1. Porous materials

Porous materials are made up of inorganic and organic materials and can have a crystalline and quasi-crystalline wall structure [1]. The porous zeolitic behavior of these materials facilitates other molecules to pass through the reversible passages or holes. This unique character of these materials is responsible to applicable in various sectors such as such as functional group adsorption, size selective sorption, molecular recognition, gas storage and catalysis. Several parameters were used to describe the porous structure, such as pore size or shape, channel dimensionality and direction, composition and features of channel walls. Among these parameters, pore size and shape are the most important. According to International Union of Pure and Applied Chemistry (IUPAC), porous materials are classified into three groups: based on the diameter of their pores, microporous (pore diameter less than < 2 nm), mesoporous (diameter of 2 ~ 50 nm) and macro porous materials (diameter larger than >50 nm). Porous materials are widely used as catalysts, adsorbents, ion-exchange agents and supports for catalysts because of their high surface area and open framework structure[2,3].

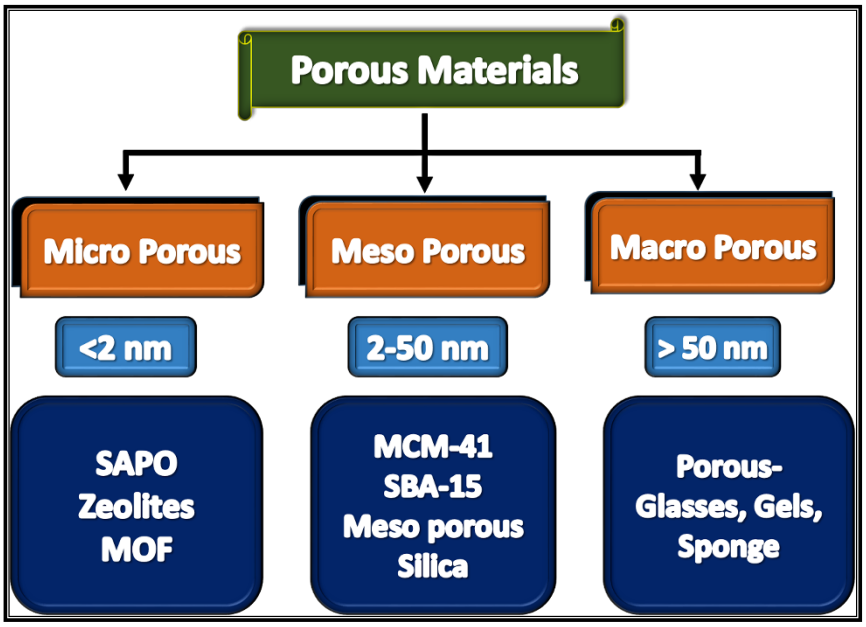

Figure.1 Classification of Porous Materials

I.2. Zeolites

The history of zeolites started with the discovery of the first mineral stilbite, by the Swedish Mineralogist Baron A.F. Cronstedt in 1756 [4]. Cronstedt found that stilbite would lose a significant amount of water during heating and called the mineral 'zeolite'. He found that the zeolitic materials are a new class of minerals with hydrated aluminosilicates of the alkali and alkaline earths. In the late 1700 through the 1800s numerous authors are studied and explained the properties of zeolite materials, including adsorption properties, reversible ion exchange dehydration studies and so on. In the year 1858 Eichorn proved that these zeolite minerals are proficient for the exchange of cataions like Na^{+} and Ca^{++} using chabazite and natrolite materials. After these innovation, several researchers founded, developed and demonstrated different type of natural and synthetic zeolites. St. Claire Deville is the first person who demonstrated the hydrothermal synthesis of a zeolite, levynite, in the year 1862 [5].

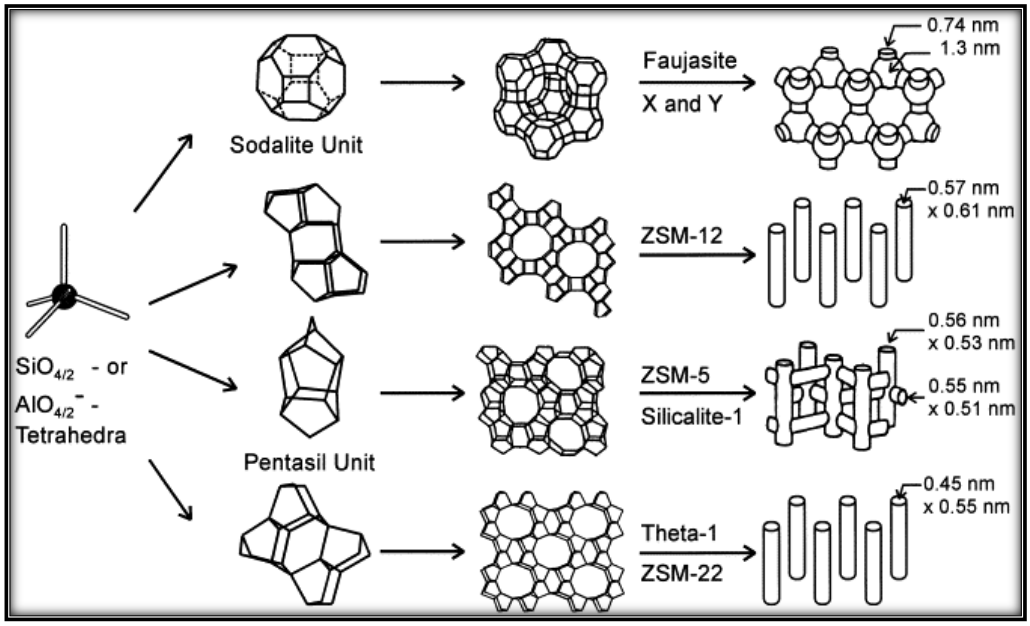

Figure 2. Different zeolite materials (Source: Internet)

In the year 1896 George Friedel developed and demonstrated that these zeolite materials can be used as sponge to occulate materials like chloroform, benzene and alcohols with dehydrated zeolites [6,7]. In the year 1909 François Grandjean found that gasses can be adsorbed by some of framework structures like chabazite. He demonstrated hydrogen gas and NH_3 gas adsorption by chabazite framework structure [8]. In 1925 Oskar Weigel and Eduard Steinhoff reported the first molecular sieve effect for the zeolite chabazite (dehydrated) with different organic vapours such as methanol, ethanol and formic acid [9]. In 1927 Leonard described the first use of X-ray diffraction for identification in

mineral synthesis [10]. Taylor and Pauling determined the first single crystal structure of zeolite minerals in 1930 [11]. Taylor revealed the structure of analcime [12]. In 1932 McBain established the term “Molecular Sieve” to define porous solid materials that act as sieves on a molecular scale [13].

By the mid-1930s, the ion exchange, adsorption, molecular sieve effects and structural properties of zeolite minerals as well as a number of reported synthesis of zeolite was described in literature. Barree's work in 1938, Samanish's in 1929, Samanishi and Hemmi's in 1934 on the zeolite adsorption and molecular sieve phenomena were carried out on crystals from basalt vugs.

Richard M. Barrer began his pioneering work in zeolite adsorption and synthesis in the mid-1930s to 1940s [14]. He presented the first classification of the known zeolites based on molecular size considerations in 1945 [15]. The first definite synthesis of zeolites, among which zeolite mineral mordenite, was described in 1948 by Richard Barrer [16] and a novel synthetic zeolite [17] much later identified as the KFI framework.

In the late 1940s Linde Division of Union Carbide Corporation initiated studies on zeolite synthesis under the direction of M. Milton and D. Breck to produce chabazite for separation and purification of air, other adsorption and molecular sieve application.

In the year 1950, Linde Company applied the use of NaA in the separation of normal and isoalkanes. In 1960, zeolites X and Y were used as catalysts for cracking reactions of hydrocarbon conversion. NaA, NaX and NaY have been widely used in the petroleum industry in reactions such as cracking, alkylation, isomerisation, shape selective reforming, hydrogenation and dehydrogenation and methanol to gasoline conversion (MTG).

The period from 1954 to the early 1980s is the golden age for the development of zeolites. Zeolites with low, medium and high Si/Al ratios were extensively explored and this greatly facilitated the application of zeolites in industrial progress [18].

By 1953, Milton and his co-workers had synthesized 20 zeolites, including 14 unknowns as natural minerals [19]. Between 1949 and 1954 Robert Milton and Donald W. Breck discovered a number of commercially significant zeolites, namely zeolite types A, X and Y using inorganic bases. Ten years later, Barrer and Benny obtained zeolite A with higher Si/Al ratios up to 3 by replacing inorganic bases with organic ones.

In 1954 Union Carbide commercialized that synthetic zeolites could be applied for industrial applications such as separation and purification purposes and implemented

their use in the drying of refrigerant gas and natural gas. The earliest applications were the drying of refrigerant gas and natural gas. In 1955 T.B. Reed and D.W. Breck reported the structure of the synthetic zeolite A [20]. In 1959 Union Carbide marketed the "ISOSIV" process for normal iso-paraffin separation, representing the first major bulk separation process using true molecular sieving selectivity. In 1959 zeolite Y based catalyst was marketed by Carbide as an isomerisation catalyst.

In 1960, Flanigen and Breck studied in detail the formation mechanism of zeolites. They reported the use of X-ray measurements to follow the crystallization of different zeolites over time [21]. They were the first to observe the S-shaped growth curves typical for zeolite synthesis, which indicates the induction period during which few zeolite crystals are formed, followed by a rapid growth which takes place over a short span of time. In order to increase the thermal stability and acidity of zeolites, D.W. Breck synthesized zeolite Y (Si/Al = 1.5 ~ 3.0), which played an extremely important role in the catalysis of hydrocarbon conversion.

In 1962 Mobil Oil Company introduced the use of synthetic zeolite X as a hydrocarbon cracking catalyst. In 1969 Grace described the first modification chemistry based on steaming zeolite Y to form an "ultrastable" Y (USY). In 1967 – 1969 Mobil Oil reported the synthesis of the high silica zeolites Beta and ZSM-5 [22].

In 1974 Henkel introduced zeolite A in detergents as a replacement for phosphates. By 2008 approximately 367000 tonnes of zeolite Y were in use in catalytic cracking [23]. In 1977 Union Carbide introduced zeolites for ion – exchange separations. In 1978 researchers at Union Carbide Corporation found a way to synthesize silicalite-1, a pure silica ZSM-5 [24]. In the 1980s extensive work was carried out on the synthesis and applications of ZSM-5 and other members of the high silica zeolite family.

In the period since the 1980s the discovery of new compositions and structures of zeolites increased tremendously: in the first edition of the Atlas of Zeolite Structure Types from 1978, only 38 structure types were described. In the second edition (1987), this increased to 64 and in the online 2011 edition, 197 different zeolite framework types were reported. According to the Structure Commission [25] of the International Zeolite Association [26], 201 zeolite framework codes are known, with the latest entry registered on October 15, 2011, clearly shows that even today zeolites attract great interest.

The increase in type and structural diversity of zeolites, as well as deep insight into zeolite properties such as thermal stability, acidity, hydrophobicity and hydrophilicity of surfaces, ion-exchange capacity, has led to application of a series of zeolites in industry. The crystallization of zeolite occurs via the formation of organic inorganic composites which are organised in the synthesis solution to form the first crystal nuclei through aggregation. Further incorporation of the composite to the nuclei gives rise to a layer-by-layer growth of the final zeolite product, as shown in Fig. 3 [27].

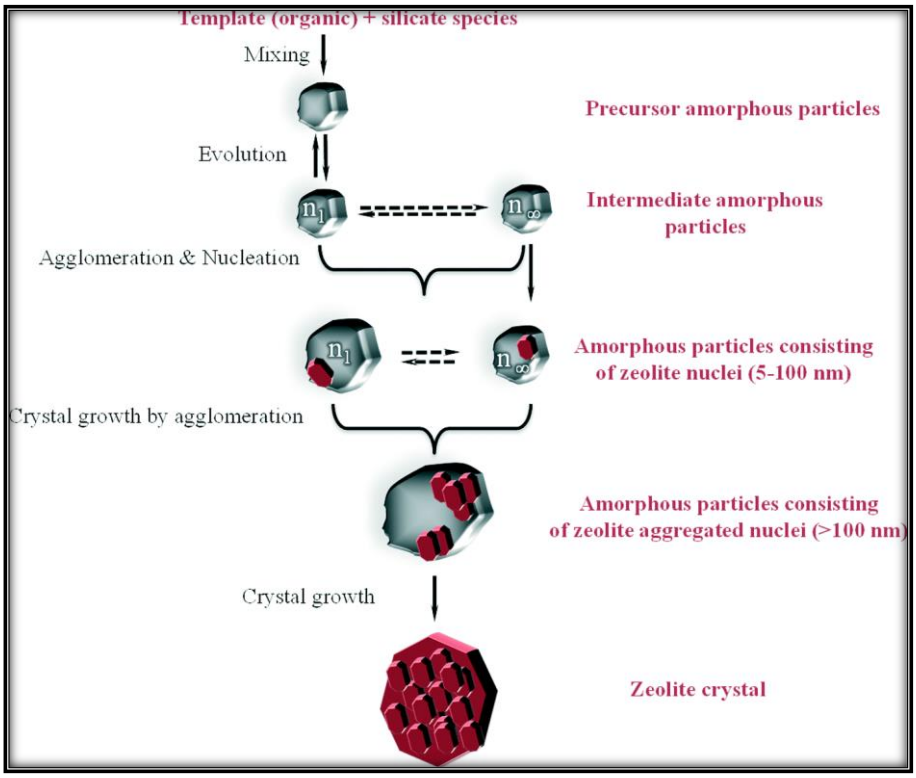

Figure 3: Scheme for zeolite crystallization.

The crystallization process involves following steps:

(1) The initial step is formation of hydrogen bonds in between the structure directing agent (SDA) and the silicate groups which are present in the initial gel

(2) After bond formation, the oligomerisation of silicates

(3) Third step of zeolite crystallization is, condensation of the silicate and the structure directing agent species to get the primary stable crystalline nuclei;

(4) The last step of is crystal growth. (Tertiary ammonium salts are used as structure directing agent for the study.

I.3. Molecular sieves

The term molecular sieves describe porous materials, which are able to selectively separate molecules on the basis of their size or shape. A common classification of

molecular sieve materials includes (i) the family of the microporous crystalline solids, which comprises zeolites, all silicoaluminophosphate molecular sieves, aluminophosphates and related materials; (ii) mesoporous solids from the M41S family; (iii) pillared clays and (iv) non-crystalline solids such as charcoals and metal oxides. Other mesoporous materials include metal oxides and non-oxides (e.g. sulfides), carbons or metals (normally not structured). Macro pores can be formed in oxides, activated carbons, polymer resins or metals. In the past half century, molecular sieves have played increasingly important role as catalysts in the petroleum refining, petrochemical and other chemical industries.

I.3.1. Aluminophosphate ($AlPO_4$) molecular sieves:

Lok, Flanigen and Wilson et al. successfully synthesized a new class family microporous crystalline natured aluminiphosphate molecular sieves ($AlPO_4$-n) in 1982 at Union Carbide Factory [28]. In addition of other elements like Si to this $AlPO_4$-n molecular sieves become SAPO-n (silicoaluminophosphate) here S Means Si. In addition of other metal ions like Fe, Co, Mg, Mn gives metalloaluminophosphate (MeSAPO-n) (Me = Fe, Mg, Mn, Zn, Co, etc) and ‘‘ElAPO-n’’ family (El = Ba, Ga, Ge, Li, As, etc.,). Here the added element is incorporated into the $AlPO_4$ [29].

So far there are over two hundred compounds available in the $AlPO_4$ molecular sieves family and these compounds will be crystallized using different kinds of templets or structure directing agents. There are numerous structure types of microporous $AlPO_4$ molecular sieves with different compositions and these composite materials differ significantly [30]. Apart from these composites, some of isostructural with respective zeolite materials, utmost $AlPO_4$ molecular sieves framework structures are unique and their elemental compositions are bit differ from the regular zeolite materials which consists of silicon and aluminium.

These zeotype materials are formed by the substitution of framework silicon atoms by phosphorous atoms and are used as membranes, heterogeneous catalysts and adsorbents [31]. Such substitutions allow the formation of larger ring structures. The thermal stability of the resulting materials is lower, but they display an improved accessibility and diffusivity in comparison to the conventional zeolite frameworks.

The substitution of heteroatoms into $AlPO_4$ framework structure has played an important role in enhancing the variety of framework structures and compositions of different kind

of microporous compounds and molecular sieves. So far Twenty above different elements had been effectively incorporated into frameworks of $AlPO_4$ molecular sieves. The different compositional and structural $AlPO_4$ frameworks and their respective metals substituted framework structured materials are having many applications like macromolecular catalysis, redox catalysis, adsorption, separation and chiral catalysis. So far there are more than 24 framework structures and close to 200 composites in $AlPO_4$ based molecular sieves. Kimura et al. reported the formation of stable mesoporous AlPOs using surfactants with long alkyl chains [32,33]. Van Nordstrand et al. have reported the synthesis of a pure silica analogue of the SAPO-5 structure, SSZ-24 [34]. Stucky et al. discovered a generalized method for preparing a large number of metallo-aluminophosphate and metallo-gallophosphate frameworks containing transition metals. The method utilizes amine SDAs and high concentrations of transition metal and phosphate in mixed solvents, typically alcohol and water. Gier et al. reported zinc and beryllium phosphates and arsenates with the X (FAU), ABW and SOD structures reminiscent of the early aluminum rich synthetic zeolite chemistry. Kaliaguine et al. have synthesized AlPO-5, which was shown to have both Lewis and Bronsted acid sites [35]. Among more than 40 structures of $AlPO_4$-n, some are zeolite analogues but there are also novel, unique structures. Davis et al. successfully synthesized the first aluminophosphate molecular sieve, VPI-5 ($(H_2O)_{42}[Al_{18}P_{18}O_{72}]$), with 18-membered ring apertures (12.7 x 12.7A°) [36]. The synthesis of VPI-5 is another milestone in the development of microporous materials.

I.3.2. Silicoaluminophosphate (SAPO) molecular sieves

There are various types of Silicoaluminophosphate molecular sieves with a distinguishable structural diversity for instance, Levynite type SAPO-35, faujasite type SAPO-37 and Chabazite type SAPO-34 etc., [37]. Out of these various SAPO molecular sieves SAPO-5, SAPO-11, SAPO-16, SAPO-20 and SAPO-31 are considered to be consisting novel structural framework. The basic framework structure of these SAPO molecular sieves are found to be tetrahedral oxide framework with the constituting elements of aluminium, phosphorus and. Silicon [38,39]. The formation of SAPO molecular sieves follows a typical substitution of silicon atoms into aluminophosphate framework. The mechanistic aspect of this substitution can plausibly follow three different routes, which are i) aluminium replaced by silicon atom, ii) phosphorous replaced by silicon atom, iii) both phosphorous and aluminium concurrently replaced by

two silicon atoms respectively. The overall framework formed by the substitution mechanisms mentioned above bring about the change in the net framework charge, which are +1 for i) mechanism, -1 for ii) mechanism and -1 for iii) mechanism respectively. Based on the mechanism of framework formation some of the SAPO molecular sieves contains net negative charge along with exchangeable cations and Brønsted acid sites. The SAPO molecular sieves contains cations and hydroxyl groups accompanied by the difference in electronegativity between constituent elements viz, Al, P and Si. As a consequence, these SAPOs will demonstration moderate to high hydrophilic surface properties. Because of these unique structural properties SAPOs can be used as catalysts, ion-exchangers and adsorbents. Since, SAPOs have more commonalities with $AlPO_4$ molecular sieves their properties like adsorption, thermal stability and pore dimensions are also resembling with $AlPO_4$. The acidic strength may vary with respect to the concentration of silicon in the framework along with framework structure.

I.3.2.1. SAPO-35:

SAPO-35 is a LEV (Levyne) type topological framework microporous material with 0.36 x 0.48 nm ring opening pore which is constructed by a single six membered ring (S6R) and a double six membered ring (D6R) with different T sites in a 2:1 ratio respectively [40]. It was synthesized using Quinuclidine, Cyclohexyleamine, and Hexamethyleneimine as the structure directing agents (SDA) for the crystallization of SAPO-35 at 200 °C reaction temperature in aqueous media [41].

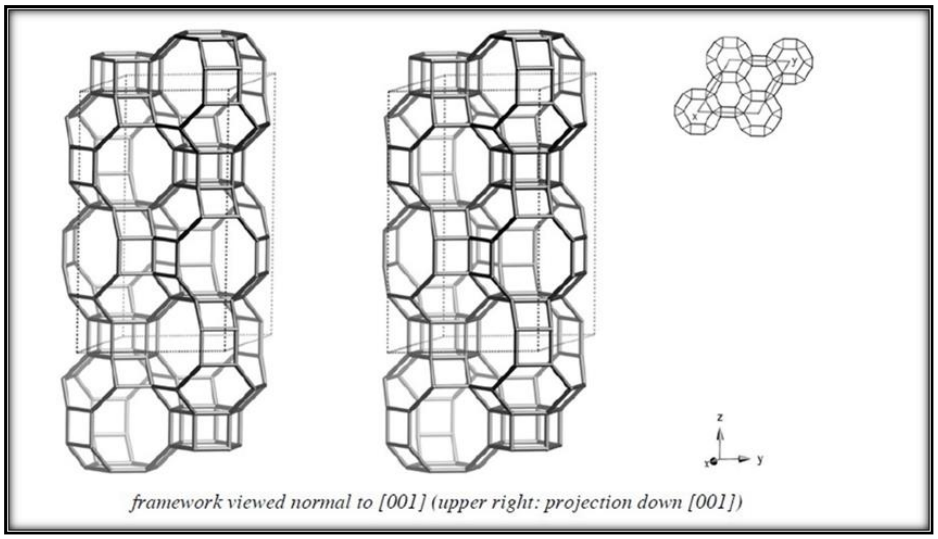

Figure 4: Framework Structure of SAPO-35

I.3.3.2. SAPO-16:

SAPO-16 is having AST type frame work topology [42,43]. The Cubic AST can be constructed by T10-units which consists of a double 4-ring (D4R) with two dangling T atoms (or two 4-1 units). The D4Rs of the T10-units are associated via the dangling T atoms into a two-dimensional Periodic Building Unit (PerBU). These vicinal PerBUs, related by a shift of ½ b (or ½ a), are associated via the dangling T atoms. Cages of (fused) 6-rings and 4-rings are formed. The framework can also be fabricated by fusion of these cages. The cavities are formed by 6-rings only [44]

I.3.3. Metal aluminophosphate (MeAPO) molecular sieves

Aluminophosphates are known to be neutral in nature [45]. Hence, they don't exhibit catalytic activity, several researchers have worked on aluminophosphates to improve the catalytic activity by chemical modifications and physical modifications like adsorption or introduce catalytic species by trapping them in to the pores of aluminophosphates. By introducing or substituting directly in to the lattice, some of the cations which may be equivalent or altervalent acquire properties like ion exchange ability and obtain acidic or basic centers in the system. Hence, by adopting hydrothermal method researchers have succeeded in formation of tetrahedral co-ordinations in the framework using di, tri and tetravalent cations. There are reports in the literature on the integration of catalytic active centers in the framework using hydrothermal method to incorporate cations [46] like Si^{4+}, Ti^{4+}, Sn^{4+}, Fe^{3+}, B^{3+}, Ni^{2+}, Co^{2+}, Mg^{2+}, Sr^{2+}, La^{3+} and V^{5+}.

The microporous materials synthesized by adopting the above mentioned method have crystalline structure and can be denoted as MeAPO-n. The pore size of these materials generally found in the range of 3 A° to 10 A°. Moreover, the as synthesized materials after calcination also contains acidic site in its framework. The constituent elements of the above synthesized materials framework have the combination of aluminium, phosphorous and metal. The variety of compositions of metal aluminophosphates mentioned above was represented with a general formula which is, $0.3R\ (Me_xAl_yP_z)O_2$. In this formula the value of x is said to be the mole fraction of metal, which varies from 0.01 to 0.25.

When the alumimiumhposphate consisting the tetrahedral units of AlO_2 and PO^{2+} was modified with divalent ions generates acidic sites in the framework along with ion-exchange capacity to the material. This phenomenon explains the substitution process of

the metal ions in the APO framework, which is evidently the substitution of Al with metal rather than the P. When the trivalent aluminum was substituted by divalent metal results in a net negative charge to the framework. Whereas, for the trivalent substituent metal the net framework charge is found to be neutral. As a consequence, the MeAPO materials possesses Bronsted acid sites as well as ion-exchange properties just like SAPO-n.

Based on the substitution type the MeAPO-n demonstrates structural multiplicity and compositional disparity. As per the reports thirteen different types of structures in the MeAPO family have been crystallized so far, which have similarities in framework topology with Zeolites and $AlPO_4$-5, $AlPO_4$-11 structures. The unique properties of MeAPOs like pore size, pore volume, adsorption capability and hydrophilic surface selectivity are more or less similar to the SAPO materials and $AlPO_4$ materials. Based on the substituent metal and structure of material the catalytic properties show a discrepancy. Interestingly, the MeAPO-n materials show less thermal and hydrothermal stability compared to those of SAPO and $AlPO_4$ materilas.

I.3.4. Metal Silicoaluminophosphate (MeAPO) molecular sieves

MeAPSO [47-49] structure types consist of framework topologies witnessed in binary ($AlPO_4$ and ternary (SAPO and MeAPO) compositional systems of MeO_2, AlO_2, SiO_2 and PO_2 tetrahedral units. The empirical chemical composition on anhydrous basis for these molecular sieves is expressed as mR $(Me_wAl_xP_ySi_z)O_2$, where w, x, y and z represent the molar fractions of Me, Al, P and Si respectively, present as tetrahedral oxides and m may vary from 0 to 0.03. Some molecular sieves with ZnO_2, AlO_2, PO_2 and SiO_2 and other molecular sieves with TiO_2, AlO_2, PO_2 and SiO_2 oxide framework structures have been reported by Lok et al. When additional elements such as Li, Be, B, Ga, Ge, As and Ti are incorporated into the framework structures, many large, intermediate and small pore molecular sieves are formed. These molecular sieves are designated as ElAPO-n [50-52] and ElAPSO-n. Quinary and senary framework compositions have been synthesized containing aluminium, phosphorous and silicon with additional combination of divalent metals [53,54].

I.4. Applications:

Zeolites firmly known as molecular sieves are usually referred to the aluminosilicate family which are having ordered pores with different pore sizes and dimensions. These materials are widely used in different industries like petroleum industry as the ion-exchangers, heterogeneous catalysts, in environmental protection these materials used as

the adsorbents, in medicine field these materials used as the drug delivery agents, also these materials used in construction industry and agriculture as well. Silicon substituted aluminophosphates are acidic in nature and theses (SAPO) materials were being used in different application studies like olefin oligomerization and organic transformations.

The substitution of different transition metals in these SAPO materials leads to the enhancement of the catalytic activity along with selectivity This improvement in selectivity may due to the acid sties in the substituted transition metal MeSAPSO's combined with unexpected spatial effects. Some of the most encouraging applications are disused below and few of these applications are commercial [55-61].

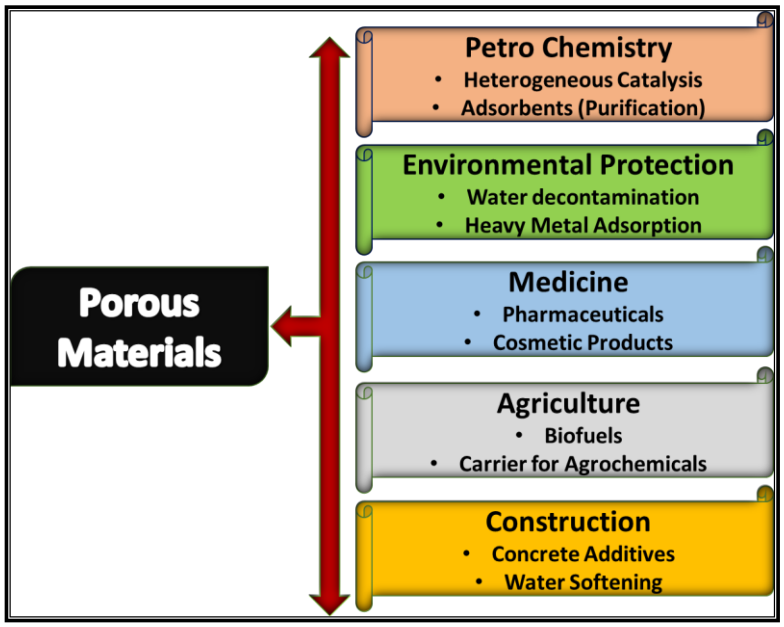

Figure.5: Different Applications of Porous Materials

I.4.1. Methanol to Olefin reaction:

MTO reaction is one of the most important reactions for the production of petrochemicals [62-65]. The catalytic conversion of MTO is one of the promising ways of converting natural gas and coal to chemicals. This MTO reaction was first proposed by Mobil Corporation in 1977. The methanol to olefin reaction is an acid catalysed reaction. Researchers widely studied this MTO reaction with different zeolites, Si incorporated molecular sieves, from these studies it was found that SAPO-34, SAPO-35 and HZSM-5 are better catalysts for the conversion of methanol-to olefins [66,67].

I.4.2. Benzaldehyde Acetalization:

The acetalization of alcohols reaction is widely used in synthetic approaches to protect the carbonyl group of the various aldehydes and ketones [68,69]. The acetals and hemiacetals are important reactants for synthesizing functional compounds like

fragrances, steroids, and pharmaceuticals. As per the available literature, many heterogeneous catalysts are there for acetalization reactions for instance, mesoporous alumino-silicates JRC-SiO-4, silica gel, and MCM-41.

I.4.3. Suzuki–Miyaura cross-coupling reaction

In the modern chemistry Pd catalyzed C-C bond formation Suzuki Miyaura coupling is a most important and useful reactions [70-73]. In the year, 2010 noble prize awarded for this reaction speaks the significance of this reaction. The resulting products of Suzuki Miyaura coupling reactions are bi-aryls [74,75]. These are the most essential ingredients of the many pharmaceuticals also in agrochemical fertilizers and natural products etc., The catalyst for Suzuki-Miyaura coupling reaction has been extensively studied with homogeneous catalysts and reported with high turnover number and yields but the major disadvantage of using homogenous catalyst is separation of the catalyst and reuse of it for multiple times [76]. To overcome this problem, researchers are focusing on development in heterogeneous catalysts with the same turnover numbers and high yield along with reusing capacity [77].

I.4.4. Photocatalysis

Photocatalytic technology refers to the rate of photo chemical reactions (oxidation or reduction) by the initiation of a catalyst which is generally a semiconductor material in presence of visible or UV light. Photocatalytic degradation of organic pollutants and photocatalytic water splitting can be simply defined as an artificial photosynthesis. In photosynthesis, plants use chlorophyll and light to generate starch (organic matter) and oxygen from carbon dioxide and water, whereas a photocatalyst can decompose organic matter into carbon dioxide and water using oxygen and water by light irradiation. It can also decompose the water into oxygen and hydrogen gases [78,79]. Therefore, photocatalysis is a promising alternative technology for photo degradation of pollutants in water or air and for production of clean renewable energy through the photo induced electrons and holes in semiconductor particles [80].

I.5 Thesis Motivation and Outline

I.5.1. Need of the Present Study

Most of the SAPOs are synthesized in presence of aqueous media [81,82]. For acid catalyzed reactions, it is advantageous to synthesis SAPOs with high silicon content to increase the number of acidic sites which are located both on dispersed silicon species and at the edge of silicon islands. However, due to poor crystallinity, and formation of

large siliceous islands at high Si concentration in the gel, the silicon content in the SAPOs is limited. It is advantageous therefore to look for synthesis procedures that allow the synthesis of highly siliceous SAPOs from a gel containing high concentration of silica. Insufficient and non-specific incorporation of Si in $AlPO_4$ lattice and poor crystallinity of the SAPOs are major problems faced during the synthesis of SAPOs. Numerous efforts have been made in the past to over-come these problems though modifications in synthesis methods such as the use of biphasic medium and novel structure directing templates.

Recently some of these molecular sieves are reported to synthesis in non-aqueous media [83-85]. Venkatathri et al, worked extensively and reported the synthesis of SAPOs in non- aqueous medium, however, using their method the time for the synthesis is relatively high. This non-aqueous media synthesis is found to be superior in many aspects, in terms of Si incorporation and crystallinity. Non-aqueous media process might create the possibility to establish a new industrial process with high efficiency. However, its limitation is it requires more crystallization time, hence more time taking process than aqueous media process. In the present study we have made an effort to reduce the synthesis time by reducing the crystallization time.

I.6. Objectives of the present work

The main objectives of the present study are as follows. The overall goal of the present study is to design and development a novel root for the synthesis of non-aqueous media SAPO molecular sieves in lesser time than the conventional process with retained properties.

1. To synthesize the Silicoaluminophosphates (SAPO-35) through non-aqueous media in lesser time using Inorganic promoters than the conventional process.
2. To synthesize Silicoaluminophosphates (SAPO-16) in very short time through non-aqueous media using Microwave Irradiation.
3. To synthesize anatase TiO_2 supported SAPO-35 molecular sieves for photochemical reaction (Methylene Blue dye degradation) application.
4. To synthesize Pd supported SAPO-35 molecular sieves as catalyst for the Suzuki-Miyaura Cross Coupling Reaction.

I.7. Scope of the present work

The current work deals with the synthesis of microporous silicoaluminophosphate molecular sieves materials (SAPO). SAPO-35 material is prepared in non-aqueous media

using hexamethylenimine (HEM) as the structure directing agent (SDA) by the conventional hydrothermal method in addition of a small quantities of inorganic promoters, similarly SAPO-16 is also synthesized in non-aqueous media using hexamethylenimine (HEM) as the structure directing agent (SDA) via microwave method. Further SAPO-35 material is substituted with Pd and Doped with TiO_2 through simple Sol-Gel method.

I.8. Organization of the thesis

Chapter – I: Introduction - need, objective, and scope.

Chapter – II: A brief description of various experimental techniques employed, methods, and materials used to synthesize, characterize, and study catalytic applications of synthesized materials.

Chapter – III: Investigation on the Promoter-Induced Rapid Non-Aqueous Media Synthesis of SAPO-35 and Methanol-to-Olefin Reaction

Chapter – IV: Synthesis of SAPO molecular sieves in Non-aqueous medium by microwave method using Hexamethyleneimine as a template.

Chapter – V: New Porous high surface area, TiO_2 Anatase/SAPO-35 Mild Bronsted acidic Nanocomposite: Synthesis, characterization and studies on its enhanced photocatalytic activity.

Chapter – VI: Pd/SAPO-35: Synthesis, Characterization and its Catalytic application studies on Suzuki-Miyaura Cross Coupling Reaction.

Chapter –VII: Summary and Conclusions.

I.9. References

[1] Boucher, E. A. J. Mater. Sci. 11, 1734–1750 (1976).

[2] Liu, T. & Liu, G. Nat. Commun. 11, 4984 (2020).

[3] Sun, M.-H. Et al. Chem. Soc. Rev. 45, 3479–3563 (2016).

[4] A.F. Cronstedt Akad. Handl. Stockholm 18 (1756) 120.

[5] H. de St Claire Deville, Comptes Rendus Acad. Sci., 54 (1862) 324.

[6] G. Friedel, C. R. Acad. Sci., Paris, 122 (1896) 948.

[7] G. Friedel, Bull. Soc. Fr. Mineral. Cristallogr., 19 (1896) 363.

[8] F. Grandjean, C. R. Acad. Sci., Paris, 149 (1910) 866.

[9] O. Weigel, E. Steinhoff, Z. Kristallogr. 61 (1925) 125.

[10] R.J. Leonard, Econ. Geol., 22 (1927) 18.

[11] W.H. Taylor, Zeitschrift fur Kristallographie, 74 (1930) 1.

[12] L. Pauling, Proc. Natl. Acad. Sci. U.S.A., 16 (1930) 453.

[13] J.W. McBain, Chapter 5, Routledge and Sons, London, UK, 1932.

[14] R.M. Barrer, Proceedings of the Royal Society A, 167 (1938) 392.

[15] R.M. Barrer, J. Soc. Chem. Ind., 64 (1945) 130.

[16] R.M. Barrer, J. Chem. Soc. (1948) 2158.

[17] R.M. Barrer, J. Chem. Soc., (1948) 127.

[18] E.M. Flanigen, Proceedings of the Fifth International Conference on Zeolites, L.V.C. Rees (Ed.), Heyden, London, (1980) 760.

[19] R.M. Milton, Molecular sieve science and technology: a historical perspective, in Zeolite Synthesis, ACS Symposium Series (eds M.L. Occelli, and H.E. Robson), American Chemical Society, Washington, D.C., 398 (1989) 1.

[20] T.B. Reed, D.W. Breck, Crystalline zeolites. II. Crystal structure of synthetic zeolite, Type A. J. Am. Chem.Soc., 78 (1956) 5972.

[21] E.M. Flanigen, D. W. Breck, in Proceedings of the 137th Meeting of the ACS, Division of Inorganic Chemistry, Cleveland, Ohio, USA, Paper no. 82: Crystalline zeolites, V-Growth of zeolite crystals from gels (1960).

[22] E.M. Flanigen, Stud. Surf. Sci. Catal. 137 (2001) 11.

[23] S. Davis, Y. Inoguchi, CEH Marketing Research Report: Zeolites, SRI Consulting (2009).

[24] E.M. Flanigen, Nature, 271 (1978) 512.

[25] http://www.iza-online.org/.

[26] http://www.iza-structure.org/.

[27] S.L. Burkett, M.E. Davis, J. Phys. Chem. 98 (1994) 4647.

[28] S.T. Wilson, B.M. Lok, C.A. Messina, T.R. Cannan, E.M. Flanigen, J. Am. Chem. Soc., 104 (1982) 1146.

[29] E.M. Flanigen, B.M. Lok, R.L. Patton, S.T. Willison, In 'New Developments in Zeolite Science and Technology.' Proceedings of the 7th International Zeolite Conference, ed. Y. Murakam, A. Lijima, J.W. Ward, Kodansha - Elsevier, Tokyo, (1986) 103.

[30] W. Vermeiren, J.-P. Gilson, Top. Catal. 52 (2009) 1131.

[31] D. Barthomeuf, J. Phys. Chem. 83 (1979) 249.

[32] T. Kimura, Y. Sugahara, K. Kuroda, Chem. Commun. (1998) 559.

[33] T. Kimura, Y. Sugahara, K. Kuroda, Chem. Mater. 11 (1999) 508.

[34] Van Nordstrand, R.A., Santilli, D.S., and Zones, S.I. in Perspect. Mol. Sieve Sci., ACS Symp. Ser. 368 (eds W.H. Flank, and T.E. Whyte, Jr.), American Chemical Society, Washington, DC, (1988) 236.

[35] M. H. Zahedi-Niaki, S.M.J. Zaidi, S. Kaliaguine, Microporous Mesoporous Mater. 32 (1999) 251.

[36] M.E. Davis, C. Saldarriaga, C. Montes, J. Garces, C. Crowder, Nature (London), 331 (1988) 698.

[37] Pyke, D.R., Whitney, P., and Houghton, H., Appl. Cat., 18, 173 (1985).

[38] Venkatathri, N.; Yoo, J. W. Appl. Catal. A Gen. 2008, 340 (2), 265–270.

[39] Yu, J.; Xu, R. Rich Acc. Chem. Res. 2003, 36 (7), 481–490.

[40] A. M. Prakash, Martin Hartmann, & Larry Kevan, Chem. Mater. 1998, 10, 3, 932–941.

[41] Lohse, U.; Vogt, F.; Richter-Mendau, J. *Cryst. Res. Technol.* **1993**, *28* (8), 1101–1107.

[42] J. Chen, J. Li, Y. Wei, C. Yuan, B. Li, S. Xu, Y. Zhou, J. Wang, M. Zhang, Z. Liu, Catal. Commun. 46 (2014) 36–40.

[43] R.X.F. W.H. Baur, Microporous and Other Framework, 2000.

[44] R.M. BARRER, Nature 249 (1974) 783–783.

[45] Pyke, D.R., Whitney, P., and Houghton, H., Appl. Cat., 18, 173 (1985).

[46] Kamble, K.R., Kulkarni, S.B., Joshi, P.N., Hegde, S.G., and Ratnasamy, P., Proc. Adv. Cat. And Cat. React. Eng. Ed. P. Kantarao, p. 129 (1986).

[47] Lok, B.M., Marcus, M.T., Kristofforse, B., and Flanigen, E.M., U.S. Pat., 604,155 (1984).

[48] Lok, B.M., Marcus, B.K., and Flanigen, E.M., Eur. Pat. Appl., EP 161,488; 161,489; 161,490 (1985).

[49] Lok, B.M., Vail, L.D., and Flanigen, E.M., Eur. Pat. Appl., EP 158,976; 158,977; 158,348; 158,349; and 159,624 (1985).

[50] Lok, B.M., Marcus, B.K., and Flanigen, E.M., U.S. Pat., 4,500,651 (1985).

[51] Flanigen, E.M., Lok, B.M., Patton, R.L., and Wilson, S.T., Stud. Surf. Sci. Catal., 28, 103 (1986).

[52] Lok, B.M., Marcus, B.K., and Flanigen, E.M., Eur. Pat. Appl., EP 158,350 (1985).

[53] B.M. Weckhuysen, R.R. Rao, J. A. Martens, R.A. Schoonheydt, Eur. J. Inorg.

Chem. 1999 (1999) 565–577.

[54] M. Hartmann, L. Kevan, Chem. Rev. 99 (1999) 635–664.

[55] C.S. Cundy, P.A. Cox, Microporous Mesoporous Mater. 82 (2005) 1–78.

[56] Y. Jin, Q. Sun, G. Qi, C. Yang, J. Xu, F. Chen, X. Meng, F. Deng, F.-S. Xiao, Angew. Chemie Int. Ed. 52 (2013) 9172–9175.

[57] K.S. Park, Z. Ni, A.P. Cote, J.Y. Choi, R. Huang, F.J. Uribe-Romo, H.K. Chae, M. O'Keeffe, O.M. Yaghi, Proc. Natl. Acad. Sci. 103 (2006) 10186–10191.

[58] S.-E. Park, D.S. Kim, J.-S. Chang, W.Y. Kim, Catal. Today 44 (1998) 301–308.

[59] F.M. Shalmani, S. Askari, R. Halladj, Rev. Chem. Eng. 29 (2013) 99–122.

[60] Y. Li, W. Yang, J. Memb. Sci. 316 (2008) 3–17.

[61] X. Li, K. Li, H. Ma, R. Xu, S. Tao, Z. Tian, Microporous Mesoporous Mater. 217 (2015) 54–62.

[62] Tian, P.; Wei, Y.; Ye, M.; Liu, Z. *ACS Catal.* **2015**, *5* (3), 1922–1938.

[63] Wang, Q.; Wang, L.; Wang, H.; Li, Z.; Wu, H.; Li, G.; Zhang, X.; Zhang, S. *Asia-Pacific J. Chem. Eng.* **2011**, *6* (4), 596–605.

[64] Dai, W.; Wu, G.; Li, L.; Guan, N.; Hunger, M. *ACS Catal.* **2013**, *3* (4), 588–596.

[65] Yarulina, I.; Chowdhury, A. D.; Meirer, F.; Weckhuysen, B. M.; Gascon, J. *Nat. Catal.* **2018**, *1* (6), 398–411.

[66] Wang, Y.; Chen, S.-L.; Gao, Y.-L.; Cao, Y.-Q.; Zhang, Q.; Chang, W.-K.; Benziger, J. B. *ACS Catal.* **2017**, *7* (9), 5572–5584.

[67] Ahn, N. H.; Seo, S.; Hong, S. B. *Catal. Sci. Technol.* **2016**, *6* (8), 2725–2734.

[68] M.W.C. Robinson, A.E. Graham, Tetrahedron Lett. 48 (2007) 4727–4731.

[69] U.S.F. Arrozi, H.W. Wijaya, A. Patah, Y. Permana, Appl. Catal. A Gen. 506 (2015) 77–84.

[70] S. Kotha, K. Lahiri, D. Kashinath, Tetrahedron 58 (2002) 9633–9695.

[71] A. Modak, J. Mondal, V.K. Aswal, A. Bhaumik, J. Mater. Chem. 20 (2010) 8099–8106.

[72] Srivastava, N. Venkatathri, D. Srinivas, P. Ratnasamy, Tetrahedron Lett. 44 (2003) 3649–3651.

[73] K. Sarkar, M. Nandi, M. Islam, M. Mubarak, A. Bhaumik, Appl. Catal. A Gen. 352 (2009) 81–86.

[74] C. Len, S. Bruniaux, F. Delbecq, V. Parmar, Catalysts 7 (2017) 146.

[75] S. Thunga, S. Poshala, N. Anugu, R. Konakanchi, S. Vanaparthi, H.P. Kokatla,

Tetrahedron Lett. 60 (2019) 2046–2048.

[76] M.A. Düfert, K.L. Billingsley, S.L. Buchwald, J. Am. Chem. Soc. 135 (2013) 12877–12885.

[77] S. Chirra, S. Siliveri, A.K. Adepu, S. Goskula, S.R. Gujjula, V. Narayanan, J. Porous Mater. (2019).

[78] M. Qamar, M. Saquib, M. Muneer, Dye. Pigment. 2005, 65, 1.

[79] L. B. Reutergådh, M. Iangphasuk, Chemosphere 1997, 35, 585.

[80] I. K. Konstantinou, T. A. Albanis, Appl. Catal. B Environ. 2004, 49, 1.

[81] N. Venkatathri, S.G. Hegde, V. Ramaswamy, S. Sivasanker, Microporous Mesoporous Mater. 23 (1998) 277–285.

[82] A.K. Sinha, S. Sivasanker, P. Ratnasamy, Ind. Eng. Chem. Res. 37 (1998) 2208–2214.

[83] Q. Gao, R. Xu, Mater. Lett. 31 (1997) 151–153.

[84] Q. Gao, S. Li, R. Xu, J. Chem. Soc. Chem. Commun. (1994) 1465.

[85] Venkatathri, N.; Hegde, S. G.; Rajamohanan, P. R.; Sivasanker, S. *J. Chem. Soc. Faraday Trans.* **1997**, *93* (18), 3411–3415.

CHAPTER-II

Materials and Methods

Chapter-II

II.1. Introduction

Catalysts' characterization is an integral part of a catalysis study wherein the properties of the catalysts are associated with their performance. The Physico-chemical characteristics of a catalyst largely depend on the condition of the experiments used during their synthesis. The data for catalysts morphology in terms of shape, size, crystallinity composition, phase, etc. is obtained by subjecting the sample to appropriate agents like photons or electrons. Such techniques of characterization can be divided into either qualitative (structure and properties) or quantitative (concentration, size, composition).

Not a single universal technique is present that gives a complete picture of a porous material. Physisorption with N_2 gas provides information about surface area, size, volume, and, relatively, the shape of the pore but the pore order is not revealed which on the other hand, is obtained by XRD and TEM studies. Morphological data and pore structure in a few cases are imaged by employing SEM and TEM for mesoporous films. Similarly, Fourier transformed infrared spectroscopy (FT-IR) reveals functional groups in the material structure and thermogravimetric analysis (TGA) about the removal of polymers and functional groups. Characterization techniques employed in the present studies, along with their applications, are listed below:

II.2. Materials

Chemicals used in the synthesis of the catalysts in the present study are as follows:

Chemical	**Formula**	**Company**
Ethylene glycol	$C_2H_6O_2$	Finar India, 99%
Aluminium isopropoxide	$Al(OCH_3H_7)_3$	Aldrich, 98%
Orthophospharic acid	H_3PO_4	S.D. Fine India, 85%
Fumed Silica	SiO_2	Aldrich, 99.9%
Hexamethyleneimine	$C_6H_{12}NH$	Aldrich, 98%
Palladium acetate	$(O_2CCH_3)_2$ Pd	Aldrich, 98%
Titanium tetraisopropoxide	$Ti[OCH(CH_3)_2]_4$	Aldrich, 98%
Methylene Blue	$C_{16}H_{18}ClN_3S$	Aldrich, 98%
2-Propanol	C_3H_8O	Merk India, >99%
$NaBH_4$	$C_6H_7BO_2$	98%,Avra India

II.3. Synthesis of Materials:

The methods which were used in the present study to synthesize the materials are hydrothermal method (SAPO-35), microwave irradiation method (SAPO-16), hydrothermal followed by sol-gel process (TiO2/SAPO-35), hydrothermal followed by sodium borohydride method (Pd/SAPO-35).

II.3.1: Synthesis of SAPO-35 in non-aqueous media using promoters:

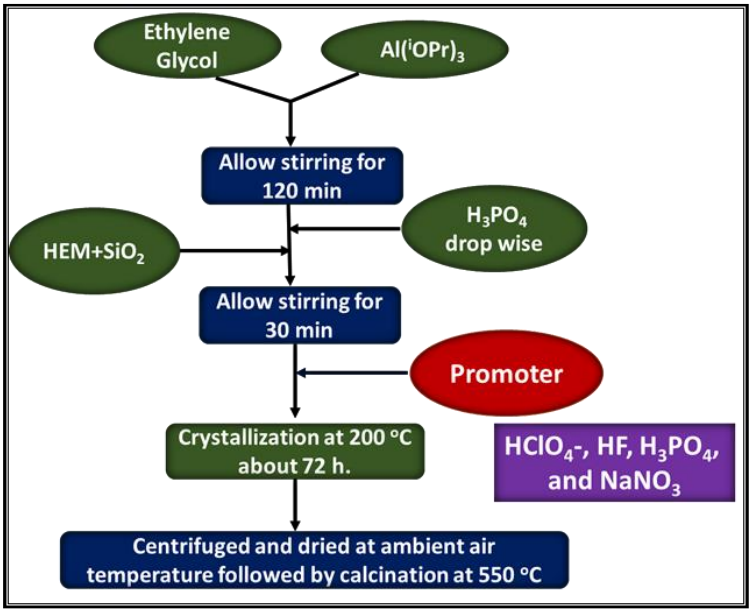

Figure 1. Synthesis of SAPO-35 in non-aqueous media using promoters

II.3.2: Synthesis of SAPO-16 in non-aqueous media using microwave oven:

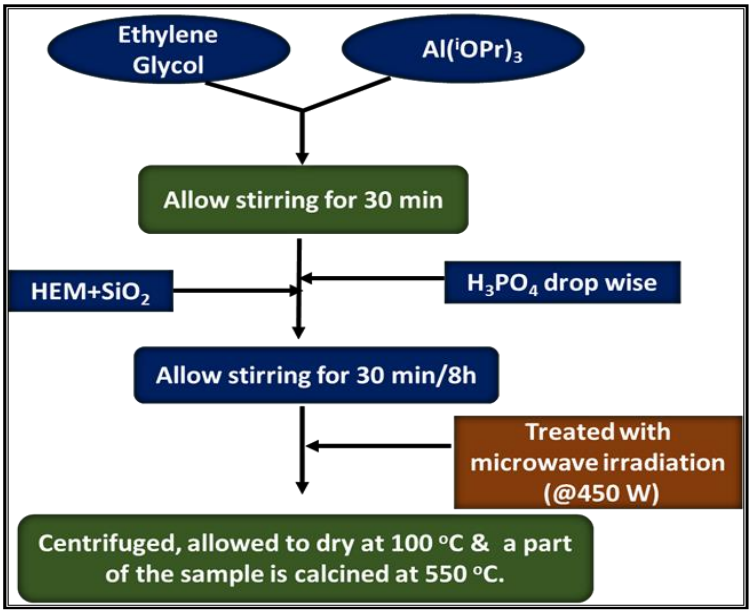

Figure 2. Synthesis of SAPO-35 in non-aqueous media using promoters

II.3.3: Synthesis of Ti/SAPO-35:

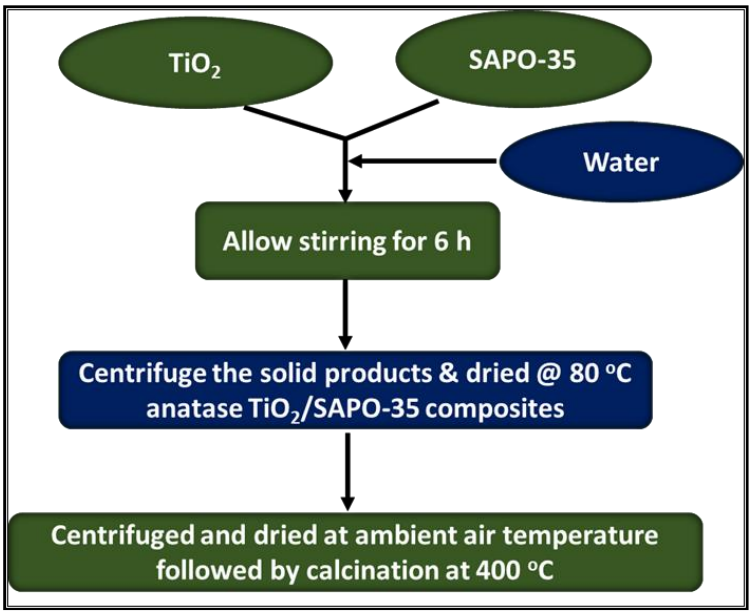

Figure 3. Synthesis of Ti/SAPO-35 by sol-gel method

II.3.4: Synthesis of Pd/SAPO-35:

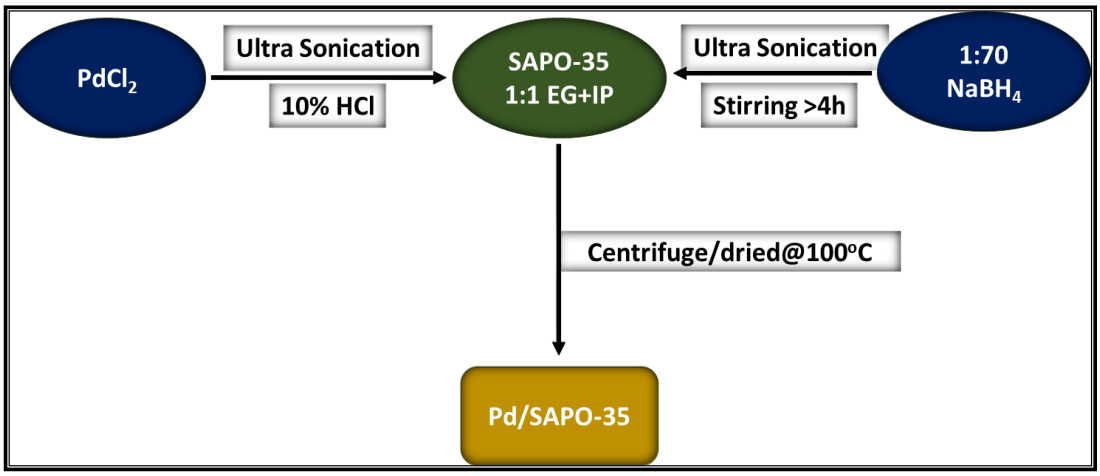

Figure 4. Synthesis of Pd/SAPO-35

II.4. Characterization of the materials

The use of following analytical techniques characterized the materials synthesized:

- Powder X-ray diffraction studies (PXRD) method for pore structure, crystallinity and phase identification
- SEM studies for morphological features
- TEM analysis for particle size and shape analysis
- Energy dispersive analysis of X-ray (EDAX) for determining elemental composition

- Thermogravimetric-differential thermal analysis (TG-DTA) for thermal behavior of as-synthesized samples
- NH_3-TPD for surface acidity.
- Brunauer, Emmett, Teller surface area analysis (BET) for surface area and pore characteristics
- FT-IR for identifying functional groups in the material framework
- UV-Vis DRS for determining metal ions coordination in functionalized materials
- XPS for surface elemental composition and binding energies of elements in the framework of the materials.
- GC to separate and analyze compounds that can undergo vaporization without decomposition.
- MAS-NMR to identify the local environment in structural framework

II.4.1 X-Ray diffraction (XRD)

XRD is among the most crucial non-destructive analytical techniques for the quantitative and qualitative solid phase analysis providing data on crystal structure and particle size of various stable compounds [1-3]. Besides, identification of the material structure, phase composition, structural arrangement of pores, phase purity, unit cell parameters, degree of crystallinity, phase transition, lattice constants, and foreign atoms existence in the crystalline lattice can also be obtained [4].

This method involves diffraction of incident X-ray beam (like Mo-Kα or Cu-Kα) by the crystal at various specific angles. This diffraction depends on X-ray wavelength, the orientation of the crystal lattice, and its structure [5, 6] and is a result of electron density. Thus, analysis of the diffraction angles gives the crystal's electron density map [7, 8].

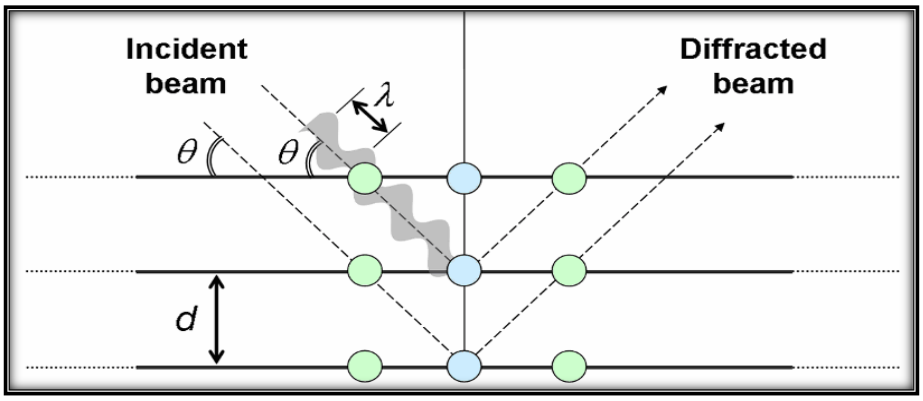

Figure 5. Bragg's Law for X-ray diffraction.

An X-ray diffractometer contains X-ray tubes that produce X-rays by the bombardment of a metal (commonly Cu and Mo) with electrons of 10-100 keV energy resulting in knocking electrons out present in the core. In this process, outer shell electrons fill the place created inner shell emitting X-ray in the process [9].

XRD principle is explained in Fig. 5 that depicts the diffraction of monochromatic X-rays of a specific wavelength (λ) from parallel crystal planes, with an incident angle θ among the plane and direction of the beam.

Diffraction of X-rays can be explained by the Bragg equation (Eqn. 2.1):

$$n\lambda = 2dsin\theta \quad (2.1)$$

Where,

n -order of the reflection

λ -wavelength

d -the distance between planes

θ -the angle between perpendicular of the wave and the reflection perpendicular.

Thus, θ and d define the intensity of the beam, which is diffracted. Distance between different planes of the crystal can be determined by measurement of diffraction intensity to varying values of 2θ. A typical diffractogram is a plot of reflected intensities against the detector angle 2θ [10].

Phase identification is also an application of XRD that can be done by comparing specimens set of reflections to that of pure reference phase or with a database, powder diffraction file (PDF) [11].

Rigaku Corporation X-ray Diffractometer Ultima-IV, Japan using Ni-filtered Cu-Ka radiation source (l = 1.5406 °A) with a 2θ scan range of 0.7–60° at 40 kV and 30 mA is used to carry out powder X-ray diffraction analysis of the samples.

II.4.2. Scanning electron microscopy (SEM)

Scanning electron microscope (SEM), another non-destructive method, employs a focused beam of electrons of high energy (typically 40 Kev) for the generation of signals at solid specimen surface, which is collected to form an image that helps to analyze sample surface. (Fig. 6). A 2D image is created from the collected data displaying spatial variation in the specified properties [12].

II.4.2.1. Principles of scanning electron microscopy (SEM)

SEM utilizes signals generated from the interaction of incident electrons of high kinetic energy electrons with the sample at various depths. The signals are of various types

like secondary electrons, diffracted backscattered electrons (help in the determination of crystal structures and orientations of minerals), backscattered electrons, heat, photons, and visible light (cathodic luminescence–CL). Secondary and backscattered electrons are used for sample imaging. Secondary electrons show sample topography and morphology, whereas backscattered electrons illustrate composition contrasts in multiphased samples.

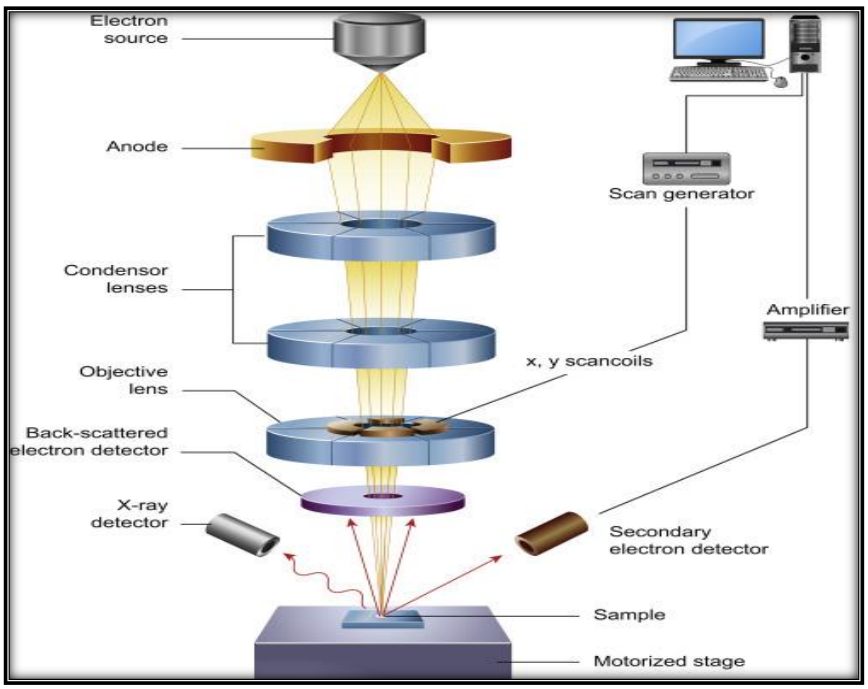

Figure. 6. *Components of SEM*

II.4.2.2. Sample preparation

Sample nature and the data required determine the sample preparation procedure that either is elaborate or simple. In general, a sample is filled into the SEM chamber with some arrangements for the prevention of charge build-up for electrically insulating samples. A coating of a thin layer of electrically insulating material like gold, carbon, or any other metal or alloy is applied for such materials. For elemental analysis, carbon is desirable, whereas metal is used for high-resolution electron imaging. JEM-2100F, JEOL, and also analyzed by TESCAN VEGA 3 LMU scanning electron microscope (SEM) operating at 10–20 kV was used for recording scanning electron micrograms of the catalysts selected.

II.4.3. Transmission electron microscopy (TEM)

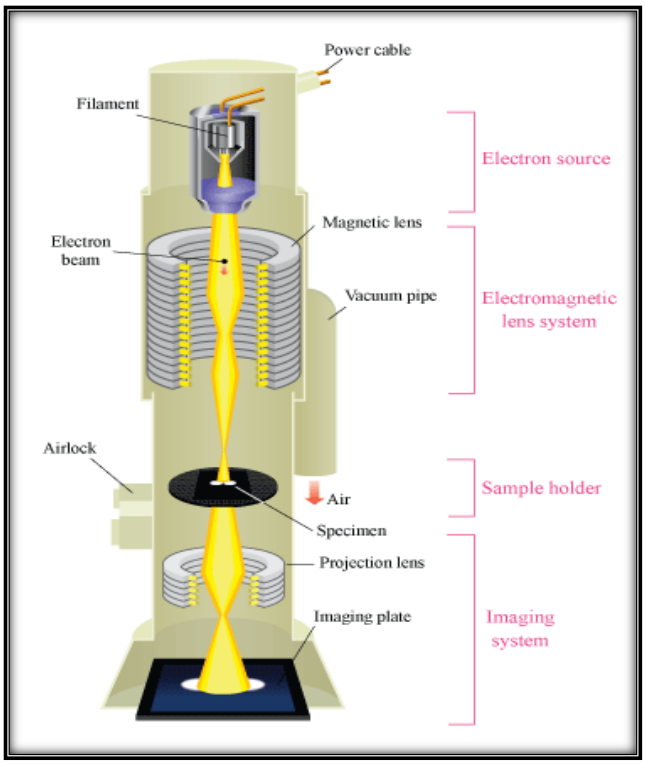

Figure 7. Schematic diagram of the core components of a TEM microscope

Transmission electron microscopy **(**TEM) is employed for mesoporous materials visualization that reveals the sample's internal components in the generated bright-field images. The images generated are black and white as the electrons generate an image. Also, a fragile sample must be required for the image to be of high quality. Thus sample preparation becomes a crucial step for the achievement of such images [13]. Since it operates under conditions of high-vacuum, TEM has excellent resolving power and a higher magnification range than the light microscope (Fig. 7). TEM recorded using JEOL JEM-2100 EM armed with a slow-scan charge-coupled device camera.

II.4.4. Energy-dispersive X-ray analysis

Energy-dispersive X-ray analysis (EDX) is a quantitative and qualitative micro-chemical technique of analysis that is used in determining the surface elemental composition of a sample. EDX, in conjunction with TEM and SEM, provides information regarding elemental analysis of a sample and elemental spatial distribution through mapping. It works on the principle of interaction of the sample with a high energy beam of charged particles such as protons, electrons, or a beam of X-rays. Secondary electron emission from atom occurs when a voltage of 10 - 20 keV is used in SEM that results in the creation of hole that is again taken place by the electron of higher energy level emitting

X-ray in this process with an energy equal to the difference in energies of high and lower energy shell. The X-ray is characteristic of the atom from which it is derived. Thus each element's image in the sample is taken by scanning of the electron beam. Whereas X-rays characteristic to the sample help in the identification and determination of different elements in the sample. EDAX spectra of the samples described in this thesis were generated on a TESCAN VEGA 3 LMU instrument. Powder samples were directly used for EDAX analysis on the sample-holder for the measurement [14].

II.4.5. Thermo Gravimetric-Differential thermal analysis (TG-DTA)

A substance on heating undergoes mechanical, chemical, or physical changes. Thermogravimetry is termed as a gain or loss of sample weight. A TGA can be performed by placing a sample pan on a precision balance present in a furnace that undergoes heating or cooling during the experimental process. The sample mass is recorded throughout the process. The environment of the sample is controlled by either an inert or a reactive sample of purge gas flowing over the sample and exiting through the exhaust. Physicochemical changes occur when sample weight varies by the change of temperature or pressure. With this technique, water loss, plasticizer loss, solvent loss, decomposition, oxidation, pyrolysis, decarboxylation, weight % of a filler, and weight % ash can be determined accurately. A microbalance measures the weight change of the sample on the heating or cooling cycle.

DTA is a dynamic method that evaluates the change in energy (heat) corresponding to chemical or physical transformations that takes place in a substance on subjection to programmed heating or cooling accompanied by a reference material that is thermally inert like alumina thereby measuring the difference in temperature between them [15]. DTA analysis provides information about thermal events such as phase changes or decomposition of the compound. This can be recorded as either temperature change or energy against time change.

The TG-DTA analysis is carried out by weighing the sample around 10-15 mg on a platinum pan, with a heating rate of 10 K/min from RT to 1073 K in nitrogen/airflow of 10 ml/min on STA 2500 Regulus NETZSCH instrument.

II.4.6. Ammonia Temperature Programmed Desorption (NH_3-TPD)

Surface acidity was measured by the temperature-programmed desorption of ammonia (NH_3-TPD) was analyzed by using (AutoChem 2910, Micromeritics, USA)

instrument. The acidity measured is characterized as three classes: weak (323–373 K), medium (423–473 K), and strong (593–773 K) as per Topsøe et al.'s [16].

II.4.7. Nitrogen adsorption-desorption isotherms

Another analytical method used in the characterization of catalyst is N_2 gas sorption that can help in analyzing the surface area, volume, and size of pores and their distribution. The application of the BET equation can do this. Stephen Brunauer, Paul Emmett, and Edward Teller came up with this theory in 1938. Nitrogen is generally employed for BET surface area analysis. A known amount of N_2 gas is discharged into the sample cell. A partial vacuum is established to maintain relative pressures less than the pressure in the atmosphere. Once saturation pressure is attained, adsorption does not occur further even on the increase of pressure. Highly precise pressure transducers can monitor this pressure change. On the formation of adsorption layers, the sample is removed and heated so that the adsorbed gas is released, which is then quantified. Measuring points were also taken during the desorption process. The adsorption-desorption measuring points on a quantity adsorbed (cm^3/g) versus relative pressure (P/Po) plot is an isotherm, where P is the absolute pressure of the last point and Po is the atmospheric pressure [17,18].

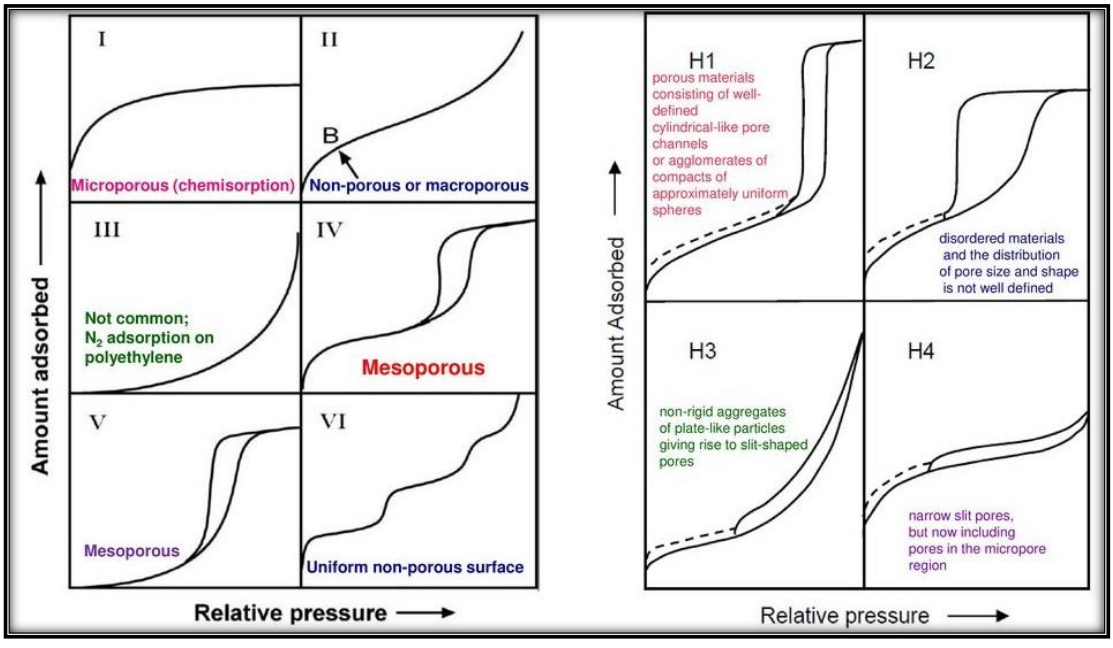

Figure 8. Illustrates different shapes of isotherms and various types of hysteresis loops.

This analytical method is significant owing to its ability to determine molecules number that is needed to form a monolayer of adsorbed gas on the surface of the solid. Multi-layer adsorption by an adsorbent forms the basis of the BET theory. Equation 2.2 is used to determine surface area by this method.

$$\frac{P}{Va(Po-P)} = \frac{1}{VmC} + \frac{(C-1)}{VmC} P/Po \quad (2.2)$$

Where,

P = adsorption equilibrium pressure

Po= saturated vapor pressure of the adsorbate

V_a = adsorbate volume corresponding to equilibrium pressure P

V_m = adsorbate volume required for a monolayer coverage at STP

C is a constant related to the heat of adsorption of adsorbate in first and subsequent layers.

According to the BET method, a plot of P / V_a (Po-P) against P/Po yields a straight line (where P/Po is in the range of $0.05 \leq P / Po \leq 0.35$). Slope ((C – 1)/ V_m C) and Intercept (1/ V_m C) of the plot permits the calculation of V_m. The specific surface area of the catalyst is calculated from Eqn. 2.3.

$$\text{Surface area } (m^2g^{-1}) = \frac{V_m A_m N}{22414 \times W} \text{ -------- (2.3)}$$

Where,

N = Avogadro number

W= sample weight

V_m= volume of gas at STP (2.414 mol^{-1})

A_m= Cross-sectional area of adsorbate gas (16.2 x 10^{-20} m^2 for N_2 at 77K)

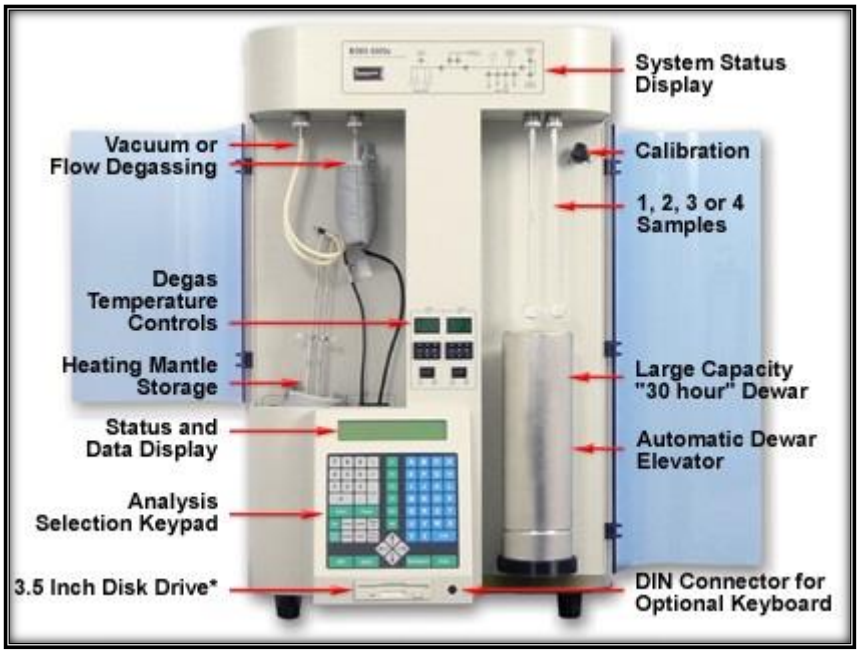

Figure 9. Quantachrome Nova 1000e Surface area and Pore size analyser.

In this work, Quantachrome Nova 1000e Surface area and Pore size analyzer (Fig. 9) was used for the measurement of catalysts surface area by nitrogen adsorption at liquid nitrogen (77 K) temperature.

II.4.8. Fourier transform infrared spectroscopy

A molecule, when subjected to infrared radiations, its atoms either rotate or vibrate in different ways at certain quantized energy levels due to change in its permanent dipole moment. This results in the absorption of some amount of radiation by the sample and transmission of rest. Thus, the spectrum generated is a representation of both absorption and transmission at the molecular level that produces a fingerprint that is unique for each sample. There are different methods for sample preparation in FT-IR. Usually, the powdered catalyst is prepared as a thin pellet by grinding a 2mg catalyst with 200mg KBr for it to be transparent to the IR beam. IR radiation region is divided into three areas, near IR, mid-IR, and far IR [19], of which the middle region extending from 4000 to 400 cm^{-1} is employed for analytical studies.

The atoms in a molecule are never stationary, and a good approximation is to treat them as a combination of point masses held together by Hooke's law of forces. By classical mechanics, it can be shown that the displacements of the masses from their mean positions are always the sum of the displacements due to a particular set of vibrations [20]. If in these set of vibrations, the masses are in phase and the motion of all the nuclei involved are such that the center of gravity of the molecule remains unaltered, then such vibrations are known as the fundamental modes of vibration of the molecule. Mostly, a normal mode is localized to a group within the molecule and hence corresponds to stretching or bending of one or few bonds only and hence associated with that particular functional group. Whether for the functional group or the entire molecule, the vibrations are universally classified either as stretching or as bending types. Stretching vibrations, which correspond to the oscillations leading to change in bond lengths, can be further sub-divided into symmetric or asymmetric stretching vibrations. Continuous change in angle between the bonds results in bending vibrations and are further sub-classified as twisting, wagging, scissoring, and rocking. FT-IR recorded within 400–4000 cm^{-1} using a PerkinElmer instrument by mixing the samples with potassium bromide.

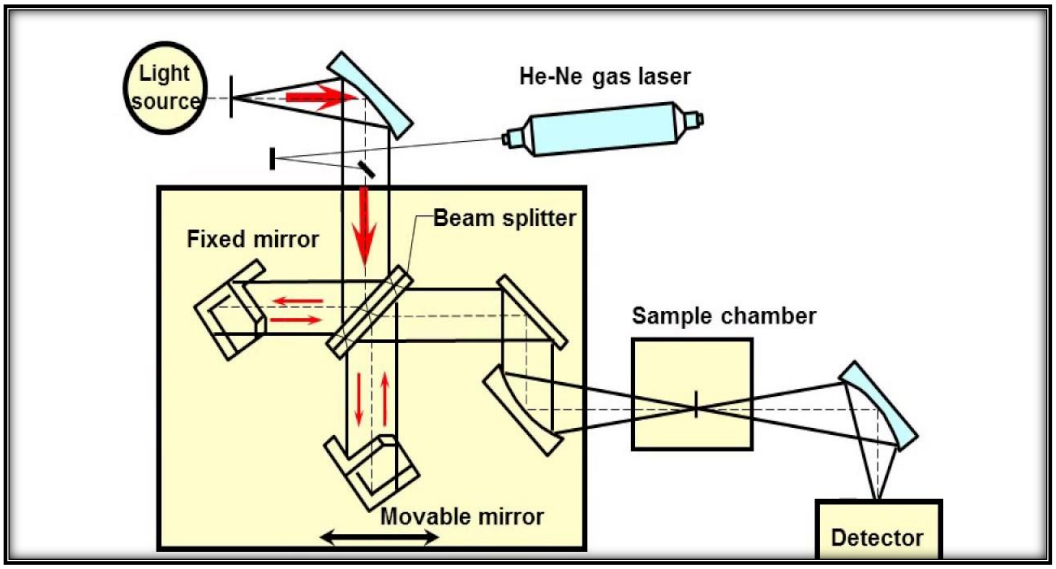

Figure 10. Schematic diagram FTIR principal

II.4.9. UV-Visible spectroscopy

UV-Visible Spectroscopy is a category of absorption spectroscopy wherein absorption of light in the ultra-violet region (200-400 nm.) by the molecule results in its electrons getting excited from the ground state to a higher energy state. Since light is an energy form, absorbance of the same leads to enhancement in the energy content of the molecules or atoms. Summation of vibrational, electrical and potential energies give the total potential energy of a molecule:

$$E_{total} = \text{Electronic} + \text{Evibrational} + \text{Erotational} \text{ ---------- } (2.4)$$

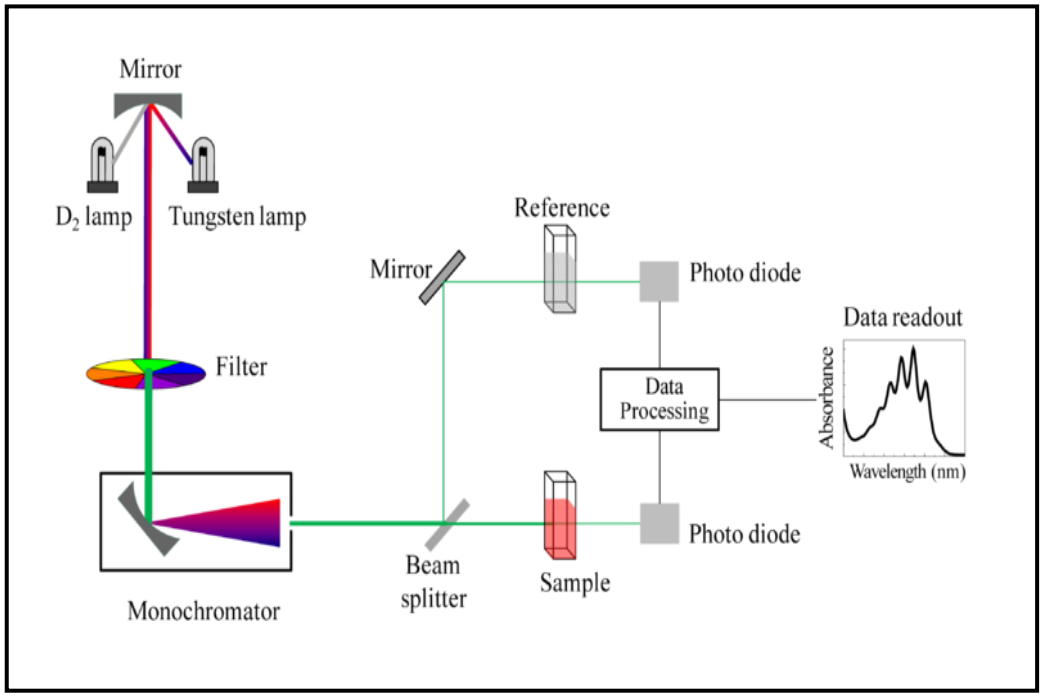

Figure 11. Schematic diagram of UV-Visible Spectroscopy

Transitions occur between different electronic levels in some atoms and molecules brought about by photons of UV and visible light. The highest occupied molecular orbital (HOMO) to the lowest unoccupied molecular orbital (LUMO) transition is the general transition that results in a molecule getting termed as excited speciesv [21,22]. LOMO is s orbitals in almost all the molecules that correspond to sigma bonds, whereas HOMO is p orbitals that are present at higher energy levels. The electron pairs that are unshared in nonbonding orbitals are present between lower and higher energy levels. The possible transitions can involve different orbitals (i.e., σ, π, n, σ* and π*) arising in different electronic transitions namely σ → σ*, n → σ*, n → π* and π → π* [23]. The transition to the first excited state associated with the HOMO to LUMO excitation is normally characterized by having low energy and high intensity.

II.4.9.1. Principle of UV spectroscopy UV spectroscopy

UV spectroscopy principle lies in obeying Beer-Lambert law, specifying that when an absorbing substance solution is made to pass a beam of monochromatic light, loss of radiation intensity with the absorbing solution's thickness is proportional to the incident radiation and solution concentration; the expression of which can be explained as:

$$A = \log(\frac{Io}{I}) = \epsilon cl \quad (2.5)$$

Where,

A = absorbance

I_0 = intensity of incident light

I = intensity of transmitted light

ϵ = molar absorptivity

C =conc. term

l = length of the sample holder (cm.)

Studies on catalytic degradation of dyes presented in this thesis were carried out by using Analytikjena Specord D 205 UV-Visible spectrophotometer [24].

II.4.10. UV-Visible diffuse reflectance spectroscopy

This is a non-destructive technique providing data on materials structure and composition [25]. It is a highly responsive and robust technique for identifying and characterizing metal ion's co-ordination and location in metal-containing robust catalysts framework [26-28]. Powdered samples UV–Visible spectra can be obtained directly through this method. This technique is apt for studying the electronic and optical properties of powders, films, pigments, etc. -In this method, when radiation interacts with samples,

absorption and scattering take place, giving rise to a reflectance spectrum due to the electronic excitation. Electronic excitations can be categorized into two d-d transitions and charge transfer transitions. The former reveals samples state of oxidation and co-ordination environment, whereas the latter are sensitive to the nature of donor and acceptor atoms. The following equation gives the percentage of reflectance:

$$Reflectance\ \% = \frac{I_s}{I_r} \times 100 \text{ --------- (2.6)}$$

Where

I_s reflected beam's intensity and

I_r is the reference standard's intensity (usually barium sulfate).

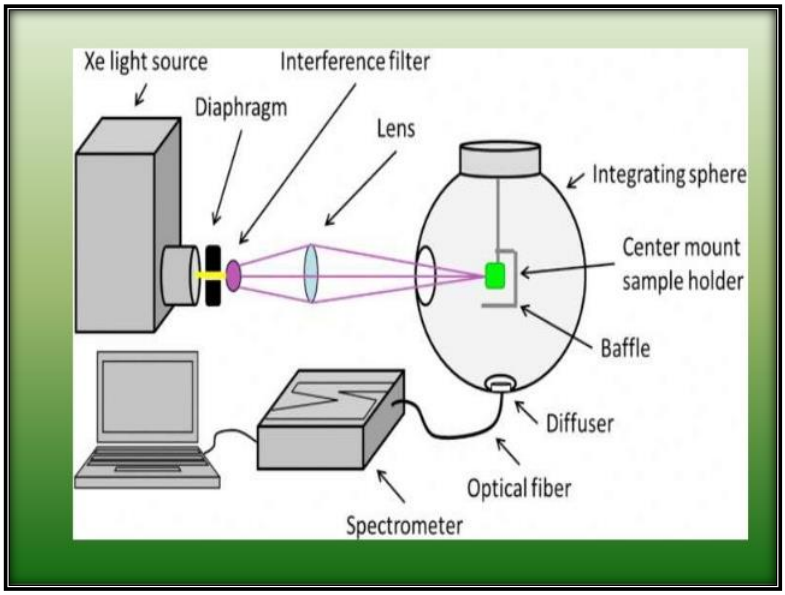

Figure 12. *Schematic representation of UV-Visible diffuse reflectance spectroscopy*

II.4.11. X-ray photoelectron spectroscopy

X-ray photoelectron spectroscopy (XPS), works on photoelectric effect for exploring elemental compositions of the surface, not limited to physical properties. The process of analysis consists of excitation of X-ray source excites to an area of 1 cm^2 and depth of about 1μm; this entire volume emits electrons. It is generally operated high vacuum (10-10 mbar pressure range). Equation (2.7) is employed to measure the kinetic energy of the electrons ejected [29] wherein hυ is the energy of photon absorbed by an atom resulting in valence electron of binding energy Eb ejection.

$$Ek = h\upsilon - Eb \text{ ---------- } 2.7$$

The spectrum generated is a plot of photoelectrons intensity, N (E) as a function of their kinetic energy Ek, vs. binding energy Eb. The labeling of peaks of the photoelectron is based on quantum numbers of electrons. For every orbital momentum l > 0, there are two

values of the total momentum: j = l + ½ and j = l – ½, each state filled with 2j + 1 electrons. This results in doubling of peaks with components intensity ratio as (l + 1)/l. 1+s subscript is omitted in cases of too small doublet split (Si 2p, Cl 2p, Al 2p). Apart from surface composition and oxidation states study, XPS has also been employed for yielding information on supported catalysts dispersion. The XPS spectra of selected samples were carried out in Thermo Fisher Scientific Theta Probe Spectrometer (East Grinstead, UK).

II.4.12. Solid-state magic angle spinning (MAS) nuclear magnetic resonance (NMR) spectra:

To identify the local environment in structural framework of the synthesized SAPO materials, ^{27}Al, ^{29}Si, and ^{31}P MAS-NMR spectroscopic studies [30,31] were carried out.

Solid-state magic angle spinning (MAS) nuclear magnetic resonance (NMR) spectra of synthesized materials were acquired in a Varian spectrometer bundled with an 8.5 T wide-bore magnet. The resonant frequencies of ^{29}Si, ^{27}Al, and ^{31}P nuclei were 70.958, 93.073 and 144.593 MHz respectively. The experiments were carried at room temperature, with the samples filled into Zirconia rotors of 4 mm diameter. All of the spectra were acquired using a home-built single-resonance 4 mm MAS probe. The ^{29}Si NMR spectra were obtained with a π/4 pulse width of 2 μs at a MAS frequency of 6 kHz; and a total of 12 k transients were acquired with a relaxation delay of 30 s. The ^{27}Al MAS NMR spectra were acquired using a π/2 pulse width of 2 μs at a spinning rate of 7 kHz; and a sum of 10 k scans were recorded with a relaxation delay of 1 s. The ^{31}P MAS NMR spectra were obtained with a π/2 pulse width of 8.5 μs at a spinning speed of 6 kHz; and a total of 1024 scans were acquired with a relaxation delay of 10 s. The ^{29}Si, ^{27}Al, and ^{31}P spectral components were referenced to tetramethylsilane (TMS) at 0 ppm, aluminum nitrate in D_2O at 0 ppm, and 85% *ortho*-phosphoric acid at 0 ppm. The data were processed using a Tecmag NTNMR software.

II.4.13. Cyclic voltammetry (CV)

Cyclic voltammetry (CV) is a versatile electroanalytical technique for the study of electroactive species [32,33]. Electrochemical measurements were carried out using CHI 619d (CH International, USA) electrochemical analyzer and All electrochemical measurements were carried out at room temperature of ca. 25 °C.

II.4.14. Product analysis

The Catalytic reaction product mixture is analyzed using Gas chromatograph, Model YL 6500 instrument from YL Instrument Co., Ltd, South Korea with a flame ionization

detector (FID) and a capillary column (TR-WAX, column length: 30 m; internal diameter: 0.53mmand thickness 1 μ). The Rhodamine B degraded products are analyzed by LC-ESI-MS (Waters 2695 Separation Module- ZORBAX Eclipse XDB-C18).

II.5. References

[1] W.H. Bragg, W.L. Bragg, Mc Millan, New York 1 (1949).

[2] S. Biz, M.L. Occelli, Catal. Rev.-Sci. Eng., 40 (1998) 329.

[3] B.K. Hodnett, John Wiley & Sons, New York, USA (2000).

[4] Antonelli D. M., Ying J. Y., Angew. Chem. Int. Ed. Engl. 1995, 34, 315.

[5] Cullity, B. D., Addison-Wesley Publishing Comp. Inc., USA, 1978.

[6] Xu, R.; Pand, W.; Yu, J.; Huo, Q.; Chen, J., 2nd Edition, Wiley-Interscience Publication, New York, 2007.

[7] Ladd, M. F. C.; Palmer, R. A., New York, 1994.

[8] Tanabe, K.; Misono, M.; Ono, Y.; Hattori, H., Kodansha/Elsevier, Tokyo/New York, 1989.

[9] Bergeret, G.; Gallezot, P., Plenum Press, New York, 1994.

[10] P. Gallezot, X-ray Techniques in Catalysis, in J.R. Anderson, M. Boudart (eds.), Springer-Verlag, Berlin, 5 (1984) 224.

[11] Brunauer, S.; Emmett, P. H.; Teller, E. J. Am. Chem. Soc. 1938, 60, 309.

[12] J.I. Goldstein, H. Yakowitz (Eds.), Plenum Press, New York, (1975).

[13] Fultz, B. Transmission electron microscopy and diffraction of materials, Springer, 2001.

[14] Goldstein J. I.; Newbury D. E.; Echlin P.; Joy D. C.; Fiori C.; Lifshin E., Springer, 3rd corrected edition, 2007.

[15] X. Gao, I.E. Wachs, J. Phys. Chem. B 104 (2000) 1261.

[16] Topsøe, N.-Y., Pedersen, K. & Derouane, E. G., J. Catal. 70, 41–52 (1981)

[17] Langmuir, I. J. Am. Chem. Soc. 1916, 38, 2221.

[18] Barrett, E. P.; Joyner, L. G.; Halenda, P. P. J. Am. Chem. Soc., 1951, 73, 373.

[19] The International Centre for Diffraction Data, 12 Campus Boulevard, Newton Square, PA 19073-3273, U.S.A.

[20] Ikeya, M (1993). New Applications of Electron Spin Resonance.

[21] S. Lacombe, H. Cardy, N. Soggiu, S. Blanc, J.L. Habib-Jiwan, J.Ph. Soumillion, Micropor. Mesopor. Mater. 46 (2001) 311.

[22] E.H. Catherine, G.S. Alan, Inorganic chemistry, 2nd Edn., Pearson Education, Prentice Hall, England, (2005).

[23] C.N. Banwell, Fundamentals of Molecular Spectroscopy Tata McGraw-Hill Pub. Co. Ltd. New Delhi (1979).

[24] B.M. Weckhuysen, R.A. Schoonheydt, Catal. Today 49 (1999) 441.

[25] G. Kortum, Springer-Verlag, Berlin, (1969).

[26] W.N. Delgass, G.L. Haller, R. Kellerman, J.H. Lunsford, Academic Press, New York (1979).

[27] Briggs, A.; Seah, M. P. Practical Surface Analysis, 2nd ed.; Vol. 1, Wiley, New York, 1990.

[28] Neimansstuedriet, J. W., Wiley-VCH Verlag, GmbH & Co, KgaA, 2007.

[29] Klinowski, J. Chem. Rev. 1991, 91 (7), 1459–1479.

[30] N. Elgrishi, K.J. Rountree, B.D. McCarthy, E.S. Rountree, T.T. Eisenhart, J.L. Dempsey, J. Chem. Educ. 95 (2018) 197–206.

[31] P. Chooto, in: Voltammetry, IntechOpen, 2019.

[32] Klinowski, J.; Anderson, M. W. Magn. Reson. Chem. 1990, 28 (13), S68–S81.

[33] Topsøe, N.-Y., Pedersen, K. & Derouane, E. G., J. Catal. 70, 41–52 (1981).

CHAPTER-III

Investigation on the Promoter-Induced Rapid Non-Aqueous Media Synthesis of SAPO-35 and Methanol-to-Olefin Reaction

Chapter-III

Investigation on the Promoter-Induced Rapid Non-Aqueous Media Synthesis of SAPO-35 and Methanol-to-Olefin Reaction

III.1. Introduction

The molecular sieves AlPOs and SAPOs are ordered porous materials and they were synthesized three decades ago[1–3] and their basic structural framework resembles certain zeolite materials for example SAPO-35 (Levyne structure)[4,5]. Contrarily, there are several other AlPOs and SAPOs reported in the literature whose structural framework doesnot resemble any zeolite material. Basically the AlPOs are neutral in nature, hence they provide no catalytic activity[6,7]. However, by introducing Silicon in to the AlPO framework makes them acidic (SAPO) in nature and hence catalytic activity can be attained [8,9]. These SAPOs possesses certain unique catalytic properties[10], for instance adsorption[11], separation[12], ion-exchange[13]. Moreover, these materials are highly stable thermally as well as chemically. There are at least two hundred different topologies of these molecular sieves have been reported in the literature so far and more studies are carrying out currently across the globe [14,15]. By virtue of its unique properties, these materials have got considerable attention from the researchers around the world.

Conventional synthesis of molecular sieves mainly involves trial and error of variation in the synthesis parameters. However, the necessity in the synthesis of molecular sieves with desired structural framework and properties has created the need to develop new synthesis methods. These synthesis methods were constructed mainly on the understanding of the mechanism of crystallization process. The new synthesis methods are hydrothermal, solvo-thermal, microwave assisted and sol-gel etc[16,17]. Among all these methods available, hydrothermal method is the most convenient process to synthesize the molecular sieves with desired morphological framework structures. This can be achieved due to the higher temperatures and autogenous pressure involve in the synthesis process.

Although the hydrothermal method is accurate in achieving the desired morphological frameworks, but the crystallization time is very much high. This makes it less feasible in the commercial synthesis of SAPOs. This limitation in hydrothermal method can be overcome by using different types of promoters[18] for example, $HClO_4^-$ and H_3PO_4.

SAPO-35 is a LEV (Levyne) type topological framework microporous material with 0.36 x 0.48 nm ring opening pore which is constructed by a single six membered ring

(S6R) and a double six membered ring (D6R) with different T sites in a 2:1 ratio respectively[19,20]. It was synthesized using Quinuclidine, Cyclohexyleamine, and Hexamethyleneimine as the structure directing agents (SDA) for the crystallization of SAPO-35 at 200 °C reaction temperature in aqueous media[4,21]. A very recent study revealed that SAPO-35 molecular sieve has been synthesized in a non-aqueous medium (ethylene glycol) using hexamethyleneimine as SDA at 200 °C temperature about 360 h as the crystallization time[22]. This non-aqueous media samples showed better crystalline nature as compared to the aqueous samples. The only drawback was it consumed more time.

MTO reaction is one of the most important reactions for the production of petrochemicals[23–26]. The catalytic conversion of MTO is one of the promising ways of converting natural gas and coal to chemicals. This MTO reaction was first proposed by Mobil Corporation in 1977. The methanol to olefin reaction is an acid catalysed reaction. Researchers widely studied this MTO reaction with different zeolites, Si incorporated molecular sieves, from these studies it was found that SAPO-34, SAPO-35 and HZSM-5 are better catalysts for the conversion of methanol-to olefins[25,27,28].

Hence, in the present study we have demonstrated the synthesis of SAPO-35 microporous molecular sieves in a non-aqueous medium through conventional hydrothermal process by adding small amounts of inorganic promoters such as $HClO_4^-$, HF, H_3PO_4, and $NaNO_3$ in order to enhance the crystallization process such that the crystallization time is reduced. The as-synthesized SAPO-35 molecular sieves from the above method were used as catalysts in the methanol-to-olefins (MTO) reaction as an application study. Moreover, we also have compared the MTO activity of conventional 360 h SAPO-35 sample with promoter used SAPO-35 samples.

III.2. Experimental Section

III.2.1 Synthesis

Aluminium isopropoxide ($Al(OCH_3H_7)_3$) as Al source, 98% purity, Sigma Aldrich, USA, Orthophosphoric acid (H_3PO_4), as the P source, 85% purity, S.D. Fine India, Fumed Silica (SiO_2) as the Si source, 99.8% purity, Sigma Aldrich, USA, Hexamethyleneimine ($C_6H_{12}NH$) as the structure directing agent 98% purity, Sigma Aldrich, USA materials are used for the synthesis without any further purification.

Table 1. Synthesis Conditions of SAPO-35

S. No.	Gel composition	Crystallization conditions	Product
1	Al_2O_3: 1.8 P_2O_5:4.9HEM: SiO_2: 49EG	360h, 200°C	SAPO-35
2	Al_2O_3: 1.8 P_2O_5:4.9HEM: SiO_2: 49EG:0.9-1.3 $HClO_4^-$	72h, 200°C	SAPO-35
3	Al_2O_3: 1.8 P_2O_5:4.9HEM: SiO_2: 49EG:1.8 $HClO_4^-$	54h, 200°C	Semi crystalline SAPO-35
4	Al_2O_3: 1.8 P_2O_5:4.9HEM: SiO_2: 49EG:1.8 $HClO_4^-$	60h, 200°C	Semi crystalline SAPO-35
5	Al_2O_3: 1.8 P_2O_5:4.9HEM: SiO_2: 49EG:0.9-1.3 $HClO_4^-$	48h, 200°C	Amorphous
6	Al_2O_3: 1.8 P_2O_5:4.9HEM: SiO_2: 49EG:0.9-1.3 $NaNO_3$	168h, 200°C	SAPO-35
7	Al_2O_3: 1.8 P_2O_5:4.9HEM: SiO_2: 49EG:0.9-1.3 HF	90h, 200°C	SAPO-35
8	Al_2O_3: 1.8 P_2O_5:4.9HEM: SiO_2: 49EG:0.9-1.3 H_3PO_4	120h, 200°C	SAPO-35
9	Al_2O_3: 1.8 P_2O_5:4.9HEM: SiO_2: 49EG:0.9-1.3 NH_4Cl	168h, 200°C	SAPO-35 with impurity phases
10	Al_2O_3: 1.8 P_2O_5:4.9HEM: SiO_2: 49EG:0.9-1.3 KOH/NaOH	168h, 200°C	Amorphous

The typical synthesis of SAPO-35 using non-aqueous media is as follows. 6.05 g of Aluminium isopropoxide and 45.5 g of ethylene glycol was taken into a clean beaker and mixed it until the solution becoming into a homogeneous solution which is approximately 2 h. 6.024 g of H_3PO_4 was added dropwise to the above solution under constant stirring condition. In another clean beaker 7.27 g of Hexamethyleneimine, 0.526 g of fumed silica taken and stirred to make it homogeneous. Further, this mixture was added to the initial gel solution and the gel ratio is Al_2O_3: 1.8 P_2O_5:4.9HEM: SiO_2: 49EG. For the standard SAPO-35 the above gel was transferred in to a Teflon lined 100 cm^3 stainless steel autoclave and programmed at 200 °C with the ramp rate of 5 °C per minute about 360 h. After the heat treatment, the resulting products were then centrifuged, washed with distilled water and dried at 80 °C about overnight. The sample was further calcined

at 550 °C in ambient atmosphere for 8 h to remove the unreacted reactant species present in the framework. Here the reaction time for the crystallization was 360 h which is very high. Therefore, to overcome this, small amounts of inorganic promoters were added to accelerate the crystallization process. For promoter used SAPO-35 samples, after addition of fumed silica and Hexamethyleneimine appropriate amounts of promoter (table. 1) was added to the gel and allowed further stirring about 2 h and subjected to crystallization at 200 °C. The reaction conditions and promoters used for synthesis SAPO-35 in a non-aqueous media are given in the Table 1.

III.2.2. Characterization

The crystalline nature and purity of all the samples were determined by powder X-ray diffraction (PXRD) on a PANalytical X´Pert diffractometer at room temperature, with a monochromated Ni filtered Cu Kα (λ = 1.5406 Å). The X-ray scan range of 2θ was from 6^o to 50^o. Morphology of the synthesized samples were analysed by JEOL JSM-6300 scanning electron microscope (SEM). To identify the framework structure, FT-IR spectra was recorded by Perkin Elmer Spectrum using KBr pellet technique in the range of 400 to 4000 cm^{-1}. Solid-state magic angle spinning (MAS) nuclear magnetic resonance (NMR) spectra of synthesized materials were acquired in a Varian spectrometer bundled with an 8.5 T wide-bore magnet. The resonant frequencies of ^{29}Si, ^{27}Al, and ^{31}P nuclei were 70.958, 93.073 and 144.593 MHz respectively. The experiments were carried at room temperature, with the samples filled into Zirconia rotors of 4 mm diameter. All of the spectra were acquired using a home-built single-resonance 4 mm MAS probe. The ^{29}Si NMR spectra were obtained with a π/4 pulse width of 2 *μs* at a MAS frequency of 6 kHz; and a total of 12 k transients were acquired with a relaxation delay of 30 s. The ^{27}Al MAS NMR spectra were acquired using a π/2 pulse width of 2 *μs* at a spinning rate of 7 kHz; and a sum of 10 k scans were recorded with a relaxation delay of 1 s. The ^{31}P MAS NMR spectra were obtained with a π/2 pulse width of 8.5 *μs* at a spinning speed of 6 kHz; and a total of 1024 scans were acquired with a relaxation delay of 10 s. The ^{29}Si, ^{27}Al, and ^{31}P spectral components were referenced to tetramethylsilane (TMS) at 0 ppm, aluminum nitrate in D_2O at 0 ppm, and 85% *ortho*-phosphoric acid at 0 ppm. The data were processed using a Tecmag NTNMR software. The X-ray photoelectron spectroscopic (XPS) analysis of synthesized materials was performed using Kratos Axis Ultra DLD spectrometer with a monochromatic Al K_α (1486.6 eV) radiation source at a power of 150 W (15 kV×10 mA). A 3×3 mm area of powder sample was sputtered with Ar ion beam (4 kV) to remove

adventitious surficial carbon prior to XPS. The wide scan survey spectra were acquired at a pass energy of 20 eV with the neutralizer turned on. The compositional analysis was analyzed with CasaXPS software using Shirley background and Gaussian-Lorentzian peak fitting routine with standard relative sensitivity factors.

III.2.3. Catalytic application study

To know the ability of catalyst, we have performed methanol to olefins (MTO) conversion under atmospheric pressure at 350 °C. The process is as follows, 1 g of calcined SAPO-35 catalyst along with 15 g of silicon carbide was taken in a stainless steel reactor with an internal diameter of 3 cm and with a length of 60 cm. This reactor was placed in a tubular furnace and pre-heated to a temperature of 550 °C for 1 h in order to remove any moisture content in the catalyst. Simultaneously the catalyst was also purged with N_2 gas with a flow rate of 150 mL/min. After the pre-heating process, the temperature was reduced to 350 °C, at this temperature the reactor was flown with 30 % methanol water mixture with a 6.5 h^{-1} weight hourly space velocity (WHSV). The resulting gas products (effluent gas) were analysed using a gas chromatography (Thermo-scientific 1101) and the column used was GRS-1, Dimethylpolysiloxane. The GC oven initial temperature was 40 °C, then the temperature was ramped at 5 °C min^{-1} to 210 °C. The detector temperature was 300 °C when during the analysis time. The yield percentage was calculated using an Equation. 1

$$Y_p = \frac{mg(out) \times Xp}{m_{MeOH}} \times 100 \quad (1)$$

Where in equation 1. Yp is yield of the product in weight percentage, mg (out) is the is mass flow rate of outlet gas product and x_p is mass fraction of product which were analysed by GC, and m_{MeoH} (in) is mass flow rate of inlet methanol.

The turnover number (TON) and Turnover frequency were calculated using the following formulas.

Turn over number (TON) = Number of moles of reactant converted per hour/ number of moles of active centres present in catalyst

Turn over frequency (TOF) = Turn over number (TON)/ number of seconds present in hour

Turn over number and frequency mention the rate of catalysis per hour and per second.

III.3. Results and Discussion

III.3.1 PXRD analysis

All the synthesized samples were analyzed using PXRD technique to identify nature of the crystallinity. Figure. 1 represents the PXRD patterns of the SAPO and promoter samples, it can be observed from Figure. 1 that, the peaks at 2θ value of 10.9, 13.3, 17.3, 21.9, 26.6, and 31.6° were corresponding miller indices of (0 1 2) (1 1 0) (1 0 4) (0 2 4) (2 2 0) and (1 3 4) planes respectively. As per the literature [JCPDS: 51–0052] it is confirmed that the synthesized SAPO-35 has a Levyne type hexagonal crystalline structure[20,29]. Furthermore, the relative crystallinity of each sample was calculated using the most prominent peak in the corresponding PXRD pattern, which was observer at 2θ value of 21.9° corresponding to (0 2 4) plane. In order to calculate the relative crystallinity of the synthesized samples the relative crystallinity of standard sample prepared at 360 h was taken as 100 %. The equation used for the calculation of relative crystallinity is given below,

$$\text{Relative Crystallinity} = \frac{Area\ under\ the\ curve\ (0\ 2\ 4) plane\ of\ particular\ sample}{Area\ under\ the\ curve\ (0\ 2\ 4) plane\ of\ the\ standard\ sample} \times 100 \quad (2)$$

The average crystallite size of all the synthesized samples was calculated using the equation 3 and results were tabulated in Table 1.

$$\text{Crystallite Size} = \frac{K\lambda}{\beta\ Cos\ \theta} \quad (3)$$

where K is the dimensionless shape factor (0.9), λ is the X-ray wavelength (1.5418 Å), β is the line broadening at half the maximum intensity at the 2θ angle and θ is the Bragg angle.

The relative crystallinity of materials synthesized in presence of $HClO_4^-$ and HF as promoters has shown a similarity with that of standard sample. This indicates that in presence of both the promoters, the crystallinity is considerably good. However, in case of materials synthesized in presence of H_3PO_4, $NaNO_3$ as promoters, the relative crystallinity is slightly less but considerably in a good amount. This reduction in relative crystallinity is may be because of the slower rate of crystallization in SAPO-35 (H_3PO_4, $NaNO_3$ as promoters) compared that of SAPO-35 ($HClO_4^-$ and HF as promoter). The average crystallite size of synthesized SAPO-35 without promoter in non-aqueous medium and aqueous medium was found to be 68 nm This value has increased to 71 nm for synthesized

SAPO-35 in presence of $HClO_4^-$ promoter. The average crystallite size of the remaining synthesized SAPO-35 material with other promoter was found to be in the range of 47-59 nm.

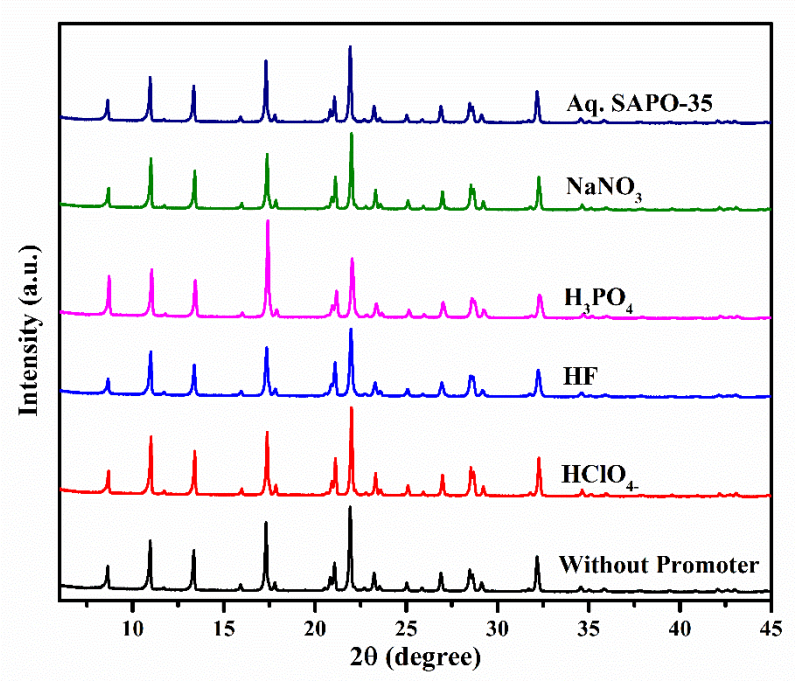

Figure 1. PXRD patterns of Std. SAPO-35, SAPO-35 in case of $HClO_4^-$ as promoter, HF as promoter, H_3PO_4 as promoter, $NaNO_3$ as promoter and aqueous media SAPO-35.

Table 2. Relative crystallinity and Average Crystallite size of the synthesized materials.

S. No.	Sample	Relative Crystallinity (%)	Avg. Crystallite Size (nm)
1	Without Promoter	100	68
2	$HClO_4^-$	99.76	71
3	HF	93.49	59
4	H_3PO_4	83.67	50
5	$NaNO_3$	77.4	47
6	Aq. SAPO-35	89.96	68

III.3.2 SEM analysis

The morphology of all synthesized SAPO-35 materials were observed through SEM. The SEM images as shown in Figure 2 revealed that, all the samples are highly crystalline in nature without any amorphous phase material except in the case of SAPO-35 synthesized using $NaNO_3$ as promoter. When the $NaNo_3$ was used as a promoter, even though the nucleation process in the reaction has occurred rapidly, the consequent

crystallization process might not has happened completely. Therefore, as a result less crystallinity was observed in the $NaNO_3$ promoter case. These SEM results are in good agreement with PXRD results as there is crystallinity nature in the synthesized materials. From SEM images it can be seen that the structure of the crystals is rhombohedral in nature and the size of the crystals was uniform throughout.

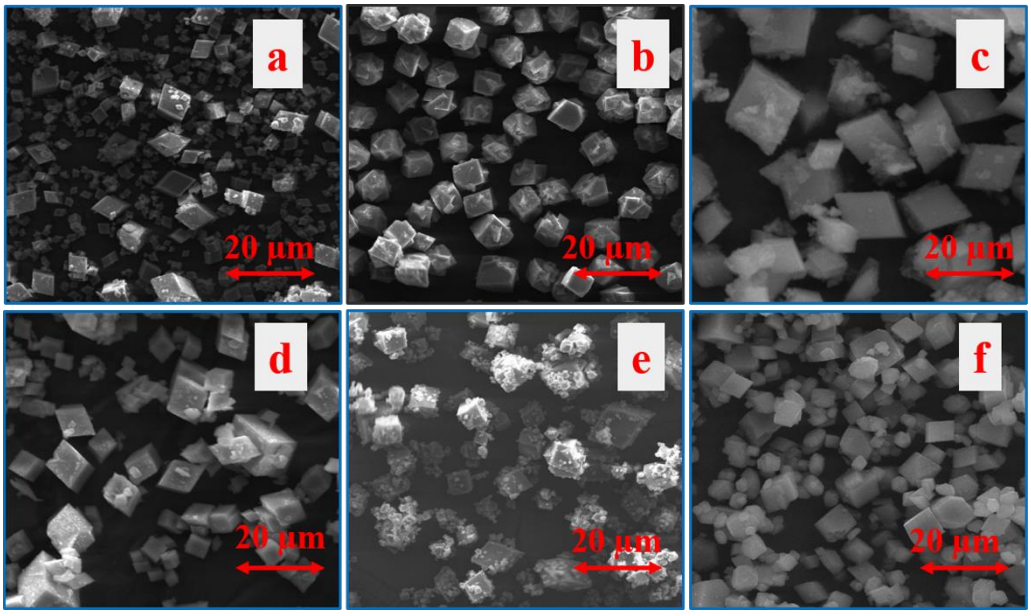

Figure 2. SEM images of a) 360 h without promoter SAPO-35, in presence of b) $HClO_4^-$ c) HF d) H_3PO_4 e) $NaNO_3$ promoters and f) SAPO-35 synthesized in aqueous media.

III.3.3 FT-IR analysis

FT-IR studies were carried out to identify the framework configuration of all SAPO-35 samples. The corresponding FT-IR spectra are illustrated in Figure 3. From these spectra we could infer that the peaks appeared at wave numbers 500, 645 cm^{-1} are corresponding to T–O–T (Where T= Si, Al, and P) symmetric stretching frequency, protonated template respectively. Whereas, the peak appeared at 750 cm^{-1} is due to T–O bending in Double 6-Ring (D6R) and T–O bending of Si tetrahedral structure. Moreover, the peak appeared in the range of 2600-3000 cm^{-1} is a consequence of the stretching frequency of -CH resultant from the organic environment like template and organic functional silane etc. The stretching vibrations around 1600 and 1400 cm^{-1} could be ascribed to physically adsorbed water molecules from the atmospheric air (i.e. H-O-H bending mode). Based on the FT-IR results it appears that the framework structure of SAPO-35 material synthesized using promoters and without using promoters is same.

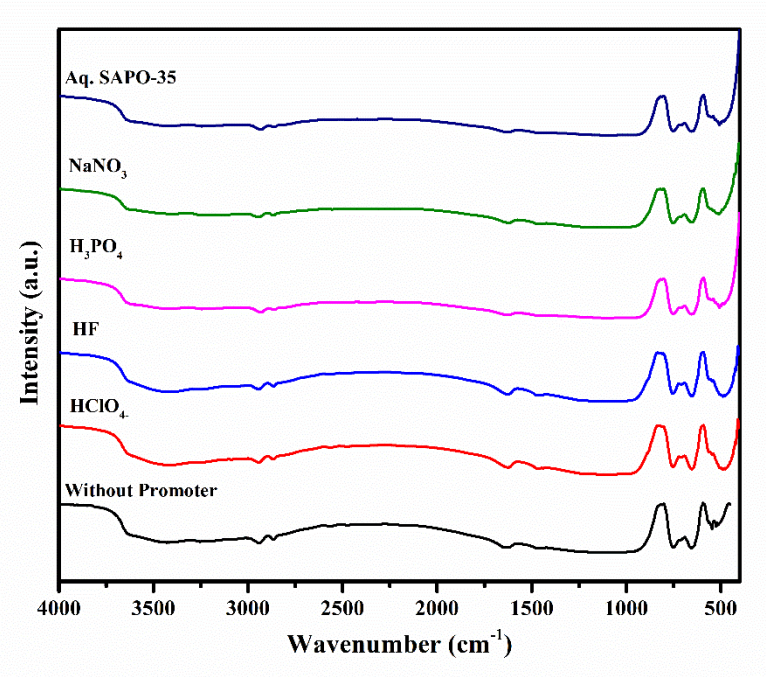

Figure. 3. FT-IR spectra of Std. SAPO-35, SAPO-35 in case of $HClO_4^-$ as promoter, HF as promoter, H_3PO_4 as promoter, $NaNO_3$ as promoter and aqueous media SAPO-35.

III.3.4 MAS-NMR studies

To identify the local environment in structural framework of the synthesized SAPO-35 materials, ^{27}Al, ^{29}Si, and ^{31}P MAS-NMR spectroscopic studies[30,31] were carried out.

The ^{27}Al MAS-NMR spectra of SAPO-35 in all cases are depicted in Figure 4. The spectrum in case of synthesized SAPO-35 without promoter at 360 h, exhibits two peaks at 41.98 ppm (strong) and 13.97 ppm (weak). The strong peak at 41.98 ppm is attributed to the tetrahedral Al $[Al(OP)_4(OH)_2]$ of the SAPO-35 framework and the weak peak at 13.97 is due to the octahedral of unreacted Al source. As SAPO-35 without promoter at 360 h the other using various promoters also exhibiting similar peaks which indicates the formation of SAPO-35 in all the cases.

The incorporation of silicon has been confirmed by the evidence of ^{29}Si MAS-NMR spectroscopic studies. The resulting ^{29}Si MAS-NMR spectra are presented in Figure 5. From the spectrum of the synthesized SAPO-35 material without promoter at 360 h, two peaks at -87.14 ppm and -93.22 ppm can be observed. Appearance of two different peaks emphasizes the incorporation of Si in both single six membered ring $[Si_{T1}(OAl)_4]$ as well as in double six membered ring $[Si_{T1}(OAl)_4]$ of framework[32,33]. From these results, the formation of Levyne type SAPO-35 framework was confirmed. The remaining materials

of SAPO-35 synthesized with promoters have also exhibited identical peaks as that of reference SAPO-35 material at 360 h. This indicated that the successful incorporation of silicon in to the framework.

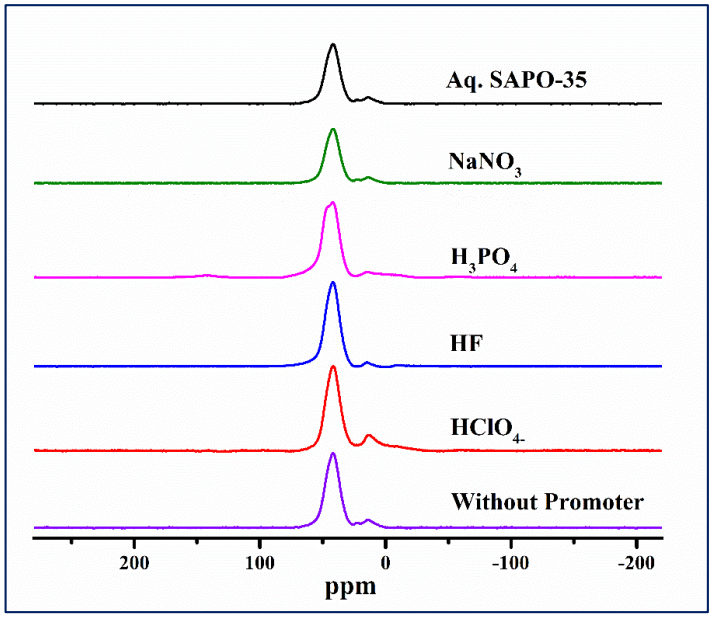

Figure 4. ^{27}Al MAS-NMR spectra of Std. SAPO-35, SAPO-35 in case of $HClO_4^-$ as promoter, HF as promoter, H_3PO_4 as promoter, $NaNO_3$ as promoter and aqueous media SAPO-35.

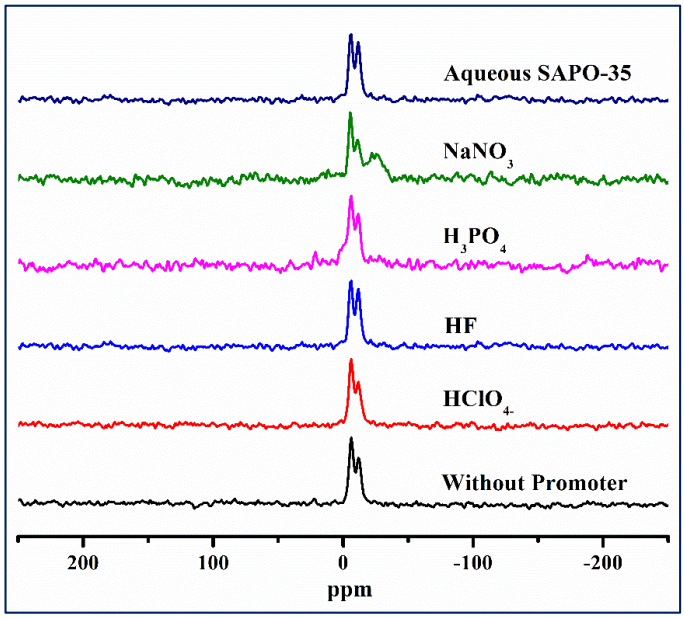

Figure 5. ^{29}Si MAS-NMR spectra of Std. SAPO-35, SAPO-35 in case of $HClO_4^-$ as promoter, HF as promoter, H_3PO_4 as promoter, $NaNO_3$ as promoter and aqueous media SAPO-35.

From ^{31}P MAS-NMR spectrum (Figure 6) of SAPO-35 material synthesized without promoter at 360 h, we can observe two peaks precisely at -25.22 ppm (strong

intense) and -31.72 ppm (weak intense). These two peaks represent phosphorus in the form of $P(Al)_4$ as tetrahedral co-ordinate with two different crystallographic T-sites[4]. The ratio of peak intensities has a value of 1.94 [P_{T1}(-25.22)/P_{T2}(-31.72)], which is very close to the theoretical value of 2. Furthermore, the ^{31}P MAS-NMR spectra of SAPO-35 material synthesized using different promoters in the present study have also demonstrated results which are identical to the results of standard material. Interestingly, the ^{31}P MAS-NMR spectrum of SAPO-35 material in case of H_3PO_4 as promoter showed one narrow (weak intense) peak at -16.67 ppm in addition to the regular peaks. This narrow peak is may be because of P species in the layered phase, where these P atoms are situated in an orderly environment even after the partial condensation of P in the layered phase as observed from the chemical shift values.

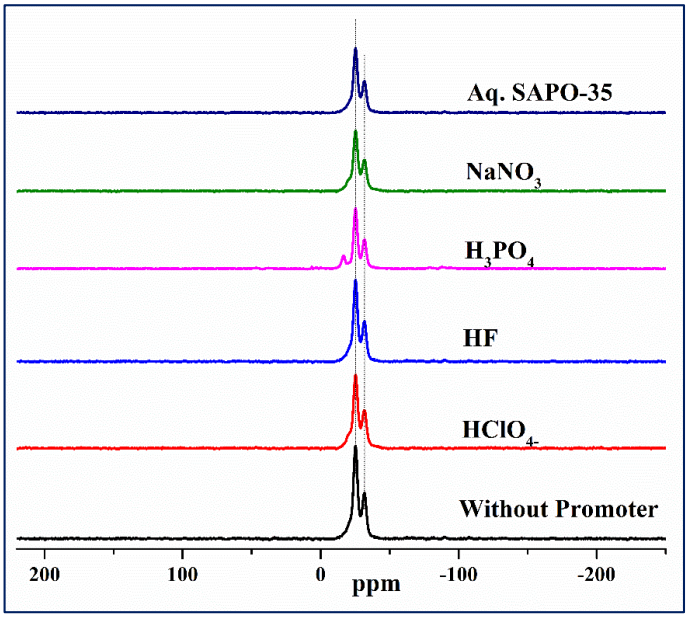

Figure 6. ^{31}P MAS-NMR spectra of Std. SAPO-35, SAPO-35 in case of $HClO_4^-$ as promoter, HF as promoter, H_3PO_4 as promoter, $NaNO_3$ as promoter and aqueous media SAPO-35.

Hence, from all the above ^{27}Al, ^{29}Si, and ^{31}P MAS-NMR spectra we can emphasize that the synthesized SAPO-35 materials using promoters were identical to the SAPO-35 synthesized without promoter at 360 h.

III.3.5 BET and XPS analyses

Surface area measurement is a significant parameter in porous materials, therefore SAPO-35 was tested by N_2 adsorption-desorption. The N_2 adsorption-desorption isotherm and the pore distribution curve of the calcinated SAPO-35 molecular sieve is presented in Table 2. BET specific surface area from the table was found to be similar for SAPO-35

synthesized with promoter and without promoter. In case of 360 h standard non-aqueous SAPO-35 materials, the surface area was 449 m^2/g with a pore volume and pore diameter about 0.22 cm^3/g, 1.97 nm respectively. Whereas, in case perchlorate and H_3PO_4 promoters used SAPO-35 materials the surface area is identical but there is a slightly difference in pore volume and pore diameter. The HF promoter used SAPO-35 material has given surface area 440 m^2/g, pore volume 0.22 cm^3/g and pore diameter 1.96 nm. Interestingly $NaNO_3$ promoter used SAPO-35 material has shown the highest surface area, pore volume and pore diameter i.e. 461 m^2/g, 0.23 cm^3/g and 2.01nm respectively. This may be due to the impure phase of SAPO-35. In all SAPO-35 materials, the isotherm is with the characteristics of microporous materials at the low relative pressure P/P_0 with a type IV hysteresis at the high relative pressure P/P_0.

The surface elemental analysis was carried out by XPS studies. The XPS results given in Table. 3 were in accordance with the theoretical values (Elemental binding energy values of respective elements) and it has been observed that, the results are supporting MAS-NMR results which confirmed the Si incorporation in SAPO-35 material.

Table 3. Textual properties of SAPO-35 materials

Gel composition	**Surface Area (m^2/g)**	**Pore Volume (cm^3/g)**	**Pore Diameter (nm)**	**Elemental composition (mol %) XPS**
Sample-1	449	0.22	1.97	$Si_{0.195}Al_{0.422}P_{0.322}$
Sample-2 ($HClO_4^-$)	446	0.22	1.97	$Si_{0.189}Al_{0.461}P_{0.361}$
Sample-3 (HF)	440	0.22	1.96	$Si_{0.186}Al_{0.468}P_{0.345}$
Sample-4 (H_3PO_4)	446	0.22	1.98	$Si_{0.177}Al_{0.466}P_{0.329}$
Sample-5 $NaNO_3$	461	0.23	2.01	$Si_{0.179}Al_{0.461}P_{0.361}$
Sample-6 (Aq. Media)	444	0.22	1.97	$Si_{0.187}Al_{0.484}P_{0.326}$

The surface elemental analysis was carried out by XPS studies. The XPS results given in Table. 3 were in accordance with the theoretical values (Elemental binding energy values of respective elements) and it has been observed that, the results are supporting MAS-NMR results which confirmed the Si incorporation in SAPO-35 material.

From all these above studies it was observed that, the formation of SAPO-35 in all the promoters used materials were showing similar textual properties.

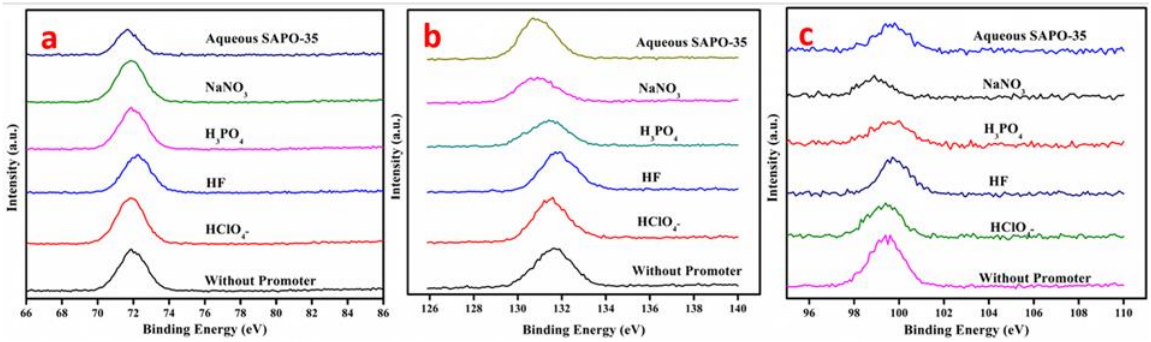

Figure 7 XPS deconvolution spectra of a) Al b) P, and c) Si.

III.3.6 Investigation of phase transformation mechanism

In general, SAPO formation occurs by reaction of Al source with P source and forms aluminium phosphate frameworks which are neutral and when the Si source is added along with the SDA, the desired SAPO products will be formed[34–36]. Here in our case also aluminium isopropoxide as the Al source and orthophosphoric acid as the P source in presence of the media, are condensed to form $AlPO_4^-$ framework. After formation of $AlPO_4^-$ framework, by addition of SiO_2 along with HEM (SDA), the replacement of Si ions with P in the $AlPO_{4-}$ framework occurred, which is called as Si/P exchange and is given in the Figure 8. Here, when we use the promoter after formation of $AlPO_4^-$ framework, the Si/P exchange process will be faster. Hence, the promoters are playing an important role in the transformation of the $AlPO_4^-$ framework to SAPO phase and in the fast crystallization growth.

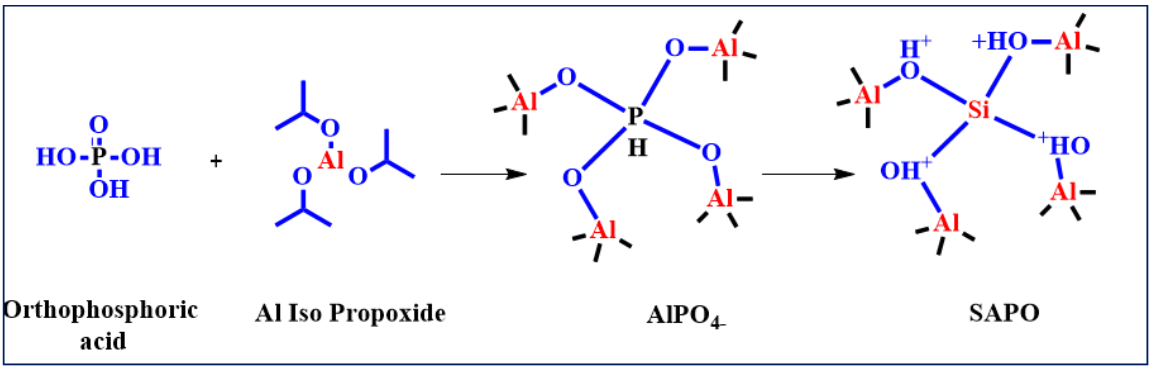

Figure 8 schematic representation of SAPO formation

The formation of SAPO's will takes place in two steps, the former one is nucleation followed by the later one which is crystal growth. In regular approach of SAPO's

preparation, the initial nucleation of the gel step takes longer time, resulting in the slower crystallization, which was the main drawback of that synthesis procedure. When a small amount of inorganic promoter was added to the reaction mixture, this will enhance the speed of the nucleation process of the gel and which leads to faster crystal growth[37].

Nucleation, the preliminary process that happens in the formation of a crystal from a solution/ liquid / a vapour, in which a small number of ions, atoms, or molecules become arranged in a pattern characteristic of a crystalline solid, forming a site upon which additional particles are deposited as the crystal grows. Supersaturation is the driving force for crystallization nucleation and growth and will ultimately dictate the final crystal size distribution.

Figure 9 represents the crystallization kinetics of SAPO-35 in presence of each promoter, in which the % of crystallisation against the reaction time was plotted. From the above plot it can be observed that, the nucleation and crystallization are very fast for the material synthesized using promoters compared to that of standard sample.

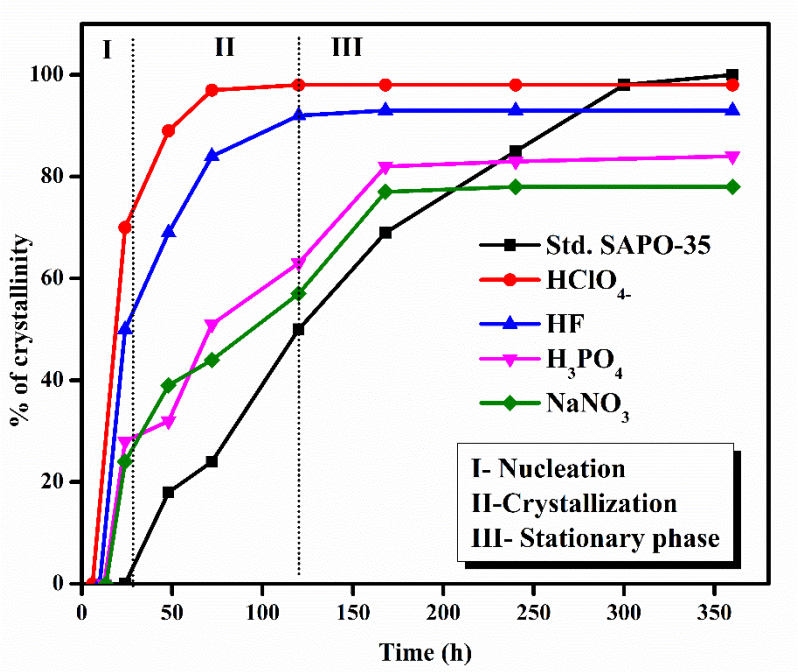

Figure 9. Crystallisation Kinetics of Std. SAPO-35, SAPO-35 in case of HClO4- as promoter, HF as promoter, H_3PO_4 as promoter, NaNO3 as promoter and aqueous media SAPO-35.

Increase in the concentration of promoter decreases the crystallization time up to a saturated level and thereafter it remains constant (at optimum concentration). The activation energy for nucleation (E_n) was calculated from the expression,

$$\frac{dln\left(\frac{1}{n}\right)}{d\left(\frac{1}{T}\right)} = -En/R$$

where 'n' is induction period, viz., the point of the crystallization at which transformation to the crystalline phase just occurs. Correspondingly, Ec, the activation energy for crystal growth was calculated as the rate of crystallization and was obtained from the point in the crystallization curve at which crystallization was 50%. The rate equation can be represented as,

$$\frac{dln\left(\frac{1}{\theta}\right)}{d\left(\frac{1}{T}\right)} = -Ec/R$$

where θ represents the time in hours for 50% crystallization.

From these results the order of the nucleation and crystallization can be given as, $HClO_4^-$>HF>H_3PO_4>$NaNO_3$>without Promoter. Interestingly the crystallinity of promoter used samples were lesser than that of sample without promoter, but the morphology is uniform compared to that of standard sample. This is may be due to the superior nucleation and faster crystallization rate.

2.7 Catalytic application study

The catalytic activity for all the synthesized SAPO-35 materials using promoters along with standard non-aqueous and aqueous SAPO-35 materials to convert methanol into olefins (MTO) was performed at 350℃ with a WHSV of 6.5 h^{-1}. MTO conversion is a reaction in which the methanol will be converted in to different types of olefins based on the catalysts used (different SAPO materials) as shown in figure 10. The obtained results are listed in Table 4. From these activity data we can observe that the standard non-aqueous SAPO-35 material's conversion activity is about 97% and major product of the reaction is 1-Butene and selectivity is over 95%. The SAPO-35 material synthesized using perchlorate as promoter has also shown similar performance, which is about 95.6% of conversion. Whereas, HF and H_3PO_4 promoter based SAPO-35 materials have obtained around 92% yield, which is slightly lower compare to the standard non- aqueous SAPO-35 and perchlorate promoter used SAPO-35 material. This is may be due to the less crystalline nature of the material which was already discussed in the previous section. Whereas, $NaNO_3$ promoter based SAPO-35 material has given the least yield conversion and least selectivity as well. This is because the impure phase of SAPO-35 and lower

crystalline nature of the material. By comparing all the above results, it could be concluded that the non-aqueous media SAPO-35 materials are superior in crystalline nature and MTO conversion reaction performance when compared to the aqueous media SAPO-35 material. Hence, it is stated that the promoter used non-aqueous SAPO-35 and standard non-aqueous SAPO-35 materials were able perform efficiently in converting methanol to olefins.

We have also calculated the Turnover number (TON) and Turnover frequency (TOF) values using the equation in the section 2.3. The turnover number value for standard SAPO-35 has been observed as 60.54. Interestingly, the turnover number for SAPO-35 in presence of $HClO_4^-$, HF, H_3PO_4 as promoters has obtained around 64 (64.78, 64.67, and 64.38 respectively). Whereas, SAPO-35 in presence of $NaNO_3$ and aqueous media SAPO-35 have shown the turnover number of 58.52 and 57.65. The turnover frequency values also found to be similar for SAPO-35 in presence of $HClO_4^-$, HF, H_3PO_4 as promoters.

Table 4 Catalytic activity of SAPO-35 Materials

S. No.	Sample	Selectivity(%)	Conversion rate (%)	TON	TOF
1	Without Promoter	99	97	60.54	0.0168
2	$HClO_4^-$	97	95.6	64.78	0.0179
3	HF	94	92	64.67	0.0179
4	H_3PO_4	94	92	64.38	0.0178
5	$NaNO_3$	90	84	58.52	0.0162
6	Aq. SAPO-35	96	87	57.65	0.0160

This MTO reaction process will be undergoing by the formation of successive construction of C-C bond(ref). MTO reaction is widely studied with SAPO-34 and the resulting products are mostly lower olefins like methylene and propene. In the present study SAPO-35 was used as catalyst, with this catalyst we have obtained the product with four carbons that is 2-Butene. Various reaction mechanisms were proposed by different researchers [38], from which most studied and mentioned reaction mechanism is direct conversion mechanisms. In this reaction mechanism the reactant methanol molecules undergo direct coupling reaction to produce olefin products. Based on the involved reaction intermediate there are twenty different kinds of mechanisms proposed by the earlier researchers[38], for instance radical species[39], oxonium ylide[40], carbocation[41], and carbine[42].

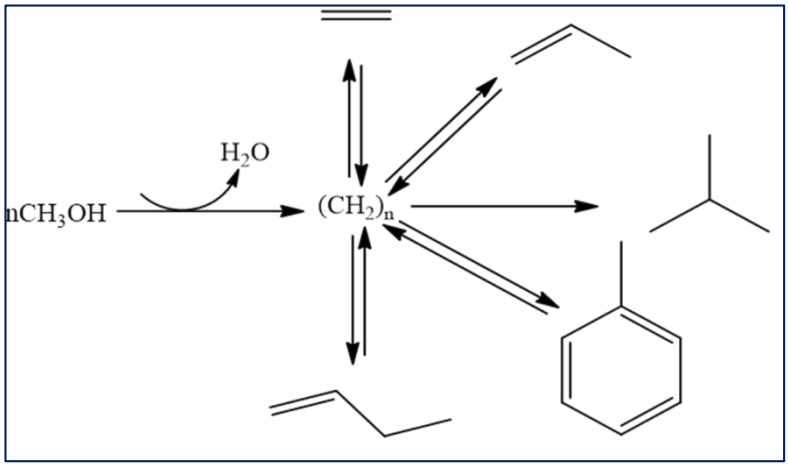

Figure. 10. Schematic MTO reaction products illustrations

III.4. Conclusions

Levyne type topological microporous SAPO-35 molecular sieves were successfully synthesized by using conventional hydrothermal method in presence of different inorganic promoters to reduce the reaction time in a typical non-aqueous media. In the present study, the reaction time was reduced by 80% which is highly recommended for the industrial commercialization. All the materials synthesized using various promoters have exhibited similar characteristics as that of the standard samples (material synthesized without using promoters), which was demonstrated using different methods in the present study. Moreover, the catalytic performance in terms of yield and selectivity of these materials in the MTO conversion reaction is found to be similar with the performance of standard material. With the help of all these studies it can be concluded that the addition of promoters has successfully reduced the time for the crystallization process which in turn reduced the time for the reaction, and the materials synthesized through this method are as effective as the standard materials in MTO conversion reaction.

III.5. References

[1] B.M. Lok, C.A. Messina, R.L. Patton, R.T. Gajek, T.R. Cannan, E.M. Flanigen, J. Am. Chem. Soc. 106 (1984) 6092–6093.

[2] N. Rajic, V. Kaucic, N.Z. Logar, in: Encycl. Catal., John Wiley & Sons, Inc., Hoboken, NJ, USA, 2011.

[3] H. Qisheng, X. Ruren, J. Chem. Soc. Chem. Commun. (1990) 783.

[4] N. Venkatathri, J.W. Yoo, Appl. Catal. A Gen. 340 (2008) 265–270.

[5] J. Yu, R. Xu, Acc. Chem. Res. 36 (2003) 481–490.

[6] Q. Gao, S. Li, R. Xu, Mater. Lett. 31 (1997) 151–153.

[7] G. Sastre, D.W. Lewis, C.R.A. Catlow, J. Phys. Chem. B 101 (1997) 5249–5262.

[8] M.E. Potter, ACS Catal. 10 (2020) 9758–9789.

[9] G. Sastre, D.W. Lewis, C.R.A. Catlow, J. Mol. Catal. A Chem. 119 (1997) 349–356.

[10] S. Samanta, N.K. Mal, P. Kumar, A. Bhaumik, J. Mol. Catal. A Chem. 215 (2004) 169–175.

[11] Y. Luo, H.H. Funke, J.L. Falconer, R.D. Noble, Ind. Eng. Chem. Res. 55 (2016) 9749–9757.

[12] M. Fischer, R.G. Bell, Phys. Chem. Chem. Phys. 16 (2014) 21062–21072.

[13] H. Chen, J. Wydra, X. Zhang, P.-S. Lee, Z. Wang, W. Fan, M. Tsapatsis, J. Am. Chem. Soc. 133 (2011) 12390–12393.

[14] S. Suresh, I.A.K. Reddy, N. Venkatathri, Microporous Mesoporous Mater. 263 (2018) 275–281.

[15] C. Zheng, Y. Li, J. Yu, Sci. Data 7 (2020) 107.

[16] X. Meng, F.-S. Xiao, Chem. Rev. 114 (2014) 1521–1543.

[17] X. Meng, L. Wang, F.-S. Xiao, in: Nanotechnol. Catal., Wiley-VCH Verlag GmbH & Co. KGaA, Weinheim, Germany, 2017, pp. 251–274.

[18] R. Kumar, A. Bhaumik, R.K. Ahedi, S. Ganapathy, Nature 381 (1996) 298–300.

[19] A.M. Prakash, M. Hartmann, L. Kevan, Chem. Mater. 10 (1998) 932–941.

[20] S. Siliveri, S. Chirra, C. Tyagi, A. Gandamalla, A.K. Adepu, S. Goskula, S.R. Gujjula, N. Venkatathri, ChemistrySelect 4 (2019) 9135–9142.

[21] U. Lohse, F. Vogt, J. Richter-Mendau, Cryst. Res. Technol. 28 (1993) 1101–1107.

[22] N. Venkatathri, S.G. Hegde, P.R. Rajamohanan, S. Sivasanker, J. Chem. Soc. Faraday Trans. 93 (1997) 3411–3415.

[23] P. Tian, Y. Wei, M. Ye, Z. Liu, ACS Catal. 5 (2015) 1922–1938.

[24] Q. Wang, L. Wang, H. Wang, Z. Li, H. Wu, G. Li, X. Zhang, S. Zhang, Asia-Pacific J. Chem. Eng. 6 (2011) 596–605.

[25] W. Dai, G. Wu, L. Li, N. Guan, M. Hunger, ACS Catal. 3 (2013) 588–596.

[26] I. Yarulina, A.D. Chowdhury, F. Meirer, B.M. Weckhuysen, J. Gascon, Nat. Catal. 1 (2018) 398–411.

[27] Y. Wang, S.-L. Chen, Y.-L. Gao, Y.-Q. Cao, Q. Zhang, W.-K. Chang, J.B. Benziger, ACS Catal. 7 (2017) 5572–5584.

[28] N.H. Ahn, S. Seo, S.B. Hong, Catal. Sci. Technol. 6 (2016) 2725–2734.

[29] N. Venkatathri, S.G. Hegde, United States Patent: US 7,037,874 B2, 2006.

[30] J. Klinowski, Chem. Rev. 91 (1991) 1459–1479.

[31] J. Klinowski, M.W. Anderson, Magn. Reson. Chem. 28 (1990) S68–S81.

[32] P. Tian, B. Li, S. Xu, X. Su, D. Wang, L. Zhang, D. Fan, Y. Qi, Z. Liu, J. Phys. Chem. C 117 (2013) 4048–4056.

[33] H.J. Jung, C.-H. Shin, S.B. Hong, J. Phys. Chem. B 109 (2005) 20847–20853.

[34] L. Zhang, Y. Huang, J. Phys. Chem. C 120 (2016) 25945–25957.

[35] L. Xu, A. Du, Y. Wei, Y. Wang, Z. Yu, Y. He, X. Zhang, Z. Liu, Microporous Mesoporous Mater. 115 (2008) 332–337.

[36] R. Vomscheid, M. Briend, M.J. Peltre, P.P. Man, D. Barthomeuf, J. Phys. Chem. 98 (1994) 9614–9618.

[37] R. Kumar, P. Mukherjee, R.. Pandey, P. Rajmohanan, A. Bhaumik, Microporous Mesoporous Mater. 22 (1998) 23–31.

[38] M. Stöcker, Microporous Mesoporous Mater. 29 (1999) 3–48.

[39] J.K.A. Clarke, R. Darcy, B.F. Hegarty, E. O'Donoghue, V. Amir-Ebrahimi, J.J. Rooney, J. Chem. Soc. Chem. Commun. (1986) 425.

[40] G.J. Hutchings, F. Gottschalk, M.V.M. Hall, R. Hunter, J. Chem. Soc. Faraday Trans. 1 Phys. Chem. Condens. Phases 83 (1987) 571.

[41] Y. Ono, T. Mori, J. Chem. Soc. Faraday Trans. 1 Phys. Chem. Condens. Phases 77 (1981) 2209.

[42] C. CHANG, J. Catal. 47 (1977) 249–259.

CHAPTER-IV

Synthesis of SAPO molecular sieves in Non-aqueous medium by microwave method using Hexamethyleneimine as a template.

Chapter-IV

Synthesis of SAPO-16 molecular sieve in Non-aqueous medium by microwave method using Hexamethyleneimine as a template

IV.1. Introduction

Alumino-phosphate ($AlPO_4$) molecular sieves were first synthesized by Union carbide in the early 1980s[1,2]. The frameworks of $AlPO_4$ molecular sieves are neutral, they usually don't show any catalytic activity, so the substitution of silicon and/metals into the framework of $AlPO_4$s results in silico alumino phosphates (SAPOs)[3], metal-substituted alumino phosphates (MeAPOs) and metal substituted silico alumino phosphates (MeAPSOs)[4,5]. Since many efforts have been stimulated to develop novel microporous and mesoporous $AlPO_4$ materials by using various methods like hydrothermal synthesis[6], Solvent-Free synthesis[7], Solvo-thermal synthesis[8], microwave irradiation[9–12], and ionothermal methods[13,14] etc. Now, these $AlPO_4$'s, SAPOs, MeAPOs, and MeAPSOs are established to approximately 200 various types including all naturally and synthetically prepared molecular sieves[15]. These materials are having considerable interest as the solid acid catalysts[16–19], as these molecular sieves show some unique characteristics like high separation[20,21] selectivity is due to their well-defined sub-nanometre pore and adsorption properties[22]. These molecular sieves possess superior thermal, mechanical and chemical properties of polymer membranes[23]. Most of them are synthesized in the laboratory in aqueous as well as non-aqueous media[24–28]. These molecular sieves can be prepared by varying the acidity, structure, and compositions [29]. The recent studies have shown that the non-aqueous media synthesis is superior to the aqueous media synthesis in many aspects, as it produces a well crystalline sample with preferable silicon incorporation [27] when Hexamethyleneimine template used. Non-aqueous media process might create the possibility to establish a new industrial process with high efficiency. However, one of its disadvantage is that the synthesis process is more time-consuming than the conventional hydrothermal method. Many efforts have been made to synthesis SAPO's in less crystallization time. Earlier microwave irradiation technique has been used to synthesize various materials like biological, organic, inorganic, and polymer nanostructured materials, particularly in the synthesizing the nanoparticles [30]. Hence, first research was focussed on microwaves mediated silico alumino phosphates synthesis [10,11,31] in

aqueous media. The main advantage is that this technique is very rapid, which leads to faster crystallization rate and low energy consumption, as a consequence the product will be of uniform size. Moreover, it results in enhancing the structural, morphological properties along with high purity materials and also enhances physicochemical properties [9,32,33]. This method is considered to be a green synthetic approach because it consumes low energy i.e., eco-friendly and is cheap. SAPO-16 is one among the silicoaluminophosphate molecular sieves with eight membered ring, small pore opening. There is only limited literature on synthesis of SAPO-16 is available and especially consume more crystallization time even in aqueous media. SAPO-16 is having AST type frame work topology[34,35]. The Cubic AST can be constructed by T10-units which consists of a double 4-ring (D4R) with two dangling T atoms (or two 4-1 units). The D4Rs of the T10-units are associated via the dangling T atoms into a two-dimensional Periodic Building Unit (PerBU). These vicinal PerBUs, related by a shift of ½ b (or ½ a), are associated via the dangling T atoms. Cages of (fused) 6-rings and 4-rings are formed. The framework can also be fabricated by fusion of these cages. The cavities are formed by 6-rings only[35]. To the best of our knowledge, there are no reports on nonaqueous media synthesis and also microwave treated synthesis of SAPO-16. Hence, the objective of our present study is to synthesize a highly efficient, economically viable, environment friendly and industrially important silicoaluminophosphate catalyst through non-aqueous media by microwave irradiation. This process is advantageous over conventional methods which take approximately 15 days for the crystallization of SAPO-16, whereas, we could synthesize this catalyst with very less crystallization time such as five minutes using microwave treatment. In this study, SAPO-16 was taken as a representative silico alumino phosphate molecular sieves and it was synthesized by microwave irradiation technique instantly using hexamethyleneimine as an organic template and ethylene glycol as the non-aqueous medium.

IV.2. Experimental

IV.2.1. Sample preparation

Aluminium isopropoxide ($Al(OCH_3H_7)_3$, 98.0%, Aldrich, USA), Orthophosphoric acid (H_3PO_4, 85.0%, S.D. fine, India), fumed silica (SiO_2, 99.8% Aldrich, USA), hexamethyleneimine ($C_6H_{12}NH$, 98.0%, Aldrich, USA) and ethylene glycol ($C_2H_6O_2$, 99.0%, S.D. Fine, India) were used for the synthesis of SAPO-16 and for catalytic

evolution Benzaldehyde (C_6H_5CHO), Methanol (CH_3OH, 99.0%, Merck India), were used without any further purification.

The SAPO-16 was synthesized by microwave method using ethylene glycol as the solvent. The procedure is briefly explained in 3 steps, which is as follows. Step1: aluminium isopropoxide was mixed with ethylene glycol under vigorous stirring to obtain a homogeneous gel. To this gel, 11.32 g of orthophosphoric acid was added drop wise. Step 2: 1.052 g of fumed silica was mixed with 7.26 g of HEM under stirring for about 15 min at room temperature, which was then added to the step1 mixture. The final composition of the obtained gel was in the ratio of Al_2O_3: $1.8P_2O_5$: 0.3-$1.2SiO_2$: 4.9HEM: 49EG. This gel was further allowed to stir for 5 min and subjected to microwave treatment at 450 W in atmospheric pressure in the air. Experiments were carried out by altering the aging time with the similar method. The crystallized products were collected after centrifugation and washed with ethanol. The products were dried at 80 ^oC for 12 h and ground to obtain a fine powder. Subsequently, the synthesized products were calcined at 550 ^oC for 8 h prior to calcination, hydrogen peroxide solution treatment was an effective way to remove the physisorbed template which chars on direct calcination.

IV.2.2. Characterisation

Powder XRD patterns were recorded on a PAN analytical advanced X-ray diffractometer using Ni filtered Cu Kα (λ = 1.5406 Å) radiation in the scan range 2θ between 6^o and 60^o. The surface morphology and composition of the samples were investigated by FE-SEM-EDX; OXFORD Instruments, INCAx-act. TEM images of the catalysts were recorded on a Technai-G2 T20 super twin instrument fitted with a 200 kV field emission gun. Samples were prepared by dispersing in isopropanol by sonication and drop casting them on copper grids. Then the grids were dried over night at 25 °C. TG/DTA analysis ware carried out on NETZSCH, STA2500 Regulus in presence N_2 atmosphere from room temperature to 1000 ^oC. N_2 adsorption–desorption isotherms were obtained on a NOVA.1000 Ver.3.7 system at 77 K. small amount of the calcined catalyst was placed in the sample cell. After degassing step, N_2 physisorption was carried out for measuring surface area. The BET equation was used to calculate specific surface area, SBET. FT-IR spectra were recorded by PerkinElmer Spectrum 100 FT-IR spectrophotometer by using the KBr pellet technique in the range of 400 to 4000 cm^{-1}. All the solid state MAS NMR experiments were performed on a VARIAN, USA Mercury plus 300 MHz NMR Spectrometer. TPD measurements were carried out on Micromeritics Auto Chem. 2910

instrument by using NH_3 as probe molecule to identify the number of acidic sites of the calcined sample. This experimental procedure as follows; 0.1 g of the calcined SAPO-16 was loaded into a U-shaped quartz sample tube. Preceding to measurements, the calcined SAPO-16 was pre-treated in He (30 mL/min) at 200 °C about 1 h, then cooled to 100 °C and a mixture of NH_3 and He (10 vol %) was nourished to the sample (30 mL/min) about 1 h. Then, the sample was flushed with He (30 mL/min) about 1 h at 100 °C. Before starting the desorption analysis, the baseline was checked for stability. TPD measurements were done in the temperature range of 100-550 °C.

To test the catalytic activity for Benzaldehyde acetalization reaction, 10 mL of methanol and 0.1 g of calcined catalyst along with 1 g of benzaldehyde were allowed to react at 80 ^oC under refluxing condition in a batch reactor. The resulting samples were collected at various intervals. The products collected after the benzaldehyde acetalization reaction were analyzed using Gas Chromatography -YL-6500 South Korea equipped with a flame ionization detector FID.

IV.3. Results and discussion

The microwave mediated synthesis of SAPO-16 at different crystallization conditions was shown in Table 1.

Table 1: Synthesis of aluminophosphates and Silicoaluminophosphates at different crystallization conditions by using Hexamethyleneimine template.

Gel composition	**Crystallization conditions**	**Product**
Al_2O_3: 1.8 P_2O_5:4.9HEM: 55H_2O (Aluminium source : Aluminium isopropoxide)	5 min, 450 W, without aging, microwave treated.	Amorphous
Al_2O_3: 1.8 P_2O_5:4.9HEM: 55H_2O (Aluminium source : catapal B)	5 min, 450 W, without aging, microwave treated.	Amorphous
Al_2O_3: 1.8 P_2O_5:4.9 HEM: 49 EG (Aluminium source : Aluminium isopropoxide)	15 days, 200 ^oC, hydrothermal	$AlPO_4$-5
Al_2O_3 : P_2O_5 : 1.16 HEM : 45 H_2O (Aluminium source : Catapal-B)	24 h, 200 ^oC, hydrothermal	$AlPO_4$-5
Al_2O_3: P_2O_5:1.35HEM: 45H_2O (Aluminium source : Catapal-B)	24 h, 200 ^oC, hydrothermal	$AlPO_4$-16

Al_2O_3 : P_2O_5 : 1.16 HEM : 45 H_2O (Aluminium source : Aluminium isopropoxide)	24 h, 200 ^oC, hydrothermal	$AlPO_4$-16
Al_2O_3: P_2O_5: 0.3 SiO_2 : 1.16 HEM: 45H_2O (Aluminium source : Catapal-B)	24 h, 200 ^oC, hydrothermal	SAPO-5
Al_2O_3: 1.8 P_2O_5: 1.2 SiO_2:4.9HEM: 20-60 H_2O: 49EG (Aluminium source : Aluminium isopropoxide)	5 min, 450 W, without aging, microwave treated.	Nano crystalline SAPO-16
Al_2O_3: 1.8 P_2O_5: 0.3-1.2 SiO_2:4.9HEM: 49EG (Aluminium source : Aluminium isopropoxide)	5 min, 450 W, without aging, microwave treated.	Nano crystalline SAPO-16 N-SAPO-16-WA
Al_2O_3: 1.8 P_2O_5: 0.3-1.2 SiO_2:4.9HEM: 49EG (Aluminium source : Aluminium isopropoxide)	5 min, 450 W, 0 to 12 h with aging, microwave treated.	Nano crystalline SAPO-16 N-SAPO-16-A
Al_2O_3: 1.8 P_2O_5: 0.3-1.2 SiO_2:4.9HEM: 49EG (Aluminium source : Aluminium isopropoxide)	15 days, 200 ^oC, hydrothermal	SAPO-35
Al_2O_3 : P_2O_5 : 0.3-1.0 SiO_2: 1.16 HEM : 45 H_2O(Aluminium source:Aluminium isopropoxide)	48 h, 200 ^oC, hydrothermal	SAPO-35

$AlPO_4$ synthesis in aqueous media resulted in amorphous materials and also SAPO synthesis with silica in presence of water resulted in amorphous materials. However, with water free, 4.9 M ratio of amine with and without aging has resulted in Nano-crystalline SAPO-16, this is may be attributed to the formation of hexamethyleneimine – silica complex, resulted in the rapid crystallization of SAPO-16 in non-aqueous medium, Where as in the case of aqueous media the inside temperature of oven is around 180-200 ^oC since the boiling point of the H_2O is 100 ^oC, so the water got evaporated and resulted in the amorphous product. The faster crystallization in case of microwave treatment is due to the direct formation of SAPO-16, whereas in case of conventional hydrothermal aqueous media synthesis, it is forming through SAPO-L lamellar intermediate [36] which takes around 24-48 h in aqueous media and 15 days in non-aqueous media at the same temperature. In order to check the physicochemical properties, the sample was prepared

by changing in aging time, at all the aging times we have got similar products and the crystallinity is slightly changed.

IV.3.1. Powder X-ray diffraction studies:

The Powder X-ray diffraction patterns of the as-synthesized with aging (N-SAPO-16-A) and without aging (N-SAPO-16-WA) and calcined (N-SAPO-16-WA) samples were shown in Fig.1. These X-ray diffraction characteristic patterns were matching with the X-ray diffraction patterns of $AlPO_4$-16 reported in the literature by S. T. Wilson etc [37], and the comparison is given in Table 2. From the obtained XRD pattern, it clearly shows that the sample is free from the impurities. It was also observed that by increasing the aging time the intensity of X-ray diffraction peaks has considerably increased. This clearly indicate that, upon aging, number of particles become mature and crystallize more.

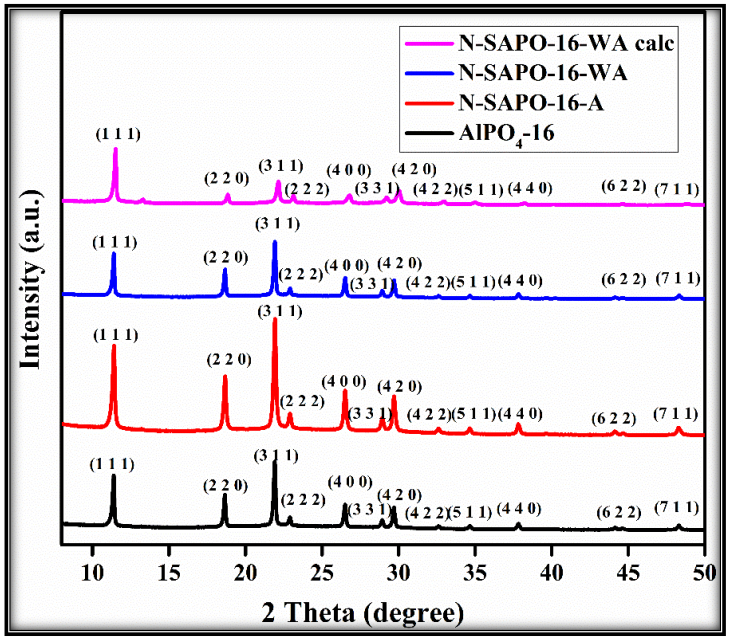

Fig. 1: Powder X-ray diffraction pattern of AST type molecular sieves.

Table 2 : Peak positions of AST type molecular sieves synthesized in the present study vs reported one.

S. No.	$AlPO_4$-16[a]		SAPO-16[b]		SAPO-16	
	2 Theta	d (Å)	2 Theta	d (Å)	2 Theta	d (Å)
1	11.3-11.5	7.83-7.69	11.41	7.75	11.43	7.73
2	18.7-18.85	4.75-4.71	18.66	4.75	18.78	4.72
3	21.9-22.2	4.06-4.00	21.91	4.05	22.03	4.03
4	26.55-26.75	3.36-3.33	26.51	3.36	26.62	3.34
5	29.75-29.95	3.00-2.98	29.69	3.00	29.82	2.99

[a]Data was taken from reference[37] [b]Data was taken from reference[36]

IV.3.2. FE-SEM/EDAX and TEM analysis:

The morphology of the as-synthesized and calcined samples of SAPO-16 were observed through FE-SEM and TEM. FE-SEM micrographs and the EDX analysis is depicted in Fig. 2A and 2B, SEM images show that the particles formed from as-synthesized without (N-SAPO-16-WA) and with aging (N-SAPO-16-A) are highly uniform and without any odd phase. The morphology of the particles did not change after calcination. EDX plot (Fig 2B) show that the presence of Al, Si, and O (0.7 Al_2O_3: 0.8 P_2O_5: 0.4 SiO_2) elements for all samples indicating the composition of SAPO. TEM micrographs as given in Fig. 2C shows that the formation of well-defined triangle shape particles. The particle size was found to be around 50-100 nm.

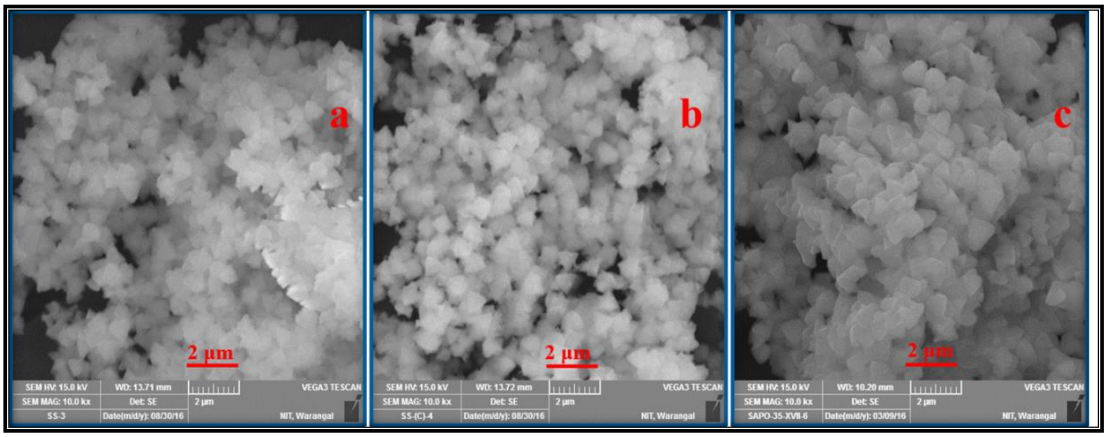

Fig. 2A. SEM micrographs of a) N-SAPO-16-WA, b) N-SAPO-16-A, c) calcined N-SAPO-16-WA

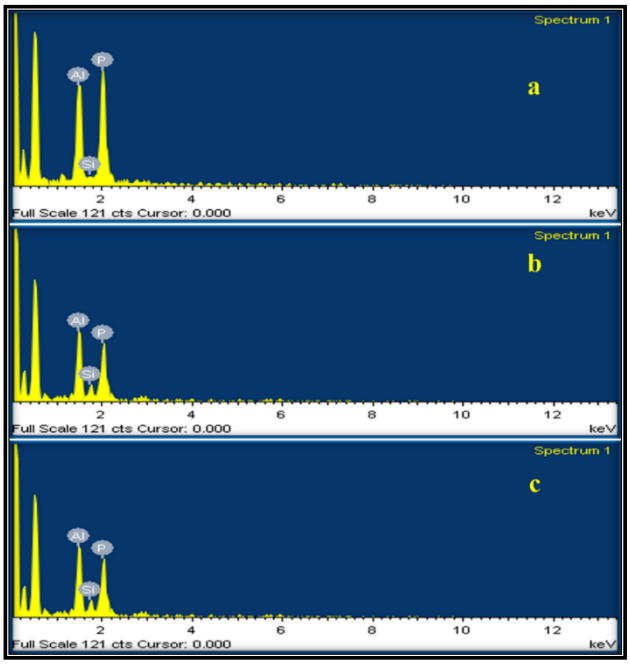

Fig. 2B. EDX plots of SAPO-16 (a) N-SAPO-16-WA, (b) N-SAPO-16-A and (c) calcined N-SAPO-16-WA samples.

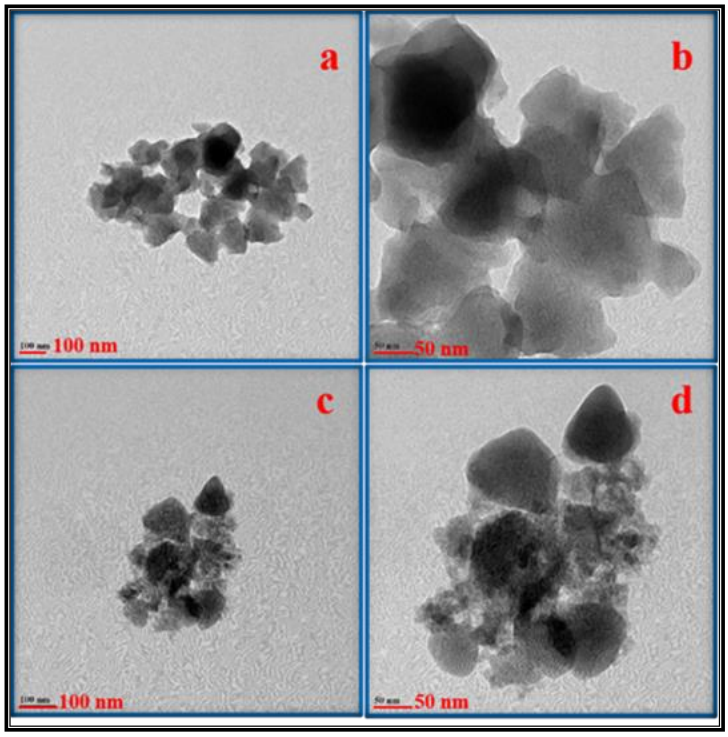

Fig. 2C. TEM Images of (a) and (b) N-SAPO-16-WA, (c) and (d) calcined N-SAPO-16-WA

IV.3.3. Thermogravimetry/Differential thermal analysis (TG/DTA):

The TG/DTA curves of SAPO-16 (both synthesized and calcined) are shown in Fig. 3. As-synthesized sample shows a weight-loss around 20 % from room temperature to 860 ^{o}C. At the lower end, i.e., the temperature region up to 256 ^{o}C, the weight loss is probably due to the loss of physisorbed water and the organic template. In the temperature range from 257 to 860 ^{o}C, we have observed an exothermic weight loss at three stages. This is due to the loss of oxidative decomposition of an organic template which has entrapped inside the cages. In general, the removal of template which has been protonated for the charge balance is more difficult compared to neutral template occluded in the channel. Calcined sample shows that only one endotherm at a lower temperature around 100 ^{o}C, with a weight loss of about 10 % due to the loss of physisorbed water. There were no other exothermic peaks observed due to the oxidative decomposition of the template.

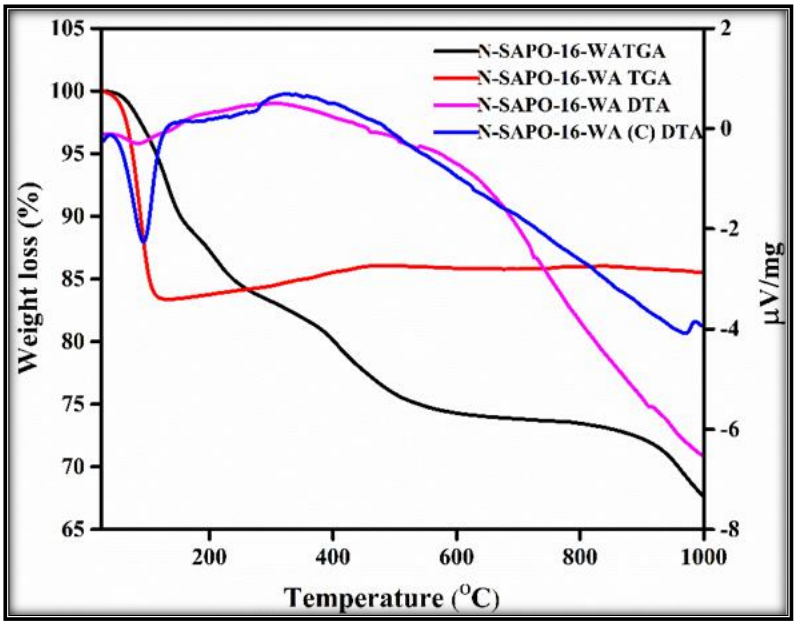

Fig. 3: Thermogravimetry/Differential thermal analysis profiles of N-SAPO-16-WA

IV.3.4. Fourier Transform Infrared (FT-IR) spectroscopic analysis

The framework vibrations of as-synthesized SAPO-16 was confirmed from the FT-IR spectrum as given in Fig. 4. It can be seen from the spectrum that, the peaks at wave numbers about 1100, 840, 640, and 470 cm^{-1} were corresponding to T–O–T (Where T= Si, Al, and P) symmetric stretching frequency [38], protonated template, T–O bending in D4R (Double 4-Ring) rings and T–O bending of Si tetrahedral respectively. The peak at wave number about 2450 cm^{-1} can be correlated to absorbed CO_2 from the atmosphere. The peaks in the range of 2650-3000 cm^{-1} appear due to the stretching frequency of -CH resultant from the organic environment like template, organic-functional silane, etc.[39]. Stretching vibration around 1650 and 1400 cm^{-1} could be attributed to physically adsorbed water i.e. H-O-H bending mode.

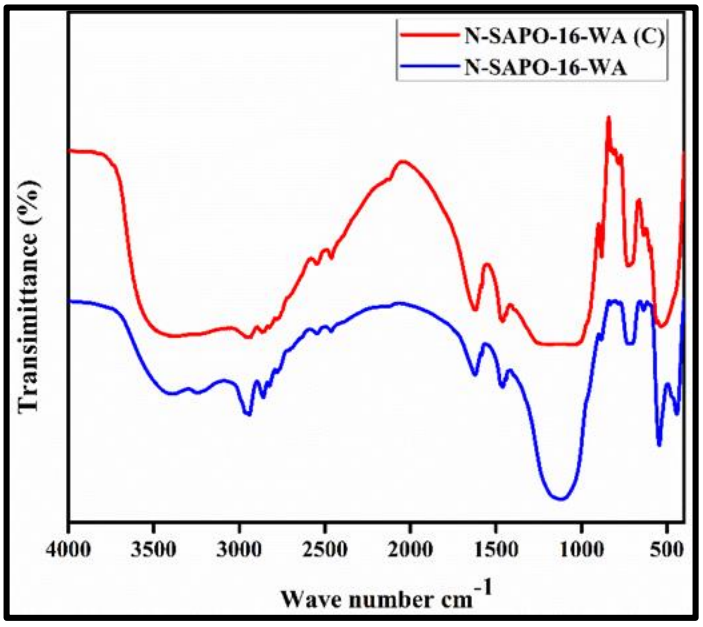

Fig. 4: Fourier Transform –Infrared Spectrum of N-SAPO-16-WA

IV.3.5. N_2 adsorption-desorption analysis:

In the characterization of porous materials surface area measurement plays a vital role, therefore N-SAPO-16-WA, N-SAPO-16-A and hydrothermally synthesized SAPO-16 (H-SAPO-16) were tested by N_2 adsorption-desorption. The N_2 adsorption-desorption isotherms of the calcined N-SAPO-16-WA, N-SAPO-16-A and H-SAPO-16 molecular sieves were depicted in Fig.5. BET specific surface area of N-SAPO-16-WA, N-SAPO-16-A and H-SAPO-16 are 270 m^2/g, 286 m^2/g, 339 m^2/g respectively. The surface area slightly increased with the aging time and also it is lower than the hydrothermal method sample. These are comparatively higher than other framework types like AFI (SAPO-5 is 214 m^2/g) and AEL (SAPO-11's 123 m^2/g) [40]. From the results, it can be emphasized that at lower relative pressure P/Po region the SAPO-16 has obtained microporous material's characteristic isotherm. But at the high relative pressure P/Po region, N-SAPO-16 has obtained characteristic isotherm of microporous materials, as a consequence it is said to be a type IV hysteresis [41].

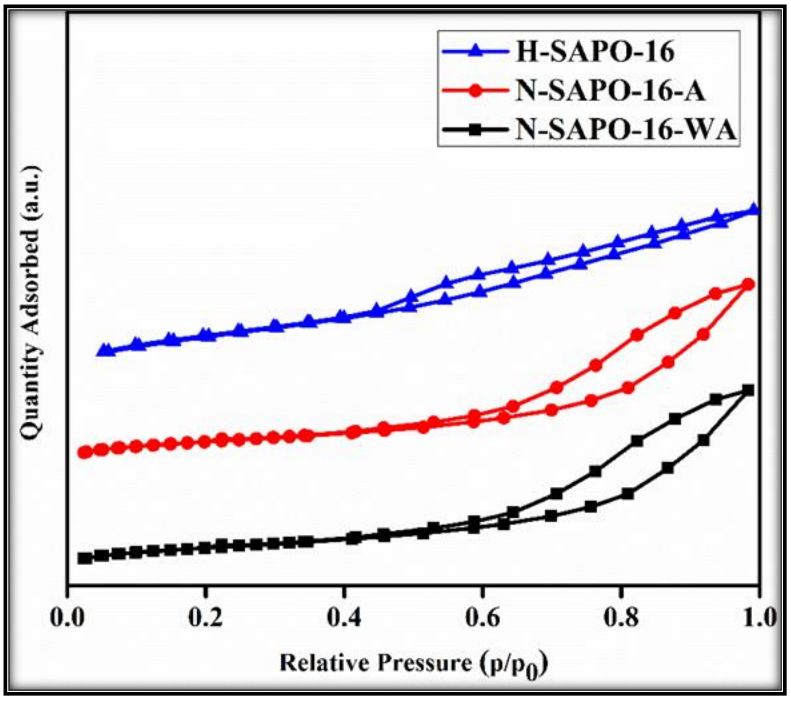

Fig. 5: N_2 adsorption-desorption isotherm of N-SAPO-16-WA, N-SAPO-16 and Hydrothermally Synthesized SAPO-16

IV.3.6 MAS – NMR spectroscopic analysis:

^{27}Al, ^{31}P and ^{29}Si MAS-NMR spectra of N-SAPO-16-WA (both as-synthesized and calcined) were recorded to ascertain the surrounding environment of these ions existing in the structural framework as shown in the Fig. 6. The ^{27}Al MAS-NMR spectra of the as synthesized samples present one broad and asymmetric peak centered at 37.7 ppm (strong) and at -15 ppm (weak) shoulder peak. They are assigned to the tetrahedral coordinated Al (Tet-Al) and the octahedral coordinated Al (Oct-Al) with an $Al(OP)_4(OH_2)_2$ [42,43] There is no change in the peak position of the calcined sample hence the Al environment remains same after calcination. The ^{31}P spectrum of N-SAPO-16-WA consisted of two peaks centered at -30.16 ppm (strong) and 2.02 ppm (weak). The peak at -30.16 ppm is clearly indicate P is fully condensed with $P(OAl)_4$ framework, and 2.02 ppm is due to partially reacted P in the reaction mixture and it was completely disappeared after calcination. The silicon incorporated in tetrahedral coordination with a different environment. The ^{29}Si NMR spectra of the sample, one a peak at -88.06 ppm arise from $Si(OAl)_3(OSi)$ or $Si(OAl)_2(OSi)_2$ environment in tetrahedral coordination and a broad peak resonance centred at -107.0 ppm which can be assigned to this is related to the presence of connectivity defects ($Si\text{-}O^-$ or Si-OH groups) and amorphous Si with $Si(OSi)_4$ [44–46].

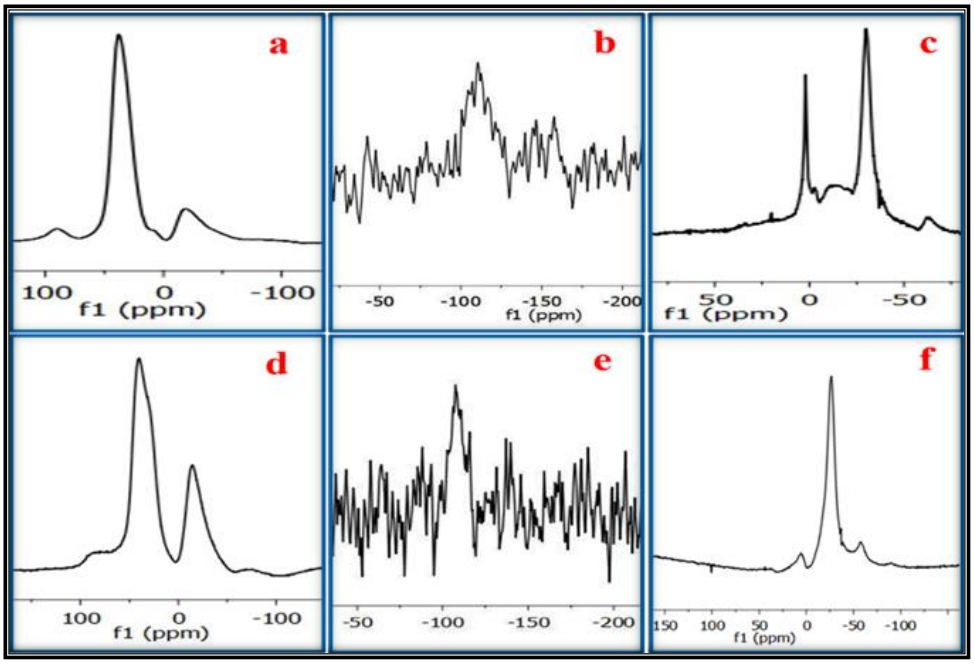

Fig. 6: MAS-NMR spectra of, as-synthesized N-SAPO-16-WA samples of ^{27}Al(a), ^{29}Si (b) and ^{31}P z(c) nuclei and calcined N-SAPO-16-WA sample of ^{27}Al(d), ^{29}Si (e) and ^{31}P (f) nuclei

IV.3.7. Temperature-programmed desorption (TPD):

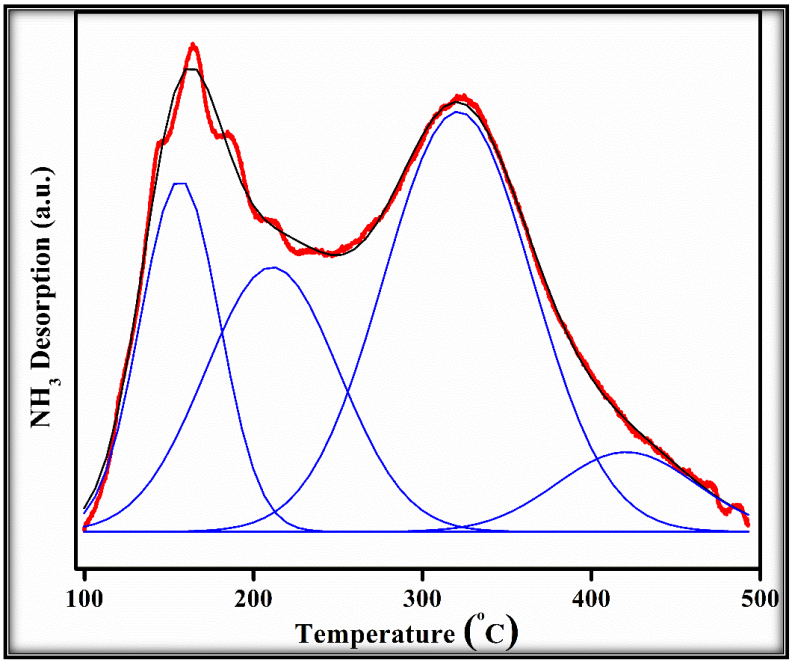

Fig.7: NH_3-TPD profile of the N-SAPO-16-WA

The acidic property of the prepared catalyst is determined using NH_3 by the probe mode. The acidic profile as given in Fig.7 show a broad peak with different strengths. It could be deconvoluted into four peaks and they are categorized as the acidic sites as weak (desorption maximum below 150 ^oC), medium/moderate (150-250 ^oC), strong (250-350

^{o}C) and very strong (350-500 ^{o}C). In Fig.7, it was found that there are one weak acidic, one medium/ moderate, one strong and one very strong acidic nature of peaks, because of which the catalytic activity can be increased. The overall acidity of the catalyst was around 1.04 mol/g.

Based on the above characterization results, the illustration of the crystallization of SAPO-16 shows that the Aluminium isopropoxide and SiO_2 are hydrolyzed and condensed to form SAPO-16 in presence of microwaves. The reduction in crystallization time is due to the total activation energy required for the nucleation followed by crystallization is given by the microwaves, hence accelerating the crystallization process, whereas the crystallization process in conventional hydrothermal method through an intermediate SAPO-L [20] which consumes more time.

IV.3.8. Catalytic activity evaluation of SAPO-16:

In order to check the catalytic activity of the calcined SAPO-16 over Benzaldehyde acetalization reaction was executed. The acetalization of alcohols reaction is widely used in synthetic approaches to protect the carbonyl group of the various aldehydes and ketones [47]. The acetals and hemiacetals are important reactants for synthesizing functional compounds like fragrances, steroids, and pharmaceuticals. As per the available literature, many heterogeneous catalysts are there for acetalization reactions for instance, mesoporous alumino-silicates JRC-SiO-4, silica gel, and MCM-41. In the present investigation, comparisons of acetalization reaction rates with catalyst and without catalyst were made.

The acetalization reaction in presence of catalyst was given by the following equation.

$$C_6H_5CHO + 2CH_3OH \xrightarrow[80^oC]{\text{SAPO-16}} C_6H_5CH(OCH_3)_2 + H_2O \quad \text{.....(1)}$$

In presence of $AlPO_4$-16, the % conversion to the product is negligible, whereas, in presence of SAPO-16 the conversion to the product is about 80% in 8 h with maximum turn over number, 14.5 x 10^{-2} and turn over frequency, 4.0 x 10^{-5} (Table 3 & 4). This clearly indicates that the catalytic activity was seen only after incorporation of Si into former $AlPO_4$, i.e., SAPO-16 acts as a better catalyst. This confirm the enhanced catalytic behavior SAPO-16. Since the results are encouraging, so this material can be useful for the conversion for the benzaldehyde acetalization reaction. The catalyst are stable and active even after the fifth with out considerable loss in conversion and selectivity (Fig. 8).

Table 3: Conversion of the reactants Turn over number (TON) and Turn over frequencies (TOF) by SAPO-16

S. No.	Time (h)	% of Conversion	TON	TOF
1	1	71	$14.5x10^{-2}$	$4.04x10^{-5}$
2	2	73	$7.45x10^{-3}$	$2.06x10^{-6}$
3	4	76	$3.89x10^{-2}$	$1.08x10^{-5}$
4	8	80	$2.05x10^{-2}$	$5.69x10^{-6}$
5	12	79	$1.35x10^{-2}$	$3.75x10^{-6}$
6	24	77	$0.65x10^{-2}$	$1.82x10^{-6}$

Table 4: Comparison of N-SAPO-16-WA with other catalysts in acetalization of benzaldehyde with methanol.

S. No.	Catalyst	Time (h)	Conversion (%)	Remark
1	N-SAPO-16-WA	1; 24	71; 80	Present work
2	SAPO-35	1;24	74; 91	Present work
3	$Cu3(BTC)_2$	2; 24	63; 78	[48]
4	Fe(BTC)	2; 24	49; 71	[49]
5	$Al_2(BDC)_3$	24	66	[49]

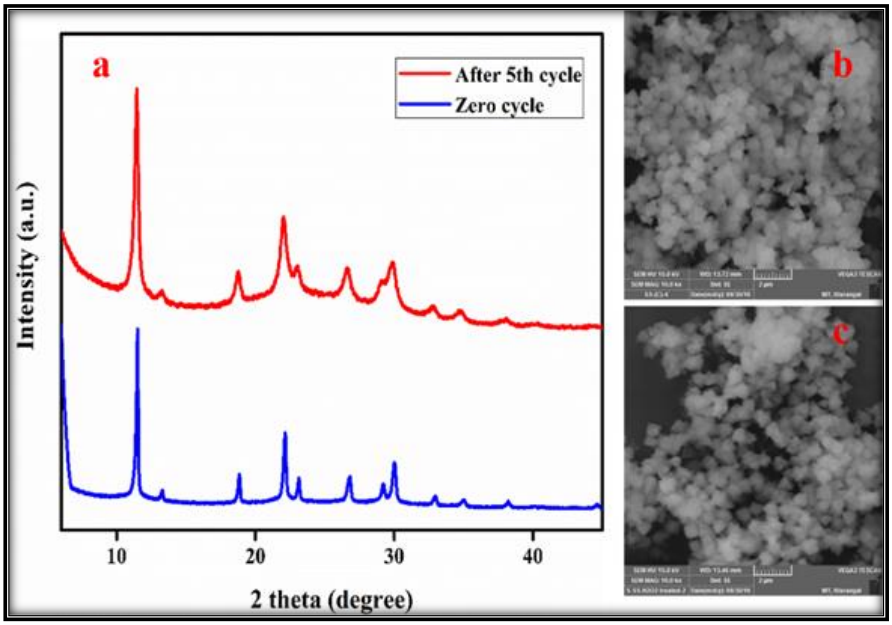

Fig. 8: a) Powder X-ray diffraction patterns, b & c) Scanning electron migrograph of 0 cycle and 5th cycle reused N-SAPO-16-WA catalysts.

IV.4. Conclusions

AST type Silicoaluminophosphate molecular sieves SAPO-16 has been synthesized in ethylene glycol media by using microwave technique with hexamethyleneimine as an organic template in rapid time against the conventional fifteen days by hydrothermal method. This synthesis root is eco-friendly, very rapid and also obtaining products were highly uniform. The synthesized SAPO-16 was found to be economic and efficient catalyst for Benzaldehyde acetalization reaction, the catalytic activity on Benzaldehyde acetalization reaction shows that the reactants have a maximum of 80 % benzaldehyde conversion in 8 h with maximum turn over a number of 14.5×10^{-2} and turn over the frequency of 4.0×10^{-5}. This method also can be applicable to synthesize other Silicoaluminophosphate molecular sieves by efficient way.

IV.5. References:

[1] B.M. Lok, C.A. Messina, R.L. Patton, R.T. Gajek, T.R. Cannan, E.M. Flanigen, J. Am. Chem. Soc. 106 (1984) 6092–6093.

[2] B.M. Lok, C. A.Messina, R.L. Patton, R.T. Gajek, T.R. Cannan, Edith M. Flanigen, Crystalline Silicoaluminophosphates US 4440871 A, 4440871 A, 1984.

[3] R. Vomscheid, M. Briend, M.J. Peltre, P.P. Man, D. Barthomeuf, J. Phys. Chem. 98 (1994) 9614–9618.

[4] B.M. Weckhuysen, R.R. Rao, J. A. Martens, R.A. Schoonheydt, Eur. J. Inorg. Chem. 1999 (1999) 565–577.

[5] M. Hartmann, L. Kevan, Chem. Rev. 99 (1999) 635–664.

[6] C.S. Cundy, P.A. Cox, Microporous Mesoporous Mater. 82 (2005) 1–78.

[7] Y. Jin, Q. Sun, G. Qi, C. Yang, J. Xu, F. Chen, X. Meng, F. Deng, F.-S. Xiao, Angew. Chemie Int. Ed. 52 (2013) 9172–9175.

[8] K.S. Park, Z. Ni, A.P. Cote, J.Y. Choi, R. Huang, F.J. Uribe-Romo, H.K. Chae, M. O'Keeffe, O.M. Yaghi, Proc. Natl. Acad. Sci. 103 (2006) 10186–10191.

[9] S.-E. Park, D.S. Kim, J.-S. Chang, W.Y. Kim, Catal. Today 44 (1998) 301–308.

[10] F.M. Shalmani, S. Askari, R. Halladj, Rev. Chem. Eng. 29 (2013) 99–122.

[11] Y. Li, W. Yang, J. Memb. Sci. 316 (2008) 3–17.

[12] X. Zhao, H. Wang, B. Dong, Z. Sun, G. Li, X. Wang, Microporous Mesoporous Mater. 151 (2012) 56–63.

[13] X. Zhao, C. Kang, H. Wang, C. Luo, G. Li, X. Wang, J. Porous Mater. 18 (2011) 615–621.

[14] X. Li, K. Li, H. Ma, R. Xu, S. Tao, Z. Tian, Microporous Mesoporous Mater. 217 (2015) 54–62.

[15] X. Meng, F. Xiao, Chem. Rev. 114 (2014) 1521–1543.

[16] M.E. Davis, Ind. Eng. Chem. Res. 30 (1991) 1675–1683.

[17] J. Chen, P.A. Wright, J.M. Thomas, S. Natarajan, L. Marchese, S.M. Bradley, G. Sankar, C.R.A. Catlow, P.L. Gai-Boyes, J. Phys. Chem. 98 (1994) 10216–10224.

[18] A.K. Singh, K. Kondamudi, R. Yadav, S. Upadhyayula, A. Sakthivel, J. Phys. Chem. C 118 (2014) 27961–27972.

[19] R. Yadav, A. Sakthivel, Appl. Catal. A Gen. 481 (2014) 143–160.

[20] M.E. Potter, M.E. Cholerton, J. Kezina, R. Bounds, M. Carravetta, M. Manzoli, E. Gianotti, M. Lefenfeld, R. Raja, ACS Catal. 4 (2014) 4161–4169.

[21] M. Moliner, C. Martínez, A. Corma, Chem. Mater. 26 (2014) 246–258.

[22] M. Fischer, R.G. Bell, Phys. Chem. Chem. Phys. 16 (2014) 21062–21072.

[23] V. Valtchev, L. Tosheva, Chem. Rev. 113 (2013) 6734–6760.

[24] A.K. Sinha, S. Sivasanker, P. Ratnasamy, Ind. Eng. Chem. Res. 37 (1998) 2208–2214.

[25] Q. Gao, S. Li, R. Xu, Mater. Lett. 31 (1997) 151–153.

[26] Q. Gao, S. Li, R. Xu, J. Chem. Soc. Chem. Commun. (1994) 1465.

[27] N. Venkatathri, S.G. Hegde, P.R. Rajamohanan, S. Sivasanker, J. Chem. Soc. Faraday Trans. 93 (1997) 3411–3415.

[28] N. Venkatathri, S.G. Hegde, United States Patent: US 7,037,874 B2, 2006.

[29] A. Galadima, O. Muraza, Ind. Eng. Chem. Res. 54 (2015) 4891–4905.

[30] A.M. Balu, D. Dallinger, D. Obermayer, J.M. Campelo, A. a. Romero, D. Carmona, F. Balas, K. Yohida, P.L. Gai, C. Vargas, C.O. Kappe, R. Luque, Green Chem. 14 (2012) 393–402.

[31] S.R. Venna, M. a. Carreon, J. Mater. Chem. 19 (2009) 3138.

[32] Y. CAO, H. WEI, Z. XIA, Trans. Nonferrous Met. Soc. China 19 (2009) s656–s664.

[33] V. Vatanpour, M.E. Yekavalangi, M. Safarpour, Sep. Purif. Technol. 163 (2016) 300–309.

[34] L. Frunza, J. Pelgrims, H. Leeman, P. Van Der Voort, E.F. Vansant, R.A. Schoonheydt, B.M. Weckhuysen, J. Phys. Chem. B 105 (2001) 2677–2686.

[35] R.M. BARRER, Nature 249 (1974) 783–783.

[36] N. Venkatathri, S.. Hegde, V. Ramaswamy, S. Sivasanker, Microporous Mesoporous Mater. 23 (1998) 277–285.

[37] all of N.Y. Stephen T. Wilson, Shrub Oak; Brent M. Lok, New York; Edith M. Flanigen, White Plains, United States Patent [191, 4,310,440, 1990.

[38] Q. Huo, R. Xu, S. Li, Z. Ma, J.M. Thomas, R.H. Jones, A.M. Chippindale, J. Chem. Soc. Chem. Commun. 0 (1992) 875.

[39] R. Yadav, M. Ahmed, A.K. Singh, A. Sakthivel, Sci. Rep. 6 (2016) 22813.

[40] a. M. Prakash, M. Hartmann, L. Kevan, Chem. Mater. 10 (1998) 932–941.

[41] Y. Fan, H. Xiao, G. Shi, H. Liu, X. Bao, J. Catal. 285 (2012) 251–259.

[42] B. Chen, Y. Huang, J. Phys. Chem. C 111 (2007) 15236–15243.

[43] C.S. Blackwell, R.L. Patton, J. Phys. Chem. 92 (1988) 3965–3970.

[44] J. Klinowski, Chem. Rev. 91 (1991) 1459–1479.

[45] T. Cheng, J. Xu, X. Li, Y. Li, B. Zhang, W. Yan, J. Yu, H. Sun, F. Deng, R. Xu, Microporous Mesoporous Mater. 152 (2012) 190–207.

[46] Y. Huang, B.A. Demko, C.W. Kirby, Chem. Mater. 15 (2003) 2437–2444.

[47] M.W.C. Robinson, A.E. Graham, Tetrahedron Lett. 48 (2007) 4727–4731.

[48] U.S.F. Arrozi, H.W. Wijaya, A. Patah, Y. Permana, Appl. Catal. A Gen. 506 (2015) 77–84.

[49] U.S.F. Arrozi, H.W. Wijaya, A. Patah, Y. Permana, Appl. Catal. A Gen. 506 (2015) 77–84.

CHAPTER-V

New Porous high surface area, TiO2 Anatase/SAPO-35 Mild Bronsted acidic Nanocomposite: Synthesis, characterization and studies on its enhanced photocatalytic activity.

Chapter-V

New Porous high surface area, TiO_2 Anatase/SAPO-35 Mild Bronsted acidic Nanocomposite: Synthesis, characterization and studies on its enhanced photocatalytic activity.

V.1. Introduction

Water pollution is one of the major global problem, this is mainly due to the effluents released from factories and other industries like mining, fuel, plastic, fishing and textile manufacturing [1,2].Textile manufacturing industry is one of the major culprit in polluting water by releasing toxic organic and inorganic pollutants[3,4]. To tackle this problemresearchers have been working to find various methods for instance photocatalysis. Photocatalysis is a method in which the selected photocatalysts absorb the photons from the light source and degrades the organic/inorganic pollutants by generating electron-hole pairs[5–7]. Researchers have developed various photocatalysts in which, Metal oxide based semiconductors are widely studied for the application of environmental protection such as polluted water treatment. Among these various oxide semiconductor photo catalysts, TiO_2 is one of the most fascinating photo catalyst, because it is cost effective, thermally stable, possess excellent optical properties and efficient in degrading toxic organic/inorganic pollutants[8–10]. Though TiO_2 has excellent features, it has limitations in the photo degradation process, i.e. larger band gap of 3.2 eV and high recombination rate which limits its photocatalytic activity[11]. To overcome these limitations, TiO_2 is doped with different materials. It was reported that Si doped TiO_2 nanocomposites exhibit higher photocatalytic efficiency over TiO_2 alone[12–18]. This is because of the enhanced separation of holes and excited electrons. Zeolite materials are well known in supporting photocatalytic materials to enhance photocatalytic efficiency. This is because of their properties like uniform pores, high adsorption and ion-exchange capabilities[19][20]. In the present study, we have utilized a novel microporous mild high surface area, Bronsted acidic SAPO-35 (LEV topology) molecular sieve to increase the photocatalytic performance[21,22]. SAPO-35 is having interesting structure which is in micro level 0.36 x 0.48 nm ring opening pore. It is an eight membered ring framework structure which is built with levyne type cage. This is constructed through single six membered ring (S6R) and double six membered ring (D6R) with different T sites in the framework, these two distribution is expected to be in the 2:1 ratio respectively. The

synthesized materials are characterized elaborately and studied their photocatalytic activity.

V.2. Experimental:

V.2.1. Materials required:

Aluminium isopropoxide ($C_9H_{21}O_3Al$, 98.0%, Aldrich, USA), Orthophosphoric acid (H_3PO_4, 85.0%, S.D.Fine, India), Fumed silica (SiO_2, 99.8% Aldrich, USA), hexamethyleneimine ($C_6H_{12}NH$, 98.0%, Aldrich, USA), Titanium iso propoxide ($C_{12}H_{28}O_4Ti$, 97% Aldrich, USA), 2-Propanol (C_3H_8O, >99% Merk India), Methylene Blue ($C_{16}H_{18}ClN_3S$, Aldrich, USA) all the reagents were used without any further purification.

V.2.2. Synthesis:

Synthesis of anatase TiO_2/SAPO-35 involves three steps. Initial step involves, mixing of 30g of H_2O to 10.86 g of aluminium isopropoxide and stirring for 30 minutes. After formation of a homogeneous slurry, added 3.04 mL of H_3PO_4 to the slurry and the resulting mixture was allowed for aging about 12 h. Then, 3.30 mL of $C_6H_{12}NH$ was added to the above solution with 10 mL of H_2O and allowed for stirring about 30 min. Later 0.453 g of SiO_2 was added for the above solution and stirred further for 30 min and the pH of the final solution is found to be less than 5. The gel composition is Al_2O_3:1.8 P_2O_5:0.3 SiO_2:1.16 HEM: 90 H_2O. The crystallization was carried out hydrothermally at 200 °C for 48 h in 100 cm^3 stainless steel autoclave lined with Teflon, using the above gel. The resulting products were centrifuged and dried at 80 °C overnight and calcined at 550 °C for 8 h in the air atmosphere.

The second step is the synthesis TiO_2 nanoparticles. A known quantity of titanium (IV) isopropoxide was dissolved in calculated amount of 2-propanol. After stirring it vigorously for 5 min, a known mixture of water and 2-propanol was added drop wise to the above solution with a burette under stirring. The final mixture was stirred for about 24 h at room temperature. The solid product was centrifuged, and dried at 80 °C temperature for over night. The obtained amorphous TiO_2 and acetic acid (Ac-OH) mixture are hydrothermally crystallized for about 24 h at 200 °C and calcined at 400 °C to obtain TiO_2 anatase.

The Third step is the synthesis of TiO_2/SAPO-35. In which, the required amount water and SAPO-35 and different weight ratios of TiO_2 anatase were sonicated in a glass beaker for about 30 min, centrifuged and the dried solid product was calcined at 400 °C.

V.2.3. Characterization:

Powder X-ray Diffraction patterns of the synthesized materials were recorded on a Ni filtered Cu Kα (λ = 1.5406 Å) PAN analytical advanced X-ray diffractometer in the scan range 2θ between 6^{o} and 80^{o}. The surface morphology of the prepared samples were studied by FE-SEM-EDX, OXFORD Instruments, INCAx-act. TG/DTA analysis carried out on NETZSCH, STA2500 Regulus in presence Nitrogen atmosphere from room temperature to 1000^{o}C. Nitrogen adsorption–desorption isotherms were obtained on a NOVA 1000 Ver.3.7 system at 77 K. FT-IR spectra recorded by PerkinElmer Spectrum with KBr pellet technique in the range of 400 to 4000 cm^{-1}. X-ray Photoelectron spectroscopic (XPS) analysis are carried out using Thermo Fisher Scientific Instrument, UK (Model: K-Alpha+) equipment with Al-Kα anode (1486.6 eV) in transmission lens mode and using a multi-channel plate (MCP) detector. All the MAS-NMR experiments were executed on ECX400-Jeol 400 MHz High Resolution Multinuclear FT-NMR Spectrometer for solids.

The photocatalytic ability of the SAPO, TiO_2/SAPO-35 composites were evaluated by the degradation of Methylene blue under sun-light irradiation, TiO_2 catalytic activity screened under UV light (400W Immersion Hg lamp, 365nm). 100mg of TiO_2 or SAPO-35 or TiO_2/SAPO-35 with 100 mL of 10^{-4} M methylene blue (Absorbtion 655 nm) were used to screen the photocatalytic degradation of methylene blue. In order to attain equilibrium and complete adsorption of methylene blue on the catalysts surface, all the methylene blue solutions were stirred for 30 minutes in the dark condition before performing the photocatalytic activity experiments. Throughout the photocatalytic processes, the sample was intermittently collected, centrifuged to separate the photo catalyst from the solution and analyzed over Perkin Elmer (Lambda 25) UV–Vis spectrophotometer.

V.3. Results and Discussion

V.3.1. Powder X-ray diffraction (PXRD)

The powder X-ray diffraction (PXRD) patterns of the as-synthesised samples were given in Fig.1. In pure SAPO-35 the diffraction patterns are found to be highly intense. The peaks observed at 2 theta values 10.98, 13.36, 17.31, 21.91, 26.61, and 31.96 represents the miller indices (012) (110) (104) (024) (220) and (134) respectively, which are the characteristic alignments of levyne type hexagonal [JCPDS: 51-0052] SAPO-35 crystalline material[23,24]. In case of anatase form of TiO_2, the XRD patterns show peaks

at 2 theta values 25.31, 37.81, 48.08, 54.06, 62.94, 69.04 and 75.30. The corresponding miller indices for these peaks are (101), (004), (200), (105), (211), (220) and (215) respectively. These results have matched well with the characteristic alignments of anatase form of TiO_2 (JCPDS no. 01-086-1157)[25–27]. The XRD results in case of 2:1 ratio of TiO_2/SAPO-35 composite clearly showed the domination of TiO_2 patterns over the SAPO-35 patterns, this is due to the excellent dispersion of TiO_2 on the surface of SAPO-35, as a consequences the SAPO-35 crystal patterns are absent. Whereas, in the case of higher SAPO-35 weight percentages, for instance 1:1 and 1:2 (w/w) TiO_2/SAPO-35 composites the SAPO-35 peaks are considerably stronger. Fig. 1b represents the calibration curve of PXRD patterns of composites, which was established by plotting the intensity of the major TiO_2 peak at 2theta value of 25.31^o of each composite and the corresponding amount of TiO_2 (w/w).

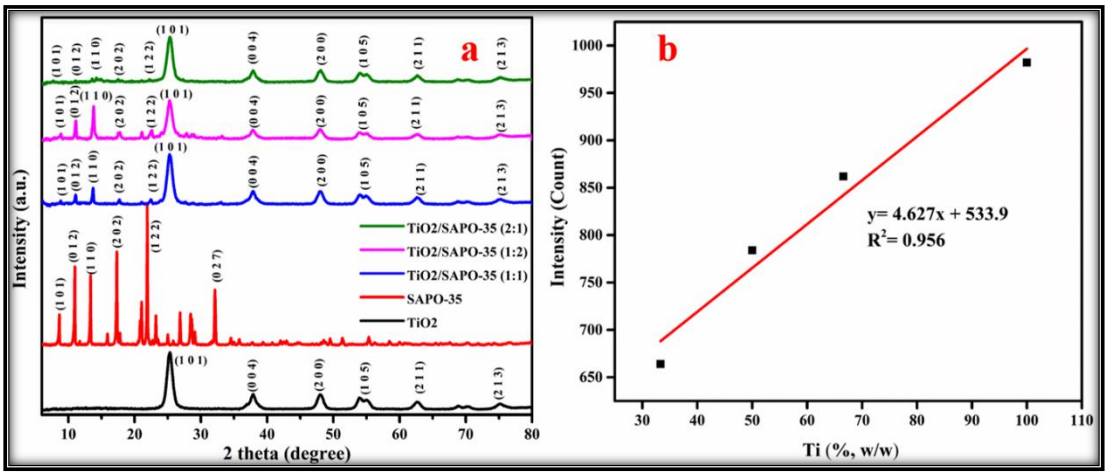

Fig.1a. PXRD patterns of the synthesized compounds, 1b Calibration curve of PXRD patterns TiO_2 and composites

V.3.2. Scanning-Electron-Microscope (SEM):

Fig. 2 represents the morphological studies of the TiO_2 anatase Nano particles (2a), SAPO-35 (2b) and TiO_2/SAPO-35 composite (2c). The FE-SEM of TiO_2 revealed the presence of particles in uniform spherical shape with size, 0.1 – 0.2 µm. The SEM image in case of pure SAPO-35 material which was shown in Fig. 2b indicated that, the crystals present in the sample are of pure rhombohedral shape with an approximate size of 5µm. The SEM image of TiO_2/SAPO-35 composite (Fig. 2c) clearly showed the well dispersed spherical shaped anatase TiO_2 nanoparticles on the surface of rhombohedral SAPO-35. These results were in good agreement with the X-ray diffraction results. EDX analysis of

TiO_2/SAPO-35 (1:1) w/w showed the surface elemental composition as 1.33 Al_2O_3 : 0.67 P_2O_5 : 0.16 SiO_2 : 6.45 TiO_2. The results reveals the surface enrichment with Al and Ti.

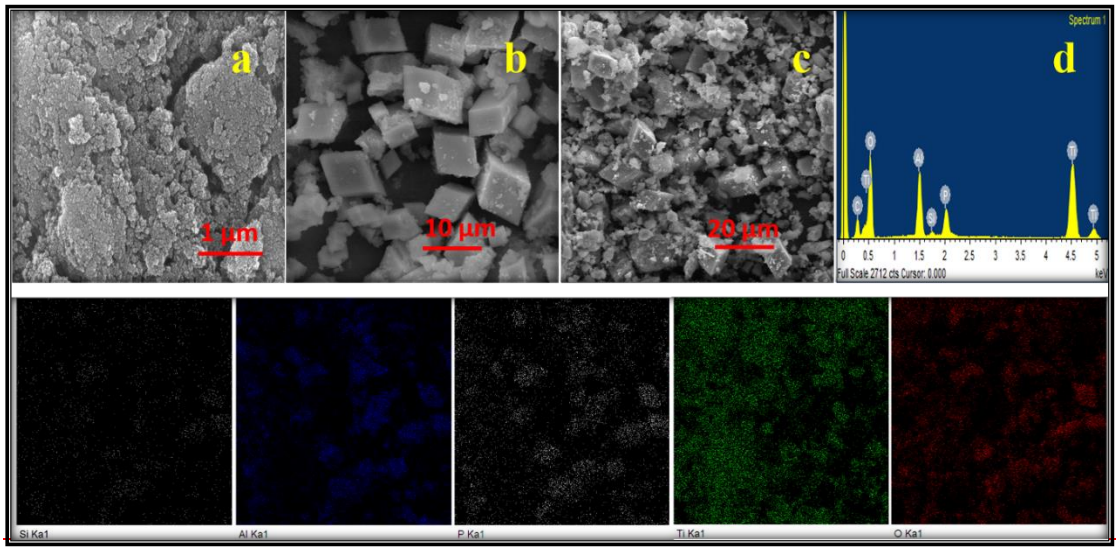

Fig. 2: Morphological studies of a) FE-SEM of anatase form of TiO_2, SEM images of b) SAPO-35 c) TiO_2/SAPO-35 (1:1) w/w d) EDX of TiO_2/SAPO-35 (1:1) w/w and corresponding elemental maps.

V.3.3. Thermogravimetry/Differential thermal analysis (TG/DTA):

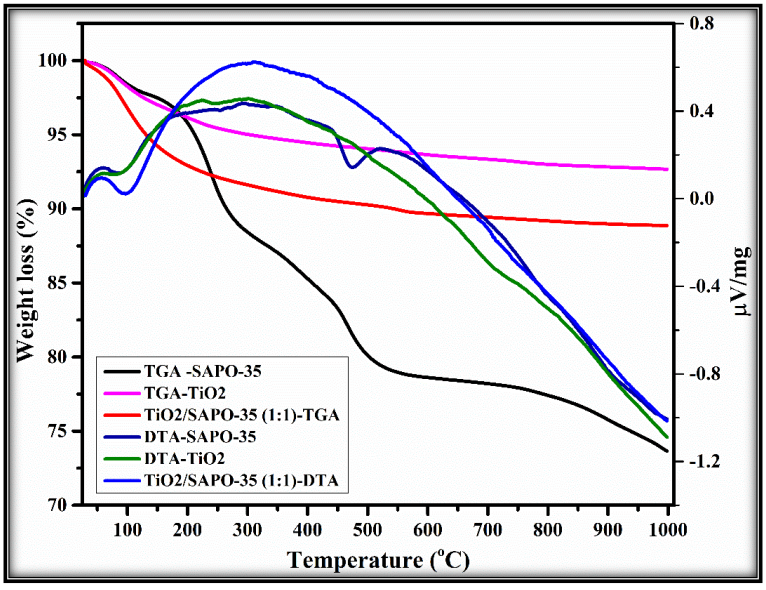

Fig. 3: TG/DTA analysis of the synthesized materials

Thermal stability of the as-synthesized TiO_2, SAPO-35 and TiO_2/SAPO-35 composite has been studied by TG/DTA analysis and the corresponding TGA curves and DTA curves are shown in Fig. 3. From the curves it can observed that, there is an endothermic weight loss around 100 ^oC in all the samples. This weight loss is mainly due to the physisorbed water from the atmospheric moisture [28,29]. The TGA curve in the

case of SAPO-35 comprises of three exothermic weight losses in the range of 100 ^{o}C to 850 ^{o}C, is due to the weight loss of oxidative decomposition of organic template in the SAPO-35 framework as well as the decomposition of unreacted organic species at this temperature range [30,31]. Whereas, the TGA curves of TiO_2 and TiO_2/SAPO-35 composite shows only one exothermic weight loss profile at a range of 550 ^{o}C - 850 ^{o}C. This is may be due to the elimination of chared organics present during prior calcination or partial phase change. In the DTA curves of all the samples at 100 ^{o}C shows endothermic peaks due to the physisorbed water and at 500 ^{o}C in pure SAPO-35 also an endothermic peak was observed due to the decomposition of unreacted organic species.

V.3.4. N_2 adsorption-desorption analysis:

From the BET adsorption isotherms as given in Fig. 4, it can be observed that, the SAPO-35 showed a hysteresis-I profile since it is a microporous material [32,33]. Whereas, the isotherm for TiO_2/SAPO-35 composite showed a hysteresis-IV profile, which is a typical mesoporous material profile [33]. The surface area of TiO2 and SAPO-35 has been studied using Nitrogen adsorption-desorption method. The surface area, pore volume and D_{BJH} of TiO_2 were found to be 85 m^2/g, 0.16 cm^3/g and 57 Å and for SAPO-35, it was found to be 448 m^2/g, 0.22 cm^3/g and 19 Å. However, for TiO_2/SAPO-35 nanocomposite, it is 222 m^2/g,0.20 cm^3/g and 28 Å which is significantly lesser than the SAPO-35. This decrease in surface area can be explained by the fact that, the TiO_2 particles were dispersed on the surface of SAPO-35, as a consequence, the available surface area got minimized. These results were in accordance with PXRD studies results.

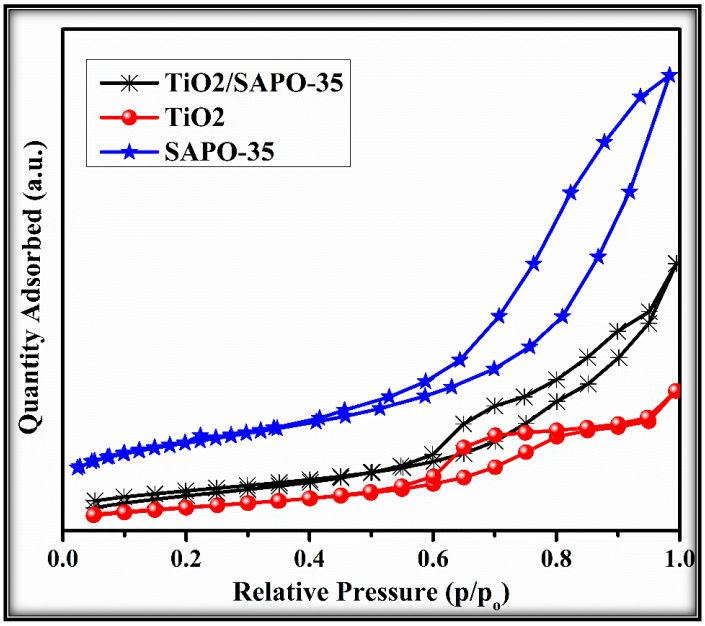

Fig. 4: Nitrogen adsorption-desorption isotherms of the synthesized materials

V.3.5. Fourier Transform Infrared (FT-IR) spectroscopic analysis

The synthesized 1:1 (w/w) TiO_2/SAPO-35 composite, along with TiO_2, and SAPO-35 are characterized by FT-IR spectroscopic as illustrated in Fig. 5. From the analysis of these spectra it has been observed that, a broad band below 1000 cm^{-1} i.e. at 770 cm^{-1} in pure TiO_2, at 490 cm^{-1} in pure SAPO-35 and at 757 cm^{-1} for TiO_2/SAPO-35 composite, were attributed to the T-O-T (T= Ti, Si, Al and P) linkage symmetric stretching frequency[34,35]. A sharp peak observed at 2362 cm^{-1} in 1:1 TiO_2/SAPO-35 composite spectrum corresponds to CO_2 stretching vibrations, which was absorbed by the composite from the atmosphere[36]. A broad band appeared at 1087 cm^{-1} in the pure SAPO-35 and 1:1 TiO_2/SAPO-35 composite spectra, is mainly because of the internal, external asymmetric and symmetric stretching vibrations of the double ring vibrations present in T–O–T linkage of SAPO-35 framework. A broad band appeared in the range of 3200-3400 cm^{-1} in all the spectra is assigned to the –OH stretching vibrations of absorbed water molecules from the atmosphere [37].

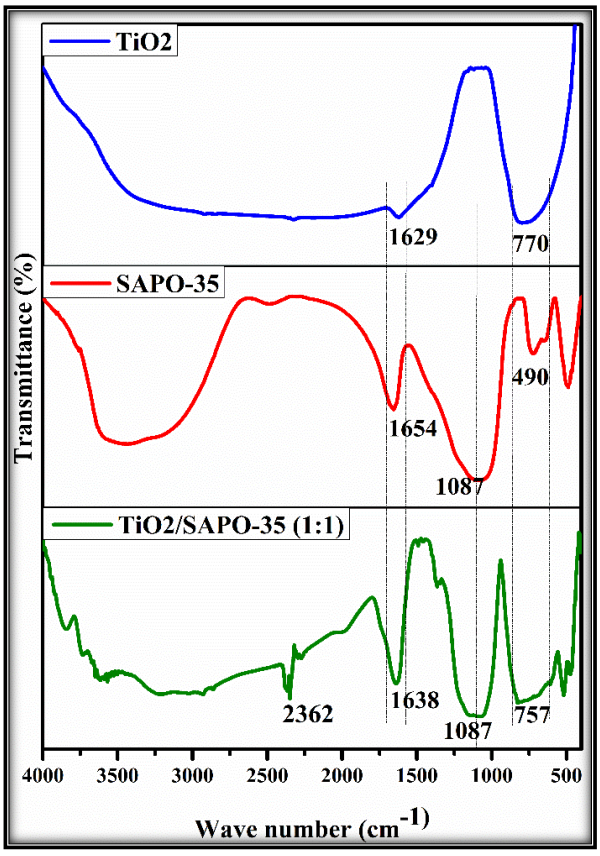

Fig. 5: Fourier Transform Infrared Spectroscopy of the calcined samples

V.3.6. X-ray Photoelectron Studies (XPS):

The XPS spectra of 1:1 TiO_2/SAPO-35 are depicted in Fig. 6. Fig. 6a spectrum consists of peaks for Titanium, Silicon, Aluminium, Phosphorous and oxygen. These are the constituent elements of the composite under study. Fig. 6(b-f) represents the deconvolution spectra for the elements Titanium, Aluminium, Silicon, Phosphorous and Oxygen, respectively. From the deconvolution spectrum of Titanium which is shown in Fig. 6b, there are two different peaks appeared at 460.4 eV and 466.1 eV, due to Titanium present in two different tetrahedral environments. The former peak in this spectrum represents the 2p 3/2 state, the later peak represents the 2p 1/2 state. In general, the 2p 3/2 state peak will be interpreted to study the respective element. Moreover, from the literature reports, the peak appeared in the range of 460.4 eV $\pm$2 eV will be because of Ti present in the form of Ti(IV) oxidation state. Hence, the peak at 460.4 eV in the present spectrum emphasizes the presence of Ti(IV) in the TiO_2/SAPO-35 composite[38,39]. The deconvolution spectrum of Silicon as is shown in Fig. 6d, only one peak is appeared at 103.3 eV. This peak is assigned to Si 2p 3/2 state. From the literature values the peak at 103.3 eV is assigned to silicon present in +4 oxidation state [40–42] in tetrahedral co-ordination. Hence, the silicon present in the TiO_2/SAPO-35 composite is confirmed as Si (IV) form. However S6R and D6R silicon are could not be differentiated.

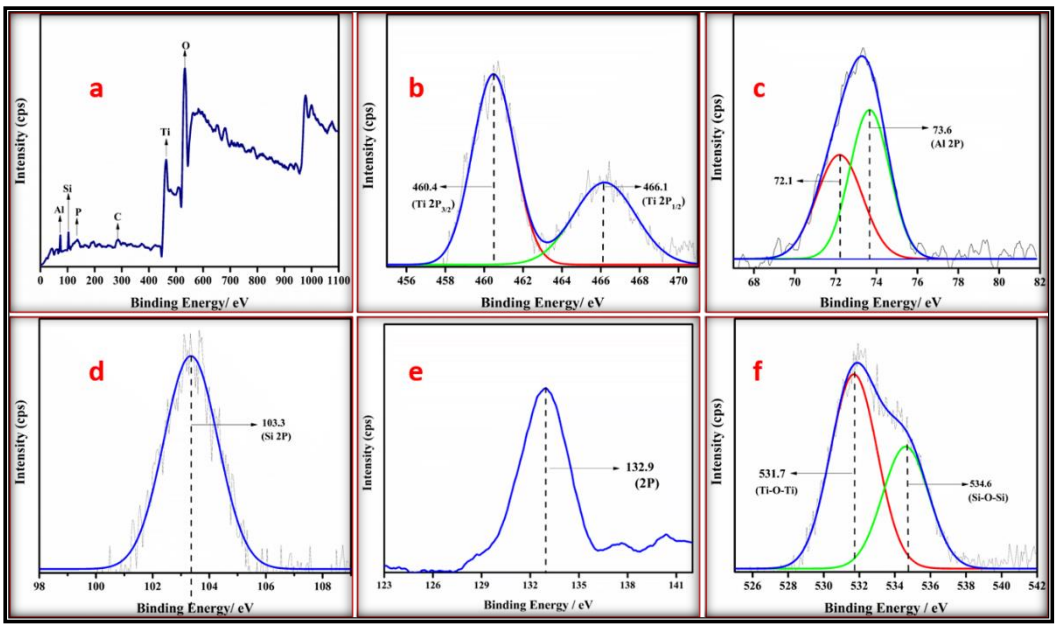

Fig. 6: XPS spectra of TiO_2/SAPO-35

Fig. 6c signifies the Aluminium deconvolution spectrum. In this spectrum we have observed two different peaks, one at 72.1 eV and the other one at 73.6 eV. The first peak at lower binding energy value is assigned to Al 2p 3/2 state and the second peak at higher

binding energy value is assigned to Al 2p 1/2 state[40,41]. General interpretation will be for 2p 3/2 peak is to analyse the respective element. From the literature Al 2p 3/2 peak at 72.1±0.1 eV represents the aluminium in +3 oxidation state. Therefore, aluminium present in the 1:1 composition is in Al (III) state. The deconvolution spectrum of Phosphorous shown in Fig. 6e contains only one peak at a binding energy value of 132.9 eV, which is of 2p 3/2 spin state of phosphorous. From the literature reports peak at 133 eV will represent the phosphorous in +5 oxidation state. Therefore, the phosphorous present in the composite is in the form of P(V)[40,41]. Fig. 6f depicts the O1s XPS deconvolution spectrum, in which we have observed two different peaks mainly 531.7 eV and 534.6 eV respectively. Based on the literature reports the former peak at lower binding energy value (i.e. 531.7 eV) is formed because of oxygen in the form of O^{2-} present in Ti-O-Ti bonding of the composite. The later peak at higher binding energy value (i,e. 534.6 eV) is because of the oxygen in the form of O^{2-} present in Si-O-Si bonding in the composite[43–45].

V.3.7. MAS – NMR spectroscopic analysis

The MAS-NMR studies were carried out to evaluate the local environment of the synthesized TiO_2 Anatase/SAPO-35 material and the results are shown in Fig. 7. From the ^{27}Al MAS-NMR spectrum, two peaks were observed, one strong intense peak at 41.3 ppm and a weak peak at 13.99 (≈14). These two represents the Al in tetrahedral and octahedral co-ordination, to be precise as $Al(OP)_4(OH)_2$[28]. From the ^{31}P MAS-NMR spectrum, it is found that two intense peaks were observed close to each other at -25.5 ppm and -31.7 ppm [46]. These two peaks represent Phosphorous present in $P(OAl)_4$ tetrahedral atmosphere in SAPO-35 framework. From the ^{29}Si MAS-NMR spectrum, we have observed four peaks one at -87.1, the other one at -91.4 ppm and a third and fourth shoulder peaks around 80 ppm probably due to Si surrounded by four Ti species. The other two peaks are assigned to Si in tetrahedral position as $Si_{T1}(OAl)_4$ and $Si_{T2}(OAl)_4$. From these MAS-NMR results, it can be emphasized that the nanocomposites are having Ti and Si in tetrahedral environment. The PXRD and SEM studies are also supports this results.

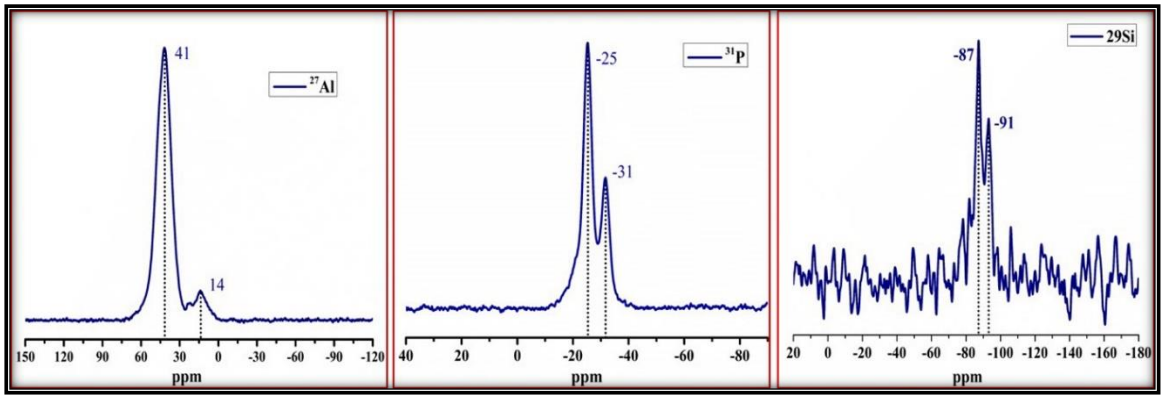

Fig. 7: MAS-NMR of Anatase TiO_2/SAPO-35 (1:1) w: w

The optical properties of the synthesized SAPO-35, TiO_2 and TiO_2/SAPO-35 composites were screened and presented in the Fig. S1 (UV-vis-DRS spectra) and Fig. S2 (Photo Luminescence spectra). From UV-vis-DRS spectra it is found that, there is a band edge shift towards higher wavelength for the composite materials from TiO_2 band edge. These results strongly reveal that the recombination rate of electron and hole pair was reduced, which is in accordance with the results of photo luminescence spectra (Fig. S2).

V.3.8. Dye degradation Studies:

The ability of TiO_2, SAPO-35, and TiO_2/SAPO-35 composite materials in degrading the methylene blue dye under sunlight irradiation condition has been studied. Initially, the degradation of methylene blue was studied under sunlight irradiation without any catalyst. This result has indicated that, there is no degradation of methylene blue took place under sunlight irradiation in the absence of any catalyst. In order to attain equilibrium and complete adsorption of methylene blue on the catalysts surface, all the methylene blue dye solutions were stirred for 30 minutes in the dark condition before performing the photocatalytic activity experiments. From the activity results, it is found that the TiO_2/SAPO-35 composite materials exhibited higher activity in degrading methylene blue under sunlight irradiation compared to the pure TiO_2 and pure SAPO-35. Moreover, among different weight ratios of composites, the 1:1 ratio TiO_2/SAPO-35 composite obtained highest Photocatalytic activity by means of degrading methylene blue completely in just 25 minutes. Whereas, the 1:2 ratio TiO_2/SAPO-35 composite and 2:1 ratio TiO_2/SAPO-35 composite could degrade the methylene blue in 50 minutes and 60 minutes respectively. The time for pure TiO_2 particles to degrade the methylene blue completely was found to be almost 90 min under UV light irradiation. Whereas, SAPO-35 was not able to degrade the methylene blue even after 120 minutes under sunlight irradiation.

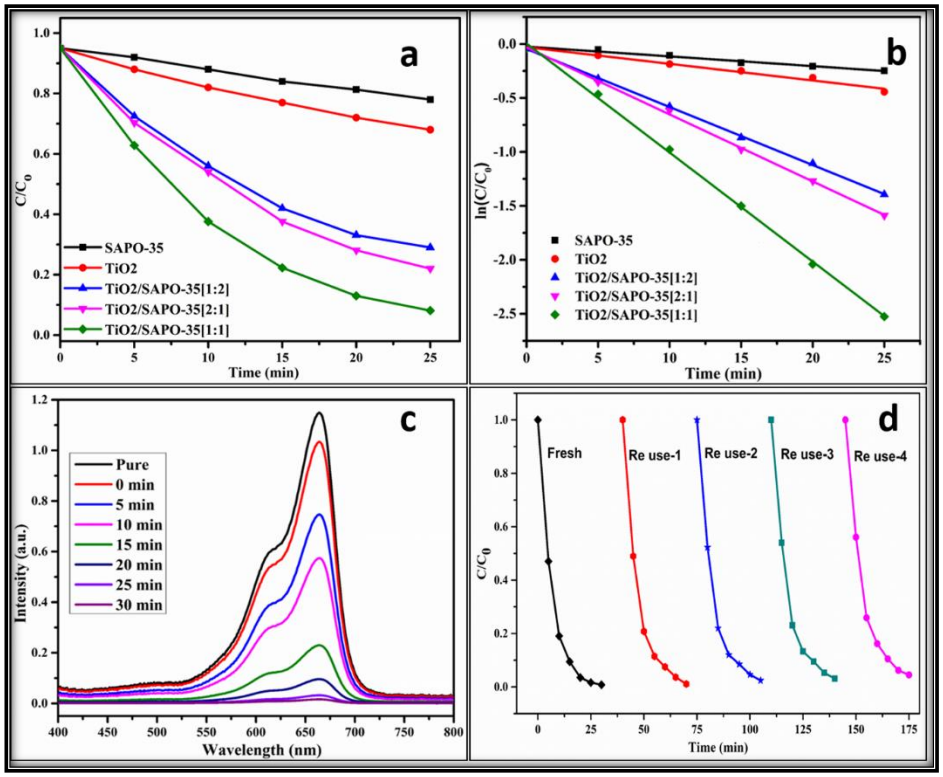

Fig. 8: Photocatalytic application a) Comparison of the photocatalytic activities of the SAPO-35, TiO_2 and TiO_2/SAPO-35 composites b) Kinetic plots of respective compounds c) UV-Visible spectrum of TiO_2/SAPO-35 [1:1] composite and d) Re-usability test of TiO_2/SAPO-35 [1:1] composite

The photocatalytic activity, kinetics and Re-usability tests of the SAPO-35, TiO_2 and TiO2/SAPO-35 are depicted in the graphs given in Fig. 8. The 1:1 TiO_2/SAPO-35 composite activity (8a) was found to be very fast, this may be because of higher number of synergetic active sites available due to the equal weight ratios of TiO_2 and SAPO-35, increasing of any of the weight ratios may lead to the decreasing in the active sites of the other, hence the time to degrade the methylene blue concentration is increasing. Stability and re-usability of the composite have been studied and given in Fig. 8d. From these results it is very clear that the composite was more stable and we can reuse even after four successive cycles. The typical reusability procedure as follows, initially 100 mg of calcined catalyst was taken into a beaker and 5 ppm methylene dye solution and allow stirring for 30 min in a dark room and photocatalytic activity has been studied under direct sunlight, after that from this mixture filtered the catalyst and repeated four times successfully. There is no catalyst loss at all and the efficiency of the catalyst is very good, even after four cycles the catalyst is showing nearly 80% degradation.

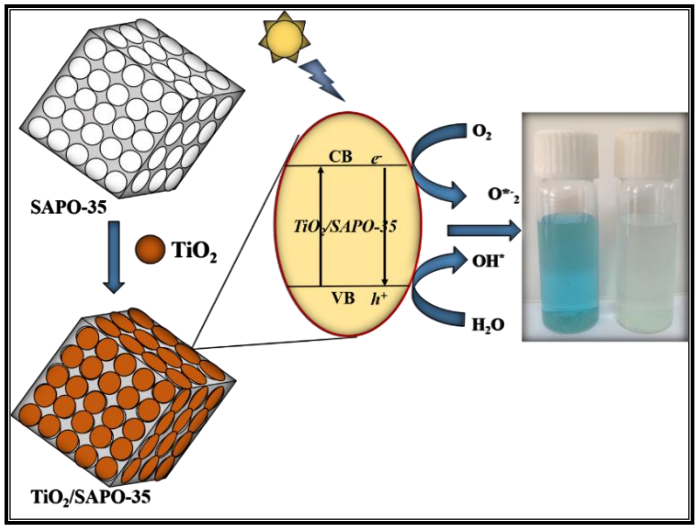

Fig. 9 : Physical photocatalytic reaction mechanism of TiO_2/SAPO-35.

Hence, from all the above analyses, the plausible mechanism of photocatalysis is depicted in Fig. 9. The band gap of TiO_2 is 3.2. Where, SAPO-35 is not having any band gap. In combination of this two will not change the band gap, however it will change the surface area as SAPO-35 surface area is more. Further, SAPO-35 is mild Bronsted acidic. It means a hydrogen donor/acceptor. Which will have the synergetic activity of the organics degradation. The methylene blue is degraded to small environmentally unharmful chemicals like CO_2, H_2O and NH_3.

V.3.9. Detection of reactive species

To know the pathway of methylene blue dye degradation with the TiO_2/SAPO-35 composite, we further investigated under direct sun light irradiation by trapping holes (h^+) hydroxyl radicals ($^{\cdot}OH$), super oxide anion radicals (O_2^{-2}) using various quenchers like Ammonium oxalate (OA), tertiary butyl alcohol (^{t}Bu-OH), Benzoquinone (BQ) respectively. From these results it confirmed that hydroxyl radicals are major responsible for the Methylene Blue dye degradation. From fig 10a it is clearly evidenced that, in case of TBA as scavenger the photocatalytic activity remarkably supressed compared to without scavenger (TiO_2/SAPO-35). In case of OA and BQ lesser suppression of photo degradation compared to the TBA. So from these results we conclude that the OH radicals are the major reactive spices for the enhancement of the photocatalytic activity of methylene blue dye. To trap the generated OH radicals which are main reactive spices for the photocatalytic activity, we used Teri phthalic acid (TA) as probe using photoluminescence spectra. The resulting product of TA is 2-hydroxyterephthalic acid, when it reacts with OH radicals which are generated during the photo degradation which

was highly fluorescent product. From Fig. 10b, the photoluminescence spectra observed the maximum intensity of the peaks is 435 nm and an excitation wavelength is about 400 nm, it reveals that the formation of OH radicals during the photocatalytic oxidation process, which is in alignment with the results of ^{t}Bu-OH quenching in fig 10a, also it witnessed that the photoluminescence intensity increases gradually with the increasing irradiation time, which reveals that OH radicals are definitely generated on the direct sunlight irradiation on the surface of TiO_2/SAPO-35.

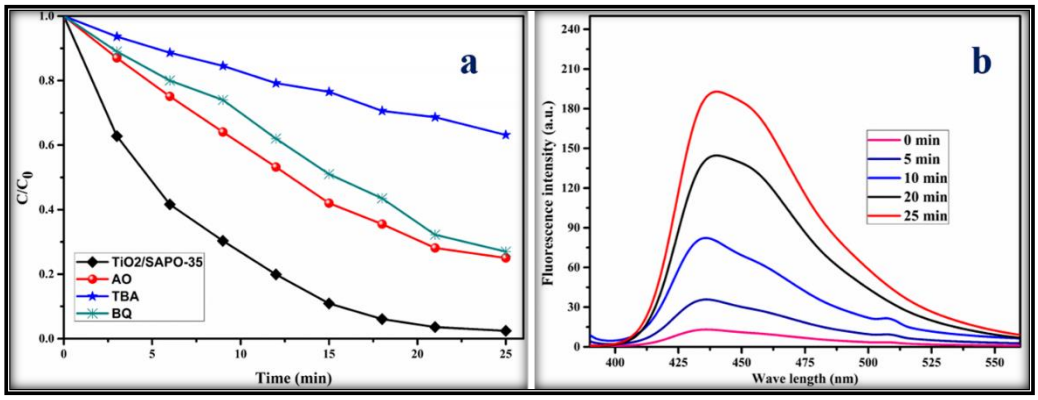

Fig.10 a) Effect of scavengers on photocatalytic degradation of methylene blue under direct sunlight irradiation b) Photo Luminescence Spectra of OH radical trapping of TiO2/SAPO-35 in TA under direct sunlight irradiation

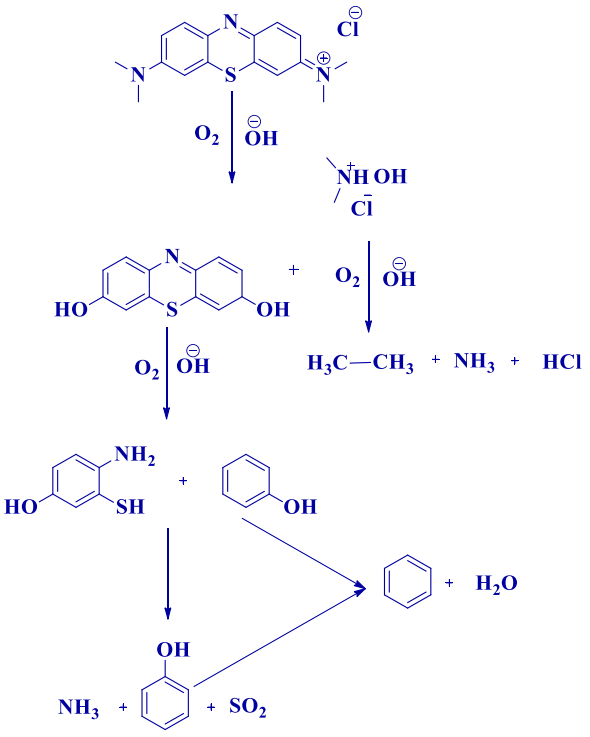

Plausible degradation pathway of methylene blue

V.4. Conclusions:

TiO_2 anatase and Microporous Silicoaluminophosphate (SAPO-35) have been synthesized by hydrothermal method. The different (w/w) ratio of TiO_2/SAPO-35 composites were prepared through sol-gel procedure. The synthesized materials are characterized in detail. The ability of these composites in degrading methylene blue has been studied under sun light irradiation. The results have shown, TiO_2/SAPO-35 composite shows excellent dye degradation ability compared to TiO_2 and SAPO-35 independently. The fine dispersion of TiO_2 anatase Nano particles on the surface of the microporous SAPO-35 resulted in the increased ability of dye degradation. As a consequence of this phenomenon, the recombination rate of electron-hole pair of these materials has minimised. All these results revealed the existence of a synergistic relation between TiO_2 and SAPO-35 in degrading methylene blue.

V.5. References

[1] J. Schneider, M. Matsuoka, M. Takeuchi, J. Zhang, Y. Horiuchi, M. Anpo, D.W. Bahnemann, Chem. Rev. 114 (2014) 9919–9986.

[2] H. Tong, S. Ouyang, Y. Bi, N. Umezawa, M. Oshikiri, J. Ye, Adv. Mater. 24 (2012) 229–251.

[3] R. Kant, Nat. Sci. 04 (2012) 22–26.

[4] http://sewreview.com/blog/water-pollution-and-the-textile-industry, (n.d.).

[5] A.K. Adepu, S. Goskula, S. Chirra, S. Siliveri, S.R. Gujjula, N. Venkatathri, J. Porous Mater. (2019).

[6] Y. Duan, J. Luo, S. Zhou, X. Mao, M. Wajid, F. Wang, Z. Chen, C. Wang, Appl. Catal. B Environ. 234 (2018) 206–212.

[7] K. Hashimoto, H. Irie, A. Fujishima, Jpn. J. Appl. Phys. 44 (2005) 8269–8285.

[8] A. FUJISHIMA, K. HONDA, Nature 238 (1972) 37–38.

[9] L. Ren, Y. Li, J. Hou, X. Zhao, C. Pan, ACS Appl. Mater. Interfaces 6 (2014) 1608–1615.

[10] W. Fan, Q. Lai, Q. Zhang, Y. Wang, J. Phys. Chem. C 115 (2011) 10694–10701.

[11] N. Roy, Y. Sohn, D. Pradhan, ACS Nano 7 (2013) 2532–2540.

[12] A. Kumar, K.L. Reddy, S. Kumar, A. Kumar, V. Sharma, V. Krishnan, ACS Appl. Mater. Interfaces 10 (2018) 15565–15581.

[13] A. Kumar, C. Schuerings, S. Kumar, A. Kumar, V. Krishnan, Beilstein J. Nanotechnol. 9 (2018) 671–685.

[14] K.L. Reddy, S. Kumar, A. Kumar, V. Krishnan, J. Hazard. Mater. 367 (2019) 694–705.

[15] A. Kumar, S. Kumar, A. Bahuguna, A. Kumar, V. Sharma, V. Krishnan, Mater. Chem. Front. 1 (2017) 2391–2404.

[16] A. Kumar, K. Kumar, V. Krishnan, Mater. Lett. 245 (2019) 45–48.

[17] I. Singh, B. Birajdar, RSC Adv. 7 (2017) 54053–54062.

[18] A. Kumar, V. Sharma, S. Kumar, A. Kumar, V. Krishnan, Surfaces and Interfaces 11 (2018) 98–106.

[19] Y. Zheng, X. Li, P.K. Dutta, Sensors 12 (2012) 5170–5194.

[20] B.M. Lok, C.A. Messina, R.L. Patton, R.T. Gajek, T.R. Cannan, E.M. Flanigen, J. Am. Chem. Soc. 106 (1984) 6092–6093.

[21] S.H. Ahn, H. Lee, S.B. Hong, Chem. Mater. 29 (2017) 5583–5590.

[22] I. Pinilla-Herrero, U. Olsbye, C. Márquez-Álvarez, E. Sastre, J. Catal. 352 (2017) 191–207.

[23] N. Venkatathri, S.G. Hegde, United States Patent: US 7,037,874 B2, 2006.

[24] X. Zhao, W. Duan, Q. Wang, D. Ji, Y. Zhao, G. Li, Microporous Mesoporous Mater. 275 (2019) 253–262.

[25] S. Bellatreche, A. Hasnaoui, B. Boukoussa, J. García-Aguilar, Á. Berenguer-Murcia, D. Cazorla-Amoros, A. Bengueddach, Res. Chem. Intermed. 42 (2016) 8039–8053.

[26] O. Jongprateep, R. Puranasamriddhi, Mater. Today Proc. 5 (2018) 10925–10931.

[27] E. Molero, B. Ferrari, A.J. Sanchez-Herencia, E. Gordo, P. Colombo, Adv. Eng. Mater. 19 (2017) 1600700.

[28] N. Venkatathri, S.G. Hegde, P.R. Rajamohanan, S. Sivasanker, J. Chem. Soc. Faraday Trans. 93 (1997) 3411–3415.

[29] M. Fan, H. Panezai, J. Sun, S. Bai, X. Wu, J. Phys. Chem. C 118 (2014) 23761–23767.

[30] R. Yadav, M. Ahmed, A.K. Singh, A. Sakthivel, Sci. Rep. 6 (2016) 22813.

[31] S. Suresh, I.A.K. Reddy, N. Venkatathri, Microporous Mesoporous Mater. 263 (2018) 275–281.

[32] C. Tropp, Chinese J. Catal. 34 (2013) 798–807.

[33] S. Storck, H. Bretinger, W.F. Maier, Appl. Catal. A Gen. 174 (1998) 137–146.

[34] S. Ashtekar, S.V. V Chilukuri, D.K. Chakrabarty, J. Phys. Chem. 98 (1994) 4878–

4883.

[35] N. Venkatathri, J.W. Yoo, Appl. Catal. A Gen. 340 (2008) 265–270.

[36] P.A. Gerakines, W.A. Schutte, J.M. Greenberg, E.F. van Dishoeck, Astron. Astrophys. 296 (1994) 1–17.

[37] S. Chirra, N. Venkatathri, Mater. Res. Express 6 (2018) 015021.

[38] K. Kočí, M. Reli, I. Troppová, M. Šihor, J. Kupková, P. Kustrowski, P. Praus, Appl. Surf. Sci. 396 (2017) 1685–1695.

[39] M.C. Biesinger, L.W.M. Lau, A.R. Gerson, R.S.C. Smart, Appl. Surf. Sci. 257 (2010) 887–898.

[40] R.B. Borade, A. Clearfield, J. Mol. Catal. 88 (1994) 249–265.

[41] S.L. Suib, A.M. Winiecki, A. Kostapapas, Langmuir 3 (1987) 483–488.

[42] S. Chirra, S. Siliveri, A.K. Adepu, S. Goskula, S.R. Gujjula, V. Narayanan, J. Porous Mater. (2019).

[43] Z. Song, J. Hrbek, R. Osgood, Nano Lett. 5 (2005) 1327–1332.

[44] T.L. Barr, Zeolites 10 (1990) 760–765.

[45] T.L. Barr, M.A. Lishka, J. Am. Chem. Soc. 108 (1986) 3178–3186.

[46] A.M. Prakash, M. Hartmann, L. Kevan, Chem. Mater. 10 (1998) 932–941.

CHAPTER-VI

Pd/SAPO-35: Synthesis, Characterization and its Catalytic application studies on Suzuki-Miyaura Cross Coupling Reaction.

Chapter-VI

Pd/SAPO-35: Synthesis, Characterization and its Catalytic application studies on Suzuki-Miyaura Cross Coupling Reaction.

VI.1. Introduction

In the scientific fraternity the role of porous materials has been drastically increased since last two decades[1,2]. Due to the special properties like high surface area, uniform and well-defined pore size, pore distribution, geometries, compositions and selective adsorption ability of porous materials many chemists and scientists are showing interest towards this microporous materials synthesis and their commercial applications[3,4]. These porous materials are classified into three based on the pore size these are microporous, mesoporous and macro porous. Each of these three porous materials have their own applications. The current trend in the scientific fraternity is energy storage like H_2, CO_2 and different catalytic applications by using these porous materials[5,6]. We are interested in the microporous materials because microporous materials are easy to prepare, thermally highly stable and having high surface area with ordered porous distribution [7]. Zeolites are the best examples for the microporous materials like CHA, LEV type topological framework structures[8].

In the modern chemistry Pd catalyzed C-C bond formation organic reactions like Heck, Suzuki Miyaura coupling are most important and useful reactions [9–12]. In the year, 2010 noble prize awarded for this reaction speaks the significance of this reaction. The resulting products of Suzuki Miyaura coupling reactions are bi-aryls [13,14]. These are the most essential ingredients of the many pharmaceuticals also in agrochemical fertilizers and natural products etc., The catalyst for Suzuki-Miyaura coupling reaction has been extensively studied with homogeneous and reported with high turnover number and yields but the major disadvantage of using homogenous catalyst is separation of the catalyst and reuse of it for multiple times [14,15]. To overcome this problems researcher are focusing on development in heterogeneous catalysts with the same turnover numbers and high yield along with reusing capacity [16].

In chemical reactions usage microwave irradiation is the new trend over the globe to minimize the energy and environment friendly which is showing great results in the fastest reactions and higher yields as well [17,18]. The interesting thing about using microwave

irradiation reaction, reactions are solvent free which is the most important aspect to avoid the wastage of the organic solvents and resulting products are simplified [19,20].

In the present work, we have studied the synthesis of Pd/SAPO-35 using hydrothermal followed by borohydride reduction method and various physico-chemical properties of prepared samples are characterized by various advanced analytical techniques. Catalytic activity was screened by using Suzuki-Miyaura Cross Coupling reaction of Benzeneboronic acid in different conditions and details are given in detail.

VI.2. Experimental

VI.2.1. Sample preparation

Al isopropoxide (Al (OCH_3H_7)$_3$) as Al source 98% Sigma Aldrich, USA, Orthophospharic acid (H_3PO_4), as the P source 85% S.D. Fine India, Fumed Silica (SiO_2) as the Si source 99.8% Sigma Aldrich, USA, Hexamethyleneimine ($C_6H_{12}NH$) as the structure directing agent 98% Sigma Aldrich, USA, $PdCl_2$ 99.8% Sigma Aldrich, USA, as the Pd source, $NaBH_4$, $C_6H_7BO_2$ 98% Avra Chemicals India, K_2CO_3 Finar Ltd, India, are used for the present work without any further purification.

SAPO-35 synthesis procedure as follows, initially 10.86 g of Al isopropoxide and 30 mL of water are taken into a clean beaker and stirred at 450 rpm about 1 h to obtain homogeneous solution. To this solution, 3.04 mL H_3PO_4 was added drop-by-drop and allowed stirring up to 12 h to form $AlPO_4$-. In another clean beaker 3.30 mL Hexamethyleneimine (HEM) solution and 0.453 g of SiO_2 fine powder as taken and mixed well with a glass rod and added to the $AlPO_4$- solution and added 10 mL of water further stirred 30 more minutes and transferred into a Teflon lined hydrothermal autoclave capacity of 100 cc. The over was programmed at 200 °C about 24 h with ramp rate of 2 °C per minutes. After 24 h program the prepared solution was centrifuged and washed with distilled water dried at ambient temperature overnight. The resulting product was collected and calcined at 550 °C about 8 h.

Pd/SAPO-35 material was prepared using the borohydride reduction process. In the first step $PdCl_2$ was taken into a beaker and did ultra-sonication in water bath about 1 h at 50 °C temperature. On the other side already prepared SAPO-35 was taken into another beaker with double distilled water and stirred the solution about 1 h, to this solution the $PdCl_2$ was added slowly under vigorous stirring. Now Aqueous $NaBH_4$ solution was prepared (Pd: $NaBH_4$ – 1:70 w/w ratio) and added to the above resulting mixture in drop by drop up to 15-

20 minutes and allowed the resulting mixture around 10 h. After the above process solution was washed with double distilled water, acetone and filtered dried at ambient temperature overnight. By following this procedure, we prepared Pd/SAPO-35 three different weight ratios (3:1, 5:1, 10:1).

VI.2.2. Characterization

Powder X Ray diffraction (PXRD) patterns were recorded on a PAN analytical advance X Ray diffractometer using Ni filtered using Cu Kα (λ=1.5064 A°) radiation in a 2Θ scan range between 6° to 80°. The morphological features are investigated by field emission scanning electron microscopy-energy dispersive spectroscopy (FE-SEM-EDX; OXFORD Instruments, INCAx-act). FT-IR spectra were recorded by PerkinElmer Spectrum 100 FT-IR spectrophotometer by using the KBr pellet technique in the range of 400–4000 cm^{-1}. N_2 adsorption–desorption isotherms studied on a NOVA.1000 Version 3.7 system at 77 K. A small amount of the calcined catalyst was placed in the sample cell. After degassing step, N_2 physisorption was carried out for measuring surface area. The BET equation was used to calculate specific surface area, SBET. X-ray Photoelectron spectroscopic (XPS) analysis are carried out using Thermo Fisher Scientific Instrument, UK (Model: K-Alpha+) equipment with Al-Kα anode (1486.6 eV) in transmission lens mode and using a multi-channel plate (MCP) detector. Electrochemical measurements were carried out using CHI 619d (CH International, USA) electrochemical analyzer and All electrochemical measurements were carried out at room temperature of ca. 25 °C.

VI.3. Results and Discussion

VI.3.1. Powder X-ray diffraction (PXRD)

All the synthesized samples were tested by powder X-ray diffraction (PXRD) to know the crystalline nature of the samples and the results are shown in Fig. 1a. From these PXRD patterns in SAPO-35 sample, the peaks appeared at 2 theta value of 10.9, 13.3, 17.3, 21.9, 26.6, and 31.6 which are corresponding miller indices (0 1 2) (1 1 0) (1 0 4) (0 2 4) (2 2 0) and (1 3 4) respectively. From these findings it is confirmed that Levyne type hexagonal crystalline material of SAPO-35 [JCPDS: 51–0052] [4,21,22]. In Pd/SAPO-35 samples 3, 5, 10 (w/w %) all the peaks of SAPO-35 material and the Pd peak was appeared at 2 theta value of 39.5 which conforms the Pd presence in the materials [23]. Fig. 1b represents the PXRD calibration curve

of the Pd/SAPO-35 sample. This is plotted by Pd peak intensity at the 2-theta value of 39.5° of the individual w/w % of each composite.

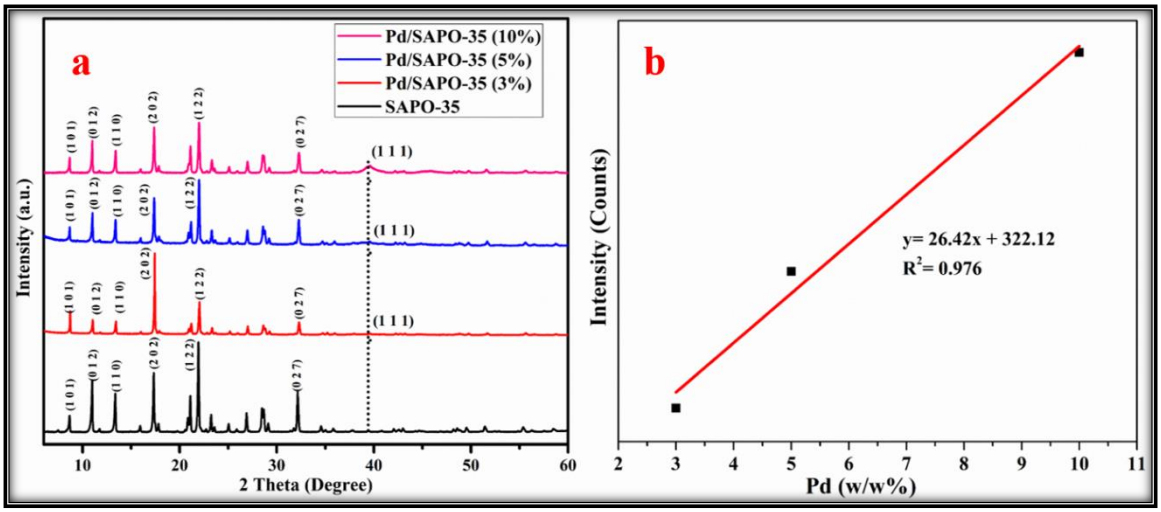

Figure 1a PXRD of the samples and 1b) Calibration curve of Pd/SAPO-35 materials.

VI.3.2. FE-SEM analysis

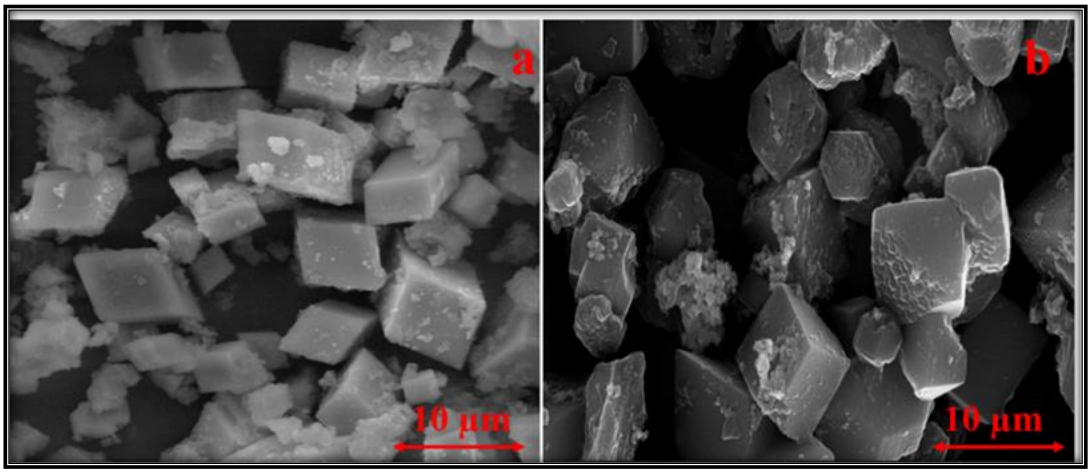

Figure 2a: SEM image of SAPO-35and 2b) FE-SEM image of Pd/SAPO-35 (10 w/w %)

Morphological features of as-synthesized SAPO-35 were observed by field emission scanning electron microscopy and the results are shown in the Fig 2a and 2b. From these figures it was found that the products SAPO-35 and Pd/SAPO-35 are in a pure form highly crystalline nature uniform size and shape, and we didn't notice any other irregular shaped impurities. All the particles are in rhombohedra with the particle size of 5µm. As the Pd particles are in Nano size we didn't notice the Pd particles from these FE-SEM images, so we

did EDX analysis and Elemental mapping and the results were shown in the Fig. 3. From EDX results the pure SAPO-35 consists of 2.66: 14.91:15.70 Si, Al, and P respectively atomic percentage whereas the Pd/SAPO-35 having the 2.55: 14.79: 13.70: 1.33 Si, Al, P and Pd respectively atomic percentage. From Fig. 3 we can clearly observe the elemental mapping for Pd/SAPO-35, after loading Pd the Pd presence we can clearly notice in the mapping results, these results are correlating with the X-ray diffraction results.

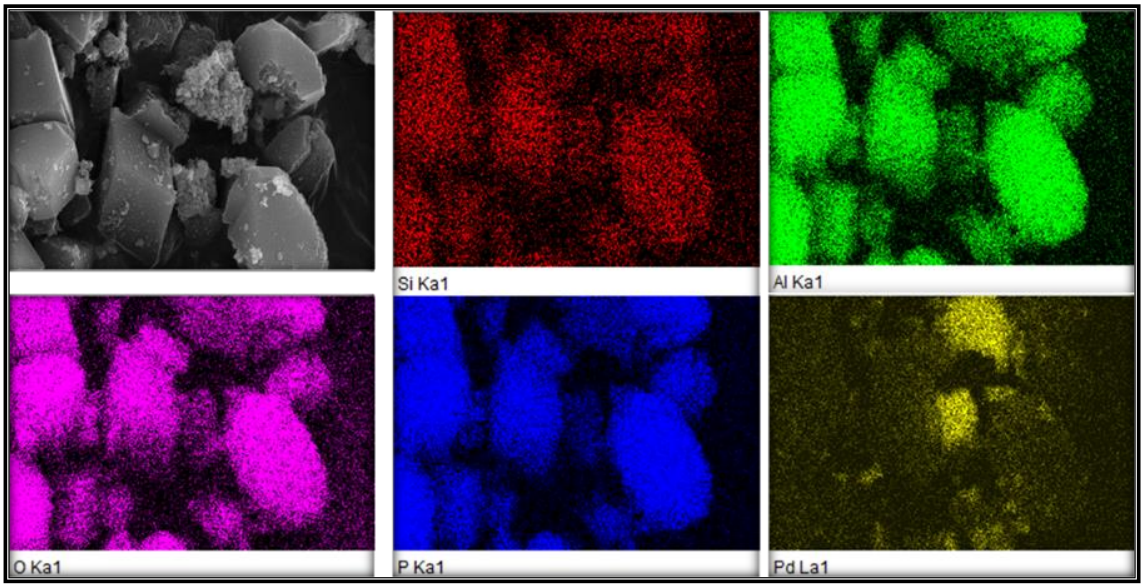

Figure 3: Elemental mapping of Pd/SAPO-35 (10 w/w %)

VI.3.3 FT-IR Studies:

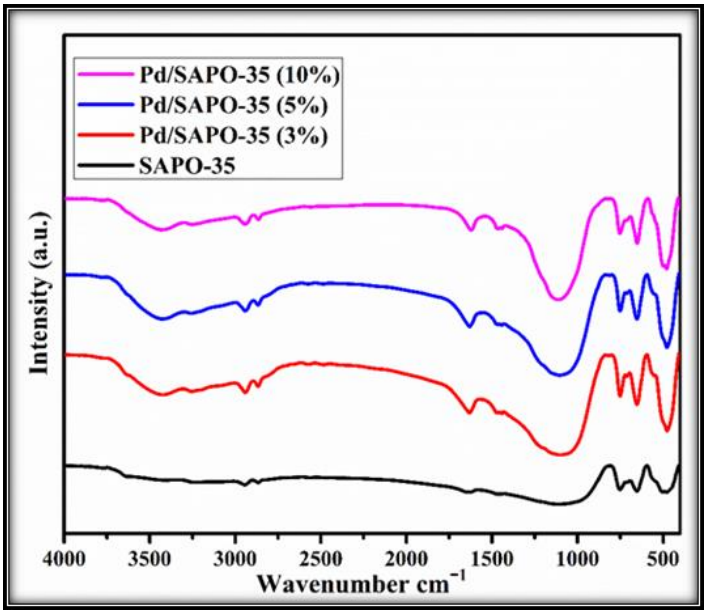

Figure 4: FT-IR spectra of prepared samples

To know the framework structure FT-IR studies were carried and the results are shown in the Fig. 4. All the samples FT-IR results are similar which shows there is no structure collapse after 550 °C calcination and post modification of SAPO-35 to Pd/SAPO-35. From the spectra a broad peak at 1100, 820, 630, 475 cm^{-1} are responsible for the T-O-T symmetrical stretching frequency where T = Si, Al, and P. The peaks at 2645-3000 cm^{-1} range are attributed due to -CH functional group's starching frequency of the organic functional silane from the template [24]. The broad peak at 1655 cm^{-1} is due to the H-O-H starching vibrations of adsorbed water.

VI.3.4. N_2 adsorption-desorption studies

N_2 adsorption-desorption studies carried to know the textual properties of the SAPO-35, Pd/SAPO-35 10% (w/w) samples and the results are given in the table 1. From these results it is found that, the initial SAPO-35 surface area is 493 m^2/g with 1.94 nm average pore diameter where as it was decreased to 211 m^2/g and 1.51 nm for the Pd/SAPO-35. The reason for the decrease in the surface area and pore size is due to the Pd particles are dispersed over the SAPO-35 surface. So as shown in the elemental mapping images the Pd particles are uniformly dispersed over the rhombohedral shaped SAPO-35 crystals hence the decrease in the surface area and pore diameter.

S. No.	Material name	BJH Surface Area (m^2/g)	Total pore volume (cc/g)	BJH Pore diameter (nm)	Average Pore diameter (nm)
1	SAPO-35	493	0.90	2.04	1.94
2	Pd-SAPO-35(10%)	211	0.64	1.60	1.51

VI.3.5. XPS studies

The XPS spectra of Pd/SAPO-35 (10% w/w) was depicted in Fig. 5. from the overlay spectra it was found the presence of Al, P, Si, O and Pd. Further to know the absolute structure of the framework we did deconvolution of each metal XPS spectra. From the Al deconvolution spectra, it was found that two different peaks at 73.1 eV and 74.6 eV which are corresponds to Al 2p 3/2 state and second peak corresponds to 2p 1/2 state. 72.3 + 0.1 represents the +3 oxidation state of the Al in the composite [4,25]. From the deconvolution spectra of P, only a single peak appeared at 139.4 eV. This binding energy corresponds to 2p 3/2 state of

phosphorous and the binding energy value 133+ 0.1 represents the +5 oxidation state of the P. So, it is conformed that the oxidation state of P is +5 [26,27]. From the deconvolution spectra of Si, we can observe a high intense narrow peak appeared at 103.3 eV which is corresponds to Si 2p 3/2 state. Hence Si is conformed that +4 oxidation state in the Pd/SAPO-35 material [28]. From the O1s deconvolution spectra there are two peaks we can observed at 531.7 and 534.6 eV. From the literature values the binding energy 531.7 eV is because of O_2 in Pd-O-Pd bonding and the peak at binding energy value of 534.6 is because of O_2 in Pd-O-Si linkage in the material. From the Pd XPS deconvolution, spectra there are three peaks observed at 334.4 eV, 336.5 eV and 342 eV. From these three peaks, the peak at lower binding energy of 335.4 eV is due to the unreacted Pd metal source Pd (0). The other two peaks at binding energy values of 335.5 eV, 342eV due to the Pd 3d 5/2 and 3d 3/2 respectively. From these results it can be conclude that the Pd is in +2 oxidation state [23,29].

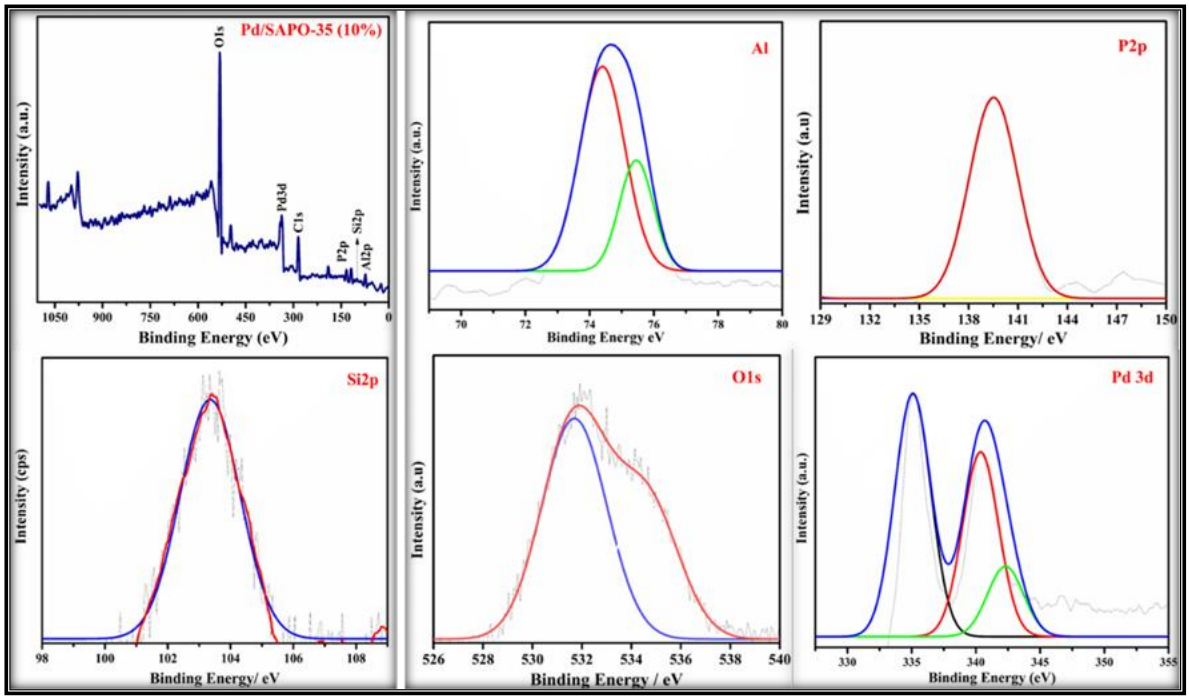

Figure 5: XPS spectra of Pd/SAPO-35 10% (w/w)

VI.3.6. Cyclic Voltammetry Studies

Along with the PXRD we have studied cyclic voltammetry for the conformation of Pd presence in the material. Because cyclic voltammetry (CV) is a versatile electroanalytical technique for the study of electroactive species [30,31]. The condition of study is 2mM Ferri cyanide solution with 100 mV/sec. From these results, we can clearly observe that the Pd metal

is the responsible for the resulting current and as the Pd weight percentage increases, the current is increasing which are depicted in Fig. 6.

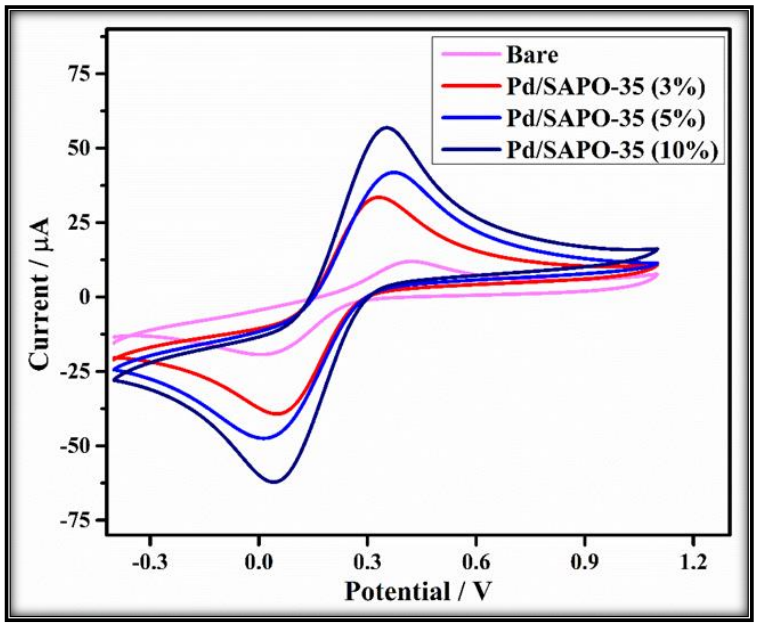

Figure 6: cyclic voltammetry of the prepared samples

VI.3.7. Suzuki-Miyaura Cross Coupling Reaction Studies

In order to check the catalytic activity of Pd/SAPO-35 we screened Suzuki-Miyaura Cross Coupling reaction. Reaction Conditions are 1mM of Benzeneboronic acid, 1mM of aryl halide, 20mg of K_2CO_3 and 10mg of calcined catalyst without organic solvent in domestic microwave oven at 360 w about 5 min. The resulting samples were collected after the Suzuki-Miyaura cross coupling reaction and analyzed using Gas Chromatography-YL-6500 South Korea equipped with a flame ionization detector FID and for further confirmation was done by the NMR. Here the main advantage of using heterogeneous catalyst we can reuse the catalyst by simply filter after several cycles, in our case we did 5 consecutive times and after 5^{th} cycle also we got over 86% of yield. All the results are given in the table 2. Also given a plausible reaction mechanism for the above reaction in Fig. 7.

The plausible reaction mechanism may take place through three steps mainly addition of organohalide, transmetallation and reductive elimination respectively. In the firsts step of reaction the Pd(II) complex reacts with organohalides by oxidative addition, at the same time under basic environment of K_2CO_3 the benzeneboronicacid forms a strong nucleophile. In the

second step this strong nucleophile attacks the Pd/SAPO-35 complex formed in the first step, this step is called transmetallation. In the final step the elimination of hydro halide takes place to form biphenyl product this step is called reductive elimination[32].

S. No.	Catalyst	R-X	Reaction Conditions	Yield (%)
1	Pd/SAPO-35 3% (w/w)	C_6H_5I	5 min @360 W	92
2	Pd/SAPO-35 5% (w/w)	C_6H_5I	5 min @360 W	96
3	Pd/SAPO-35 10% (w/w)	C_6H_5I	5 min @360 W	99
4	Pd/SAPO-35 3% (w/w)	C_6H_5Br	5 min @360 W	86
5	Pd/SAPO-35 5% (w/w)	C_6H_5Br	5 min @360 W	91
6	Pd/SAPO-35 10% (w/w)	C_6H_5Br	5 min @360 W	94

NMR spectral data of 1,1'-Biphenyl: White solid; yield 96%; MP 68-69 °C;

^{1}H NMR (400 MHz, $CDCl_3$) δ 7.69 (d, J = 8.1 Hz, 4H), 7.53 (t, J = 7.5 Hz, 4H), 7.44 (t, J = 7.2 Hz, 2H).

^{13}C NMR (100 MHz, $CDCl_3$) δ 141.3, 128.9, 127.4, 127.3.

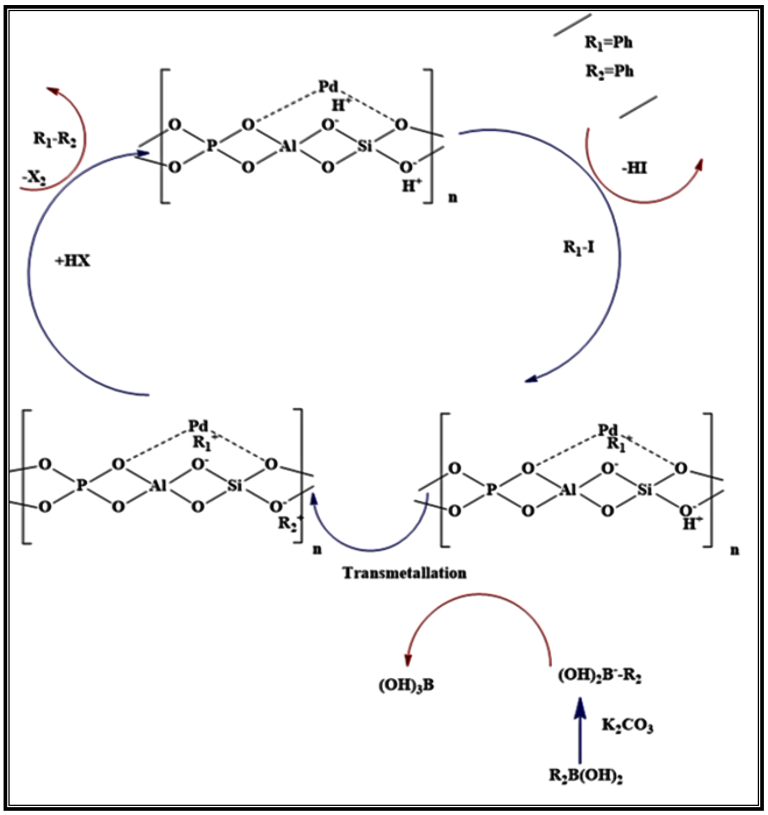

Figure 7: Plausible reaction mechanism of Suzuki-Miyaura Cross Coupling reaction using Pd/SAPO-35

VI.4. Conclusion

Levyne type microporous SAPO-35 prepared by conventional hydrothermal method and post modified it with Pd metal loading by borohydride reduction process. Synthesized material has been characterized in detailed and studied Suzuki-Miyaura Cross Coupling reaction under microwave irradiation without using organic solvents. The results are promising and process is eco-friendly.

VI.5. References

[1] S. Das, P. Heasman, T. Ben, S. Qiu, Chem. Rev. 117 (2017) 1515–1563.

[2] S. Rashidi, J.A. Esfahani, N. Karimi, Renew. Sustain. Energy Rev. 91 (2018) 229–247.

[3] H. Dai, Y. Shen, T. Yang, C. Lee, D. Fu, A. Agarwal, T.T. Le, M. Tsapatsis, J.C. Palmer, B.M. Weckhuysen, P.J. Dauenhauer, X. Zou, J.D. Rimer, Nat. Mater. (2020).

[4] S. Siliveri, S. Chirra, C. Tyagi, A. Gandamalla, A.K. Adepu, S. Goskula, S.R. Gujjula, N. Venkatathri, ChemistrySelect 4 (2019) 9135–9142.

[5] M.-H. Sun, S.-Z. Huang, L.-H. Chen, Y. Li, X.-Y. Yang, Z.-Y. Yuan, B.-L. Su, Chem. Soc. Rev. 45 (2016) 3479–3563.

[6] Y. Li, Z.-Y. Fu, B.-L. Su, Adv. Funct. Mater. 22 (2012) 4634–4667.

[7] R. Glaser, J. Weitkamp, The Application of Zeolites in Catalysis, n.d.

[8] Y. Li, L. Li, J. Yu, Chem 3 (2017) 928–949.

[9] S. Kotha, K. Lahiri, D. Kashinath, Tetrahedron 58 (2002) 9633–9695.

[10] A. Modak, J. Mondal, V.K. Aswal, A. Bhaumik, J. Mater. Chem. 20 (2010) 8099–8106.

[11] R. Srivastava, N. Venkatathri, D. Srinivas, P. Ratnasamy, Tetrahedron Lett. 44 (2003) 3649–3651.

[12] K. Sarkar, M. Nandi, M. Islam, M. Mubarak, A. Bhaumik, Appl. Catal. A Gen. 352 (2009) 81–86.

[13] C. Len, S. Bruniaux, F. Delbecq, V. Parmar, Catalysts 7 (2017) 146.

[14] S. Thunga, S. Poshala, N. Anugu, R. Konakanchi, S. Vanaparthi, H.P. Kokatla, Tetrahedron Lett. 60 (2019) 2046–2048.

[15] M.A. Düfert, K.L. Billingsley, S.L. Buchwald, J. Am. Chem. Soc. 135 (2013) 12877–12885.

[16] S. Chirra, S. Siliveri, A.K. Adepu, S. Goskula, S.R. Gujjula, V. Narayanan, J. Porous Mater. (2019).

[17] P. Priecel, J.A. Lopez-Sanchez, ACS Sustain. Chem. Eng. 7 (2019) 3–21.

[18] D. Gangrade, L. Sd, M. Al, Int J Res Pharm Sci 5 (2015) 37–42.

[19] A. Ricci, SOLVENTLESS REACTIONS UNDER MICROWAVE ACTIVATION: SAFETY AND EFFICIENCY AT THE SERVICE OF CUSTOMER-FRIENDLY CHEMISTRY, n.d.

[20] V. Polshettiwar, R.S. Varma, Acc. Chem. Res. 41 (2008) 629–639.

[21] A.M. Prakash, M. Hartmann, L. Kevan, Chem. Mater. 10 (1998) 932–941.

[22] Narayanan Venkatathri Sooryakant G. Hegde, United States Patent, US007037874B2, 2006.

[23] L. Sun, S. Zhang, W. Bao, W. He, RSC Adv. 5 (2015) 53320–53325.

[24] R. Yadav, M. Ahmed, A.K. Singh, A. Sakthivel, Sci. Rep. 6 (2016) 22813.

[25] C.D. Wagner, D.E. Passoja, H.F. Hillery, T.G. Kinisky, H.A. Six, W.T. Jansen, J.A. Taylor, J. Vac. Sci. Technol. 21 (1982) 933–944.

[26] T.L. Barr, M.A. Lishka, J. Am. Chem. Soc. 108 (1986) 3178–3186.

[27] S. Suresh, I.A.K. Reddy, N. Venkatathri, Microporous Mesoporous Mater. 263 (2018) 275–281.

[28] J.W. Ma, W.J. Lee, J.M. Bae, K.S. Jeong, S.H. Oh, J.H. Kim, S.H. Kim, J.H. Seo, J.P. Ahn, H. Kim, M.H. Cho, Nano Lett. 15 (2015) 7204–7210.

[29] P. Wu, Y. Huang, L. Kang, M. Wu, Y. Wang, Sci. Rep. 5 (2015).

[30] N. Elgrishi, K.J. Rountree, B.D. McCarthy, E.S. Rountree, T.T. Eisenhart, J.L. Dempsey, J. Chem. Educ. 95 (2018) 197–206.

[31] P. Chooto, in: Voltammetry, IntechOpen, 2019.

[32] S. Chirra, S. Siliveri, A.K. Adepu, S. Goskula, S.R. Gujjula, V. Narayanan, J. Porous Mater. 26 (2019) 1667–1677.

CHAPTER-VII

Summary and Conclusions.

Chapter-VII

Summary and Conclusions

This chapter summarizes, concludes the present work and have the outlook for the future work.

VII.1 Summary

This thesis consists of VII chapters. Chapter I describes the general introduction of the present work, Chapter II describes the experimental and characterization techniques used for analysis, Chapters III, IV, V and VI were about the original research work done on the development of silicoaluminophosphate molecular sieves and their catalytic applications. Finally, Chapter VII (This chapter) focuses mainly on the summary and conclusions.

VII.2 Conclusions

During the course of this research work, a number of conclusions have been reached, regarding the preparation, characterization and different catalytic application studies.

Chapter I: Chapter I describes the general background of Catalysis, Classification of Porous materials, state of the problem, objective and scope of the present work. It is also describing Literature review on present work, synthetic methodology and evolution of SAPO molecular sieves and their catalytic applications.

Chapter-II: Chapter-II deals with the detailed experimental procedures of the synthesized materials, Chemicals used to synthesize the materials and Characterization techniques used for the analysis of the prepared materials.

Chapter-III: Chapter-III investigates an Investigation on Promoter Induced Rapid Non-Aqueous Media Synthesis of SAPO-35 and MTO reaction. Levyne type topological microporous SAPO-35 molecular sieves were successfully synthesized by using conventional hydrothermal method in presence of different inorganic promoters to reduce the reaction time in a typical non-aqueous media. In the present study, the reaction time was reduced by 80% which is highly recommended for the industrial commercialization. All the materials synthesized using various promoters have exhibited similar characteristics as that of the standard samples (material synthesized without using promoters), which was demonstrated using different methods in the present study. Moreover, the catalytic performance in terms of yield and selectivity of these materials in the MTO conversion reaction is found to be similar with the performance of standard

material. With the help of all these studies it can be concluded that the addition of promoters has successfully reduced the time for the crystallization process which in turn reduced the time for the reaction, and the materials synthesized through this method are as effective as the standard materials in MTO conversion reaction.

Chapter IV: Chapter IV examines the detail study of Synthesis of SAPO-16 molecular sieve in Non-aqueous medium by microwave method using Hexamethyleneimine as a template. AST type Silicoaluminophosphate molecular sieves SAPO-16 has been synthesized in ethylene glycol media by using microwave technique with hexamethyleneimine as an organic template in rapid time against the conventional fifteen days by hydrothermal method. This synthesis root is eco-friendly, very rapid and also obtaining products were highly uniform. The synthesized SAPO-16 was found to be economic and efficient catalyst for Benzaldehyde acetalization reaction, the catalytic activity on Benzaldehyde acetalization reaction shows that the reactants have a maximum of 80 % benzaldehyde conversion in 8 h with maximum turn over a number of 14.5×10^{-2} and turn over the frequency of 4.0×10^{-5}. This method also can be applicable to synthesize other Silicoaluminophosphate molecular sieves by efficient way.

Chapter-V: Chapter-V examines New Porous high surface area, TiO_2 Anatase/SAPO-35 Mild Bronsted acidic Nanocomposite: Synthesis, characterization and studies on its enhanced photocatalytic activity. TiO_2 anatase and Microporous Silicoaluminophosphate (SAPO-35) have been synthesized by hydrothermal method. The different (w/w) ratio of TiO_2/SAPO-35 composites were prepared through sol-gel procedure. The synthesized materials are characterized in detail. The ability of these composites in degrading methylene blue has been studied under sun light irradiation. The results have shown, TiO_2/SAPO-35 composite shows excellent dye degradation ability compared to TiO_2 and SAPO-35 independently. The fine dispersion of TiO_2 anatase Nano particles on the surface of the microporous SAPO-35 resulted in the increased ability of dye degradation. As a consequence of this phenomenon, the recombination rate of the electron-hole pair of these materials was minimized. All these results revealed the existence of a synergistic relation between TiO_2 and SAPO-35 in degrading methylene blue.

Chapter-VI: Chapter-VI deals with Pd/SAPO-35: Synthesis, Characterization and its Catalytic application studies on Suzuki-Miyaura Cross Coupling Reaction. Levyne type microporous SAPO-35 prepared by conventional hydrothermal method and post modified

it with Pd metal loading by borohydride reduction process. Synthesized material has been characterized in detailed and studied Suzuki-Miyaura Cross Coupling reaction under microwave irradiation without using organic solvents. The results are promising and process is eco-friendly.

Chapter-VII: This chapter describes the relevant conclusions drawn from the work carried out.

Future outlook of the Present Study:

1. This promoter based non-aqueous media synthesis can be applicable for synthesis of various SAPO materials like SAPO-34, SAPO-11, SAPO-54 etc.
2. This route of synthesis (promoter based non-aqueous media synthesis) can be commercialised in a piolet scale.
3. Using TiO_2/SAPO-35 material can be used for other dyes degradation like Rhodamine-B, methyl orange etc.
4. SAPO-35 material can be used as the adsorbents for CO_2, H_2 gases storage.

List of Publications, Conferences and Bio-data

List of Publications, Conferences, and Bio-data

List of Publications

1. **Siliveri Suresh**, Sai Siva Kumar Pinnepalli, Deepak Joshi, Suman Chirra, Srinath Goskula, Sripal Reddy, Gujjula, Nathan A. Oyler, Venkatathri Narayanan. (2021) An Investigation on Promoter Induced Rapid Non-Aqueous Media Synthesis of SAPO-35 and MTO reaction. **ACS omega** 6 (8), 5661-5669.

2. **S Suresh**, IAK Reddy, N Venkatathri. (2018) Synthesis of SAPO-16 molecular sieve in non-aqueous medium by microwave method using hexamethyleneimine as a template. **Microporous and Mesoporous Materials**, 263, 275-281.

3. **S Siliveri**, S Chirra, C Tyagi, A Gandamalla, AK Adepu, S Goskula, SR Gujjula, N Venkatathri. (2019) New Porous High Surface Area, TiO_2 Anatase/SAPO-35 Mild Brønsted Acidic Nanocomposite: Synthesis, Characterization and Studies on its Enhanced Photocatalytic activity **ChemistrySelect,** 4(31), 9135–9142.

4. **Suresh Siliveri**, Suman Chirra, Srinath Goskula, Sripal Reddy Gujjula, Venkatathri Narayanan. (2021) Pd/SAPO-35: Synthesis, Characterization and its Catalytic application studies on Suzuki-Miyaura Cross Coupling Reaction. **Materials Today: Proceedings** 45, 3778-3783.

5. Suman Chirra, Li-Fang Wang, Himanshu Aggarwal, Ming-Fong Tsai, Siva Sankari Soorian, **Siliveri Suresh,** Srinath, Goskula, Sripal Reddy Gujjula, N. Venkatathri, (2021). Rapid synthesis of a novel nano-crystalline mesoporous faujasite type metal-organic framework, ZIF-8 catalyst, and $NaBH_4$ assisted, enhanced catalytic Rhodamine B Degradation **Materials Today Communications**, 26, 101993

6. S Chirra, Raju, **S Siliveri**, Naresh Yadav, S Goskula, SR Gujjula, V Narayanan, (2021). Synthesis of a novel bifunctional mesoporous Ti-SBA-15-SO_3H catalyst and studies on their enhanced performance and kinetic modeling of lactic acid esterification reaction with n-butanol. **Materials Today: Proceedings,** 45, 3699-3708.

7. Adepu, A. K., Siliveri, S., **Chirra, S.,** Goskula, S., Gujjula, S. R., Anumula, R., & Narayanan, V, (2020). A novel porous Fe3O4/Titanosilicate/g-C3N4 ternary nanocomposites: Synthesis, characterization, and their enhanced photocatalytic activity on Rhodamine B degradation under sunlight irradiation. **Journal of Water Process Engineering**, 34, 101141.

8. AK Patan, SK Thamida, S Suranani, **S Siliveri**, V Narayanan, (2020), Experimental investigation of start-up dynamics for various heating effects in batch reactive distillation to produce methyl acetate **International Journal of Chemical Reactor Engineering,** 18 (4)

9. Chirra, S., **Siliveri, S.**, Gangalla, R., Goskula, S., Gujjula, S. R., Narayanan, V. (2019). Synthesis of new multivalent metal ion functionalized mesoporous silica and studies of their enhanced antimicrobial and cytotoxicity activities. **Journal of Materials Chemistry B**, 7(45), 7235–7245.

10. AK Adepu, **S Siliveri**, S Chirra, S Goskula, SR Gujjula, R Anumula, N Venkatathri, (2019) Synthesis of a high-surface area $V_2O_5/TiO_2–SiO_2$ catalyst and its application in the visible light photocatalytic degradation of methylene blue, **RSC Advances** 9 (42), 24368-24376

11. S Chirra, **S Siliveri**, AK Adepu, S Goskula, SR Gujjula, V Narayanan, (2019), Pd-KIT-6: synthesis of a novel three-dimensional mesoporous catalyst and studies on its enhanced catalytic applications **Journal of Porous Materials,** 26 (6), 1667-1677

12. AK Adepu, S Goskula, S Chirra, **S Siliveri,** SR Gujjula, N Venkatathri, (2019). Magnetically separable porous titanosilicate/Fe_3O_4 hybrid nanocomposites with enhanced photocatalytic performance under UV light **Journal of Porous Materials** 26 (5), 1259-1267.

13. A Rajini, C Suman, A Ajay Kumar, **S Suresh**, N Venkatathri, (2016). Titanium aminophosphates as efficient, economical, and recyclable catalysts for the synthesis of xanthenediones **Synthetic Communications,** 46 (20), 1671-1677.

14. R Anumula, AK Adepu, S Chirra, **S Siliveri,** V Narayanan, (2015). Titanium aminophosphates: synthesis, characterization and crystal violet dye degradation studies, **RSC advances** 6 (1), 507-514.

List of national and international conferences

1. Functional Nanomaterials in industrial & Clinical Applications: Academy- Industry-Clinical Meet" (14th to 16th July 2020, UCLan, Preston, UK), "Pd/SAPO-35: Synthesis, Characterization and its Catalytic application studies on Suzuki- Miyaura Cross Coupling Reaction". (Poster Presentation)
2. International Conference on Materials for the millennium (MATCON-2019), CUSAT, Kochi, March 14-16th 2019. "Photocatalytic degradation of methylene blue over TiO2/SAPO-35 heterojunction". (Poster Presentation)

3. 7th Asia Pacific Congress on Catalysis, The Hotel Lalith, Mumbai, 17-21st January 2017. “Microwave-mediated rapid non-aqueous media synthesis of a novel Nano crystalline, silico-aluminophosphate SAPO-16 catalyst”. (Poster Presentation).

Bio-Data

Personal Information:

Suresh Siliveri

Research Scholar, Department of Chemistry

National Institute of Technology, Warangal, Telangana, India, 506 004.

+91-9959499849

siliverisuresh007@gmail.com
siliverisuresh007@student.nitw.ac.in

Gender: Male | **Date of Birth:** 05-07-1990 | **Nationality:** Indian

https://scholar.google.co.in/citations?user=xEgIS6cAAAAJ&hl=en

https://www.researchgate.net/profile/Siliveri_Suresh

Education and Training:

Institute/College /School	University/Board	Course	Division	Year of Study
Nizam College, Hyderabad India	Osmania University, Hyderabad, Telangana, India. http://www.osmania.ac.in/	M.Sc. Chemistry	First Class CGPA:7.44	July 2011 – May 2013
Government Degree College, Siddipet	Osmania University, Hyderabad, Telangana, India. http://www.osmania.ac.in/	Bachelor of Science Mb. Z. C	First Class (63.77%)	July 2007 – June 2010)
Prathibha Junior College, Siddipet	Board of Intermediate Education, Hyderabad http://bie.telangana.gov.in/	Intermediate	First Class (85.70%)	June 2005-April 2007
Gayathri Vidhyalayam	Board Secondary Education http://bse.telangana.gov.in/	SSC	First Class (87.66%)	April-2005

Work Experience:

- ✓ Having more than five years of research experience in National Institute of Technology, Warangal.
- ✓ Good expertise in synthesis of various SAPO molecular sieves through aqueous media and non-aqueous media through hydrothermal and Microwave methods.
- ✓ Well expertise in operating a wide variety of instruments for physicochemical characterizations.
- ✓ Familiar with FT-IR, UV-Vis, PXRD, BET, TG-DTA, DSC, SEM, EDAX, TEM, Raman spectroscopy, NH_3-TPD, MAS-NMR, and Gas Chromatography.
- ✓ Well expertise in operating High Temperature Furnace, Microprocessor controlled oven, Probe sonicator.

Computer Skills:

- ✓ Proficient in using a variety of software Chem office,
- ✓ Mendeley Reference Manager.
- ✓ Origin 8.0 and 9.0, Microsoft Office.
- ✓ For a broad range of data measurement, plotting, analyses and publication writings

Honors and Awards:

- ✓ Qualified in All India level Graduate Aptitude Test in Engineering (GATE- 2015)
- ✓ Qualified in State Eligibility Test for Telangana and Andhra Pradesh States for Assistant professor/Lectureship (SET-TS & AP-2014)
- ✓ Receiving scholarship from Department of Science and Technology- Science and Engineering Research Board (DST-SERB), Government of India, for pursing Ph.D. in the Department of Chemistry, NIT-Warangal.
- ✓ Received Best Poster award in Research Conclave-2018 at National Institute of Technology, Warangal, India.